University of Illinois at Urbana-Champaign

ACRC

Air Conditioning and Refrigeration Center A National Science Foundation/University Cooperative Research Center

Fractionation of R-407C in Brazed Plate Evaporators at Low Mass Flux

D. A. Tallitsch and P. S. Hrnjak

ACRC CR-41 July 2001

For additional information:

Air Conditioning and Refrigeration Center
University of Illinois
Mechanical & Industrial Engineering Dept.
1206 West Green Street
Urbana, IL 61801

(217) 333-3115

Prepared for
The Trane Company
under supervision of
Jon Hartfield

The Air Conditioning and Refrigeration Center was founded in 1988 with a grant from the estate of Richard W. Kritzer, the founder of Peerless of America Inc. A State of Illinois Technology Challenge Grant helped build the laboratory facilities. The ACRC receives continuing support from the Richard W. Kritzer Endowment and the National Science Foundation. The following organizations have also become sponsors of the Center.

Amana Refrigeration, Inc.
Arçelik A. S.
Brazeway, Inc.
Carrier Corporation
Copeland Corporation
Dacor
Daikin Industries, Ltd.
DaimlerChrysler Corporation
Delphi Harrison Thermal Systems
Frigidaire Company
General Electric Company
General Motors Corporation
Hill PHOENIX
Honeywell, Inc.
Hussmann Corporation
Hydro Aluminum Adrian, Inc.
Indiana Tube Corporation
Invensys Climate Controls
Kelon Electrical Holdings Co., Ltd.
Lennox International, Inc.
LG Electronics, Inc.
Modine Manufacturing Co.
Parker Hannifin Corporation
Peerless of America, Inc.
Samsung Electronics Co., Ltd.
Tecumseh Products Company
The Trane Company
Thermo King Corporation
Valeo, Inc.
Visteon Automotive Systems
Wolverine Tube, Inc.
York International, Inc.

For additional information:

Air Conditioning & Refrigeration Center
Mechanical & Industrial Engineering Dept.
University of Illinois
1206 West Green Street
Urbana, IL 61801

217 333 3115

Abstract

This investigation explored the effects of fractionation and distribution of R-407c in brazed plate evaporators with an emphasis at low mass flux. Experiments were performed in parallel with R-22. A parametric study was performed with nominal and reduced mass fluxes, with and without distributor and with various orientations of the evaporator. Also, operating conditions were varied to investigate the effect of refrigerant inlet quality and superheat at the exit of the evaporator. This investigation took an evaporator as part of a system approach rather than evaluating local heat transfer.

All experiments show that R-407c is a viable replacement for R-22. Overall heat transfer coefficients for R-407c were essentially equal to that of R-22 when operating at nominal conditions. U-values for R-407c at low mass flux were up to 15% less than R-22. However, R-407c U-values were approximately 10% greater than R-22 when operating with a saturated refrigerant outlet condition.

Contrary to expectations, only slight fractionation was seen for all test conditions and evaporator configurations. It was concluded that lower inlet quality slightly increases refrigerant composition shift. Also seen in this investigation was greater composition shift at greater mass flux for individual experiments. This condition could be related to significant oil hold-up seen at low mass flux.

A distributor was developed in this investigation to allow better distribution when operating with refrigerant flow in the downward direction. While downward flow did not have an effect on refrigerant composition shift in this investigation, this orientation may be useful for other applications where more severe fractionation is seen.

Other issues addressed were superheat instability and oil hold-up in the evaporator. Liquid droplets were seen at the exit of the evaporator when operating with low superheat. Also, it was found that up to 35% of the volume of the evaporator could be filled with oil even when operating at nominal capacity.

Table of Contents

List of Figures

Page

List of Tables

Nomenclature

A	Gas Chromatograph Output Value
A	Heat Transfer Area
C	Nusselt Number Coefficient
Cp	Constant Pressure Specific Heat
Cre	Constant for Water Side Heat Transfer Coefficient Correlation
dh	Hydraulic Diameter
G	Refrigerant Mass Flux
h	Enthalpy
h	Average Heat Transfer Coefficient
k	Conductivity
LMTD	Log Mean Temperature Difference
M	Mass Flow Rate
n	Nusselt Number Exponent
Q	Heat Exchanged
T	Temperature
U	Overall Heat Transfer Coefficient
V	Volume
w	Weight factors for calculation of refrigerant composition
x	Mass Fraction
y	Exponent for Water Side Heat Transfer Coefficient Correlation

Greek Symbols

μ	Viscosity
ρ	Density

Dimensionless Groups

Pr	Prandtl Number
Re	Reynolds Number

Subscripts

R-32	Refrigerant R-32
R-125	Refrigerant R-125
R-134a	Refrigerant R-134a
w	Water
r	Refrigerant
in	Inlet of Evaporator
out	Outlet of Evaporator
2ph	Two Phase
sup	Superheated

Chapter 1.0. Introduction

The concern over the depletion of the ozone layer due to the release of greenhouse gases has led to the development of international agreements and United States legislation that will limit the production and use of chlorinated refrigerants. The refrigeration industry is spending much time and effort to develop replacements for the next century. Many alternative refrigerants have been evaluated for feasibility, but all have drawbacks that could include the redesign of refrigeration components. The most promising alternatives are mixtures of non-chlorinated refrigerants, since concentrations can be chosen such that the mixture has similar thermodynamic properties to the chlorinated refrigerants they are replacing. The use of such refrigerants would not require the redesign or resizing of components. However, other drawbacks exist such as temperature glide, lubricant compatibility and fractionation.

One potential replacement for the widely used chlorinated refrigerant R-22 is R-407c, a ternary mixture of R-32, R-125 and R-134a (23%, 25%, 52%), all of which are non-chlorinated refrigerants. It is widely accepted that R-407c will severely fractionate in shell and tube heat exchangers. The study reported in this paper concentrated on the fractionation of R-407c in plate evaporators and the thermal consequences of that fractionation.

This study consisted of six series of experiments to evaluate the effects of low mass flux, improved refrigerant distribution, varied evaporator exit quality/superheat and downward refrigerant flow on the magnitude of refrigerant fractionation and thermal performance. Various anomalies were discovered during this study, including superheat instability and oil hold-up in the plate evaporator.

The report is organized as follows: background information is provided in Chapter 2; the experimental facility is described in Chapter 3; experimental procedures are outlined in Chapter 4; experimental results are presented in Chapter 5; results of miscellaneous experiments are discussed in Chapter 6; conclusions of this study are made in Chapter 7; data reduction methods are presented in Chapter 8; and experimental error is calculated in Chapter 9. Raw data, analysis results, miscellaneous figures and EES equations can be found in the appendices in tabular form.

Chapter 2.0. Background

Over the last two decades, the Montreal Protocol, an international environmental agreement, has established phase-out requirements for CFC (chlorofluorocarbons) and HCFCs (hydro-clorofluorocarbons) due to the ozone-depleting nature of chlorine. The Montreal Protocol is carried out in the United States as the Clean Air Act, which calls for the phase-out of R-22 (HCFC) production by the year 2030. R-22 is the most common refrigerant for screw, scroll, and reciprocating air conditioners and chillers. As such, R-22 systems leaks could contribute significantly to the depletion of the ozone layer. With this reason, much research has been performed on so-called "drop-in" R-22 substitutes. The EPA has compiled a list of substitutes that was determined to be acceptable (http://www.epa.gov/ozone/title6/snap/lists/homeac.html). This study involves one of those refrigerants, R-407c, marketed under several trade names including SUVA 9000® by DuPont.

R-407c is blend consisting of 23/25/52 weight percent of R-32, R-125 and R-134a, respectively. Although described by DuPont as a near-azeotropic blend, zeotropic behavior has been observed through various studies when operating with low mass flow rates in shell and tube evaporators. A zeotropic blend acts like a typical mixture, retaining some of the individual properties of each component. The behavior of zeotropic blends is characterized by temperature glide and fractionation.

2.1. Understanding Temperature Glide and Fractionation

Temperature glide is defined as the change in boiling point (or condensation) temperature when evaporating (or condensing) in a heat exchanger. The term fractionation is used to describe the difference in composition of the liquid and vapor phases of a zeotropic mixture. Temperature glide and fractionation are interrelated, as the change is temperature is related to the shift in liquid and vapor composition. The magnitude of temperature glide is proportional to the magnitude of fractionation.

The vapor phase of a zeotropic blend in a closed volume and at steady state is rich in the higher-pressure component(s). This explains why most emphasis in the industry has been placed upon studying the effect of system leaks. If vapor leaks occur while the system is not operating, the higher-pressure component(s) will primarily escape changing the system composition. This is undesirable and will degrade system performance.

Leaks that occur during operation will typically not change the system composition since the system composition is relatively uniform. When the system does not operate, there is difference in composition between vapor and liquid phase and consequently potential for preferential leak of some component. During operation, however, there is the potential for fractionation to occur in components where both liquid and vapor are present, such as the evaporator. Under normal conditions, there is enough turbulence in heat exchangers where liquid and vapor are present to prevent fractionation. However, should mass flow rates be reduced below design conditions there is the potential for liquid to pool and fractionation to occur. The liquid pool would have a high concentration of the low pressure component(s), whereas the circulating refrigerant would have a high concentration of the high-pressure component(s). This scenario is plausible since the maximum capacities of most systems are rarely challenged. This leads

manufacturers to employ variable speed compressors into their systems to improve efficiency and avoid cycling.

2.2. Experimental Approach

As briefly discussed in Chapter 1, this study concentrated on the fractionation of R-407c in plate evaporators and the thermal consequences of such condition. The objective of this study was to evaluate R-407c performance under various plate evaporator configurations to show that R-407c is a viable replacement for R-22, and perhaps suggest possible ways to improve performance.

Three brazed plate heat exchangers were used in this study, one nominally sized at three tons (HX A) and two at twenty tons (HX B and HX C), where HX C had an internal distributor. A custom distributor was developed as part of this study to enable operation with downward refrigerant flow and is described in further detail later. The following six experiments were performed as a part of this study:

Experiment 1	**Baseline Experiments** – Small evaporator (HX A) resulting in design mass flux
Experiment 2	**Reduced Mass Flux** – Large evaporator (HX B) resulting in low mass flux
Experiment 3	**Refrigerant Distributor** – Large evaporator (HX C) with built-in distributor
Experiment 4	**Saturated Exit Conditions** – Large evaporator (HX C) with built-in distributor operating with a saturated exit condition
Experiment 5	**Downward Flow** – Large evaporator (HX B) with custom distributor operated with downward refrigerant flow
Experiment 6	**Downward Flow with Saturated Exit Conditions** - Large evaporator (HX B) with custom distributor operated with downward refrigerant flow and saturated exit conditions

The main objectives of these experiments were to determine the impact of the following on the circulating refrigerant composition:

- low mass flux
- improved refrigerant distribution
- varied evaporator exit quality/superheat
- downward refrigerant flow

Chapter 3.0. Experiment Facility

All data were acquired using a facility located in the Air Conditioning and Refrigeration Center (ACRC) at the University of Illinois at Urbana-Champaign.

3.1. Chiller

The chiller shown schematically in Figures 3.1 through 3.3 was used in this study. The components are listed in Table 3.1. With the exception of the evaporator, expansion valve, suction line and compressor, the apparatus was unchanged throughout the investigation. The evaporator was replaced or modified as required in the experiment matrix. The thermostatic expansion valve used during Experiments 1-3 was replaced with a manual expansion valve during Experiment 4 to obtain better stability when operating with a saturated exit condition. A heater was added in parallel to the suction line static mixer for use during Experiments 4 and 6 to allow for operation of the evaporator with a saturated outlet condition. The compressor was replaced twice with identical models after two compressor failures.

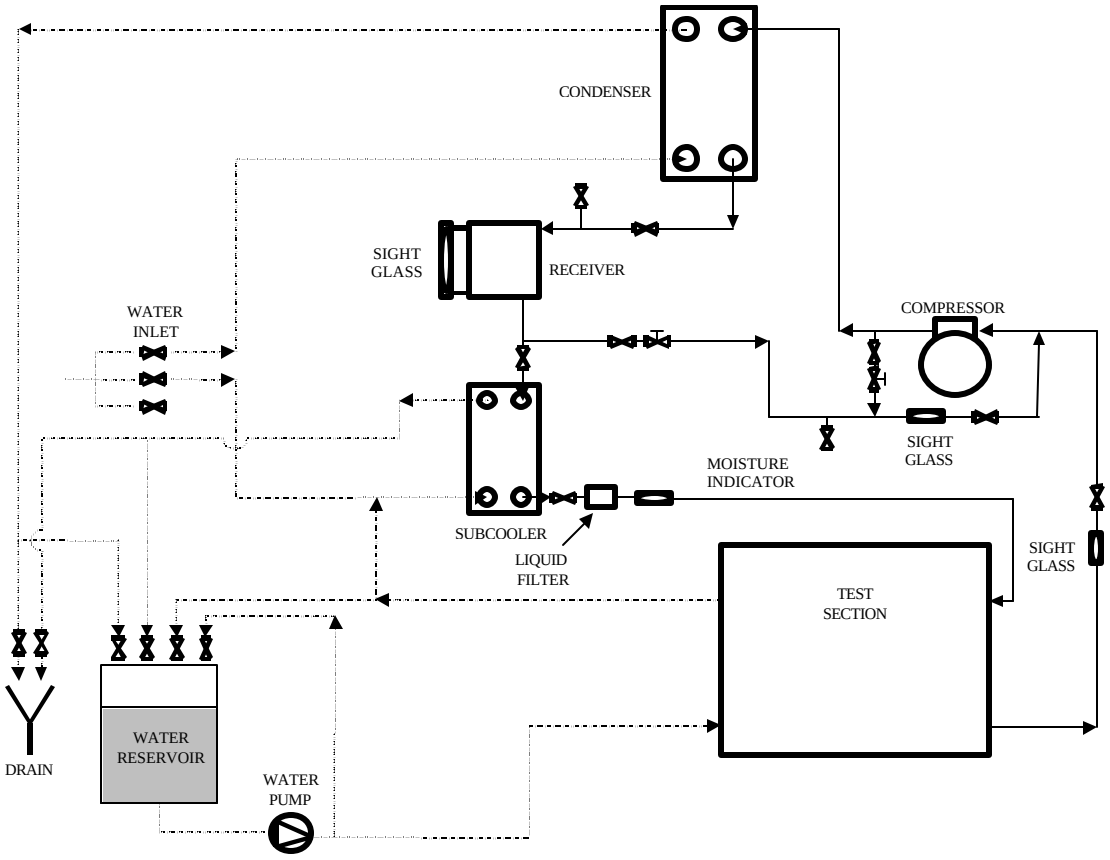

Figure 3.1 Schematic of chiller used for investigation

Table 3.1 List of chiller components

Component	Manufacturer	Model Number
Compressor	Copeland	Model ZR57K3 - PFV scroll hermetic
Condenser	SWEP	Model B15x40
Subcooler	SWEP	Model B8x20
Water Pump	Dayton	Model 9K679 (3/4 hp centrifugal pump)
Oil	Mobile	EAL Arctic Series 60105-4 (POE) ISO Viscosity Grade 22

3.1.1. Refrigerant Loop

The refrigerant loop consists of a scroll compressor, condenser, receiver, subcooler, and a test section. The test section consists of an expansion device, evaporator, and instrumentation to collect pressure, temperature, and mass flow rate. See Section 3.1.3 for a detailed description of the test section.

Refrigerant flow rate is regulated using the compressor bypass shown in the schematic. Hot vapor from the exit of the compressor is mixed with liquid refrigerant from the receiver. This flow is then directed to the suction line. The evaporating liquid refrigerant cools the vapor from the compressor discharge to a temperature that allows for proper operation of the compressor. A sight glass is used to visually ensure complete evaporation of liquid refrigerant.

All tubing and components from the subcooler to the compressor were well insulated to minimize heat transfer to the environment and to decrease uncertainty of measurements.

3.1.2. Water Loop

The first component in the water loop, a 5 gallon tank, serves as a mixer which provides water at constant temperature to the pump. A leakoff line maintains the tank at a predetermined level and maintains constant head to the centrifugal pump. This ensures steady water flow rate. Water can be supplied to the subcooler from the faucet or the return from the test section. Return water from the subcooler can be directed back to the tank or to the drain. Cooling water is supplied to the condenser from the faucet. The hot water return from the condenser is used to provide the heat load to the evaporator and to regulate the water tank temperature.

3.1.3. Test Section Description and Schematic

Figure 3.2 shows the test section configuration during Experiments 1 through 4. The test section for Experiment 5 and 6 with downward flow is shown in Figure 3.3. The instruments are chosen to determine inlet and outlet conditions (temperature, pressure, quality and enthalpy) for each experimental run.

Note that a heater was added in parallel to the static mixer for use in Experiment 4 and 6 to allow operation with saturated refrigerant exit conditions. Differential pressure across the heater and heater outlet temperature was recorded.

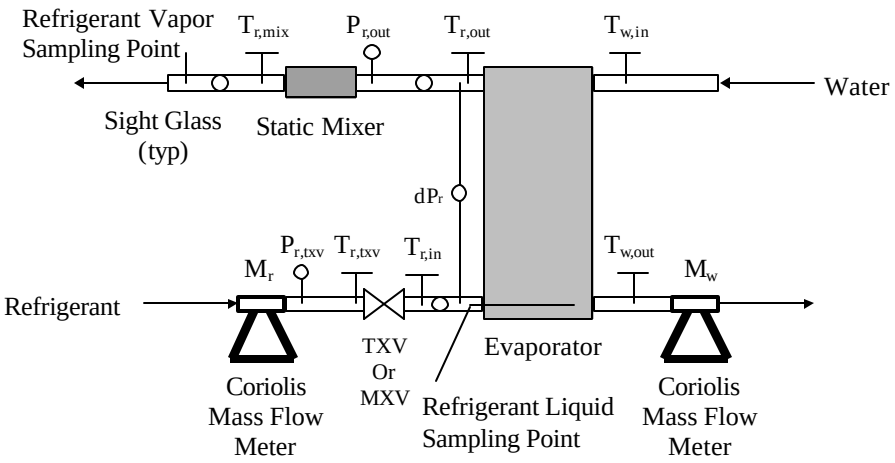

Figure 3.2 Test section during Experiments 1-4 (note that a heater was in parallel to the static mixer for test 4, similar to that seen in Figure 3.3)

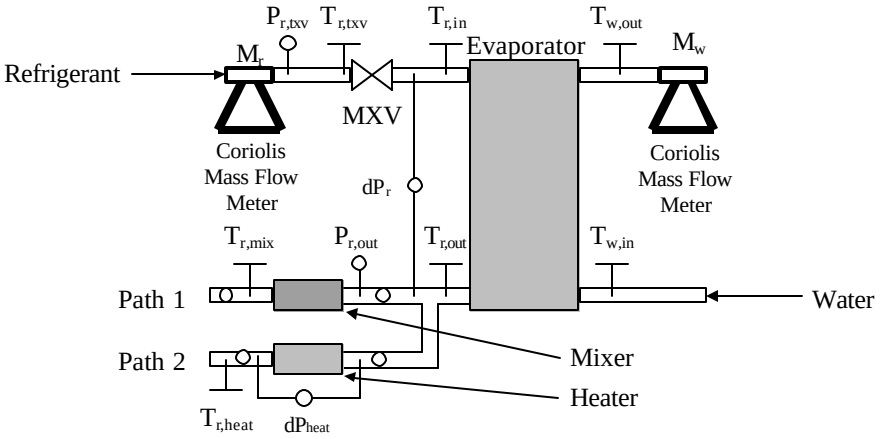

Figure 3.3 Test section during Experiment 5-6

3.1.4. Refrigerant Distributor for Downward Flow

Fractionation of refrigerant occurs at the bottom of evaporator, at low mass fluxes. If refrigerant was distributed evenly from the top, such phenomenon would be prevented. Turn of refrigerant flow down induces distribution problems. Being aware of problems with adequate distribution to ensure good wetting of evaporator surfaces, we designed a distributor to minimize maldistribution among plates when operating with downward flow of refrigerant. Figure 3.4 shows the configuration and component list. The first distributor, conventionally used in DX coils (Sporlan Type 1127), which evenly distributes the refrigerant among outlets is located immediately after the manual expansion valve. Flow leaves the distributor in 29 identical length 1/8" tubes and then enters a second distributor that directs the flow downward into the evaporator. This second distributor is cylindrical, fills the complete cavity of the evaporator header, and can be rotated to direct flow at an angle in the evaporator to decrease maldistribution within the channel. More detailed drawings of the refrigerant distributor are shown in Figures 3.5 and 3.6. Pictures taken during assembly are shown in Figure 3.7.

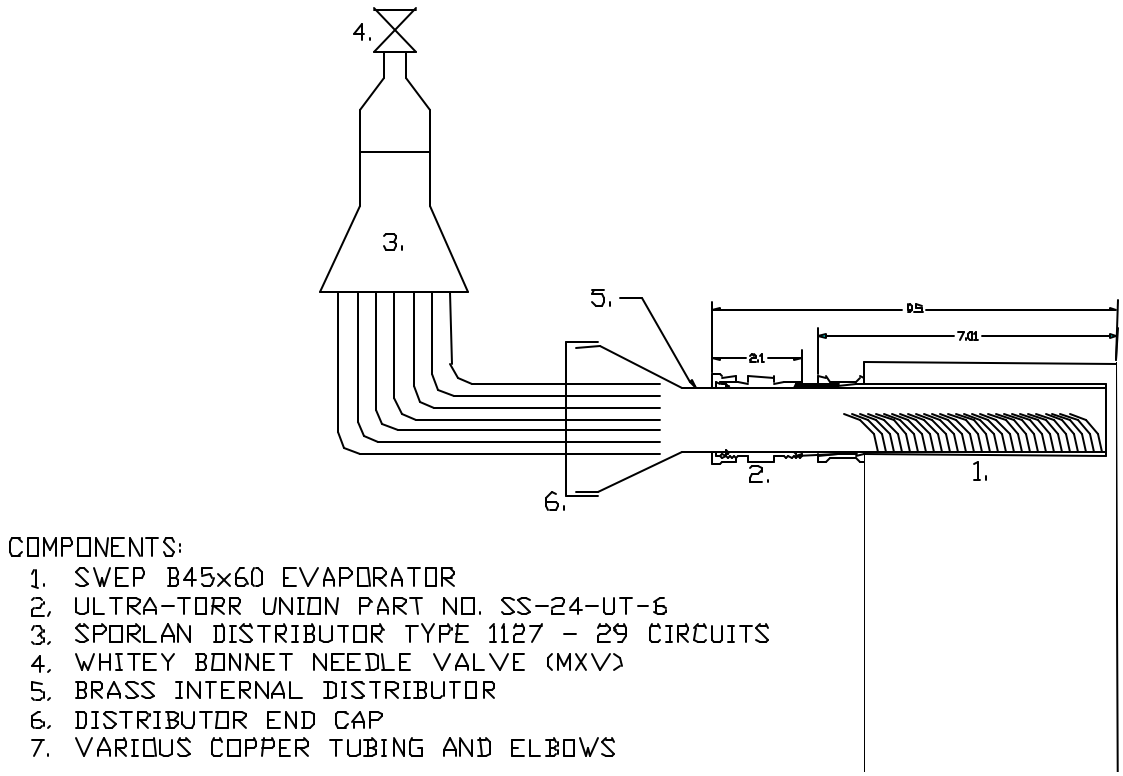

Figure 3.4 Custom distributor inserted into inlet header of evaporator to improve refrigerant distribution when operating with downward refrigerant flow

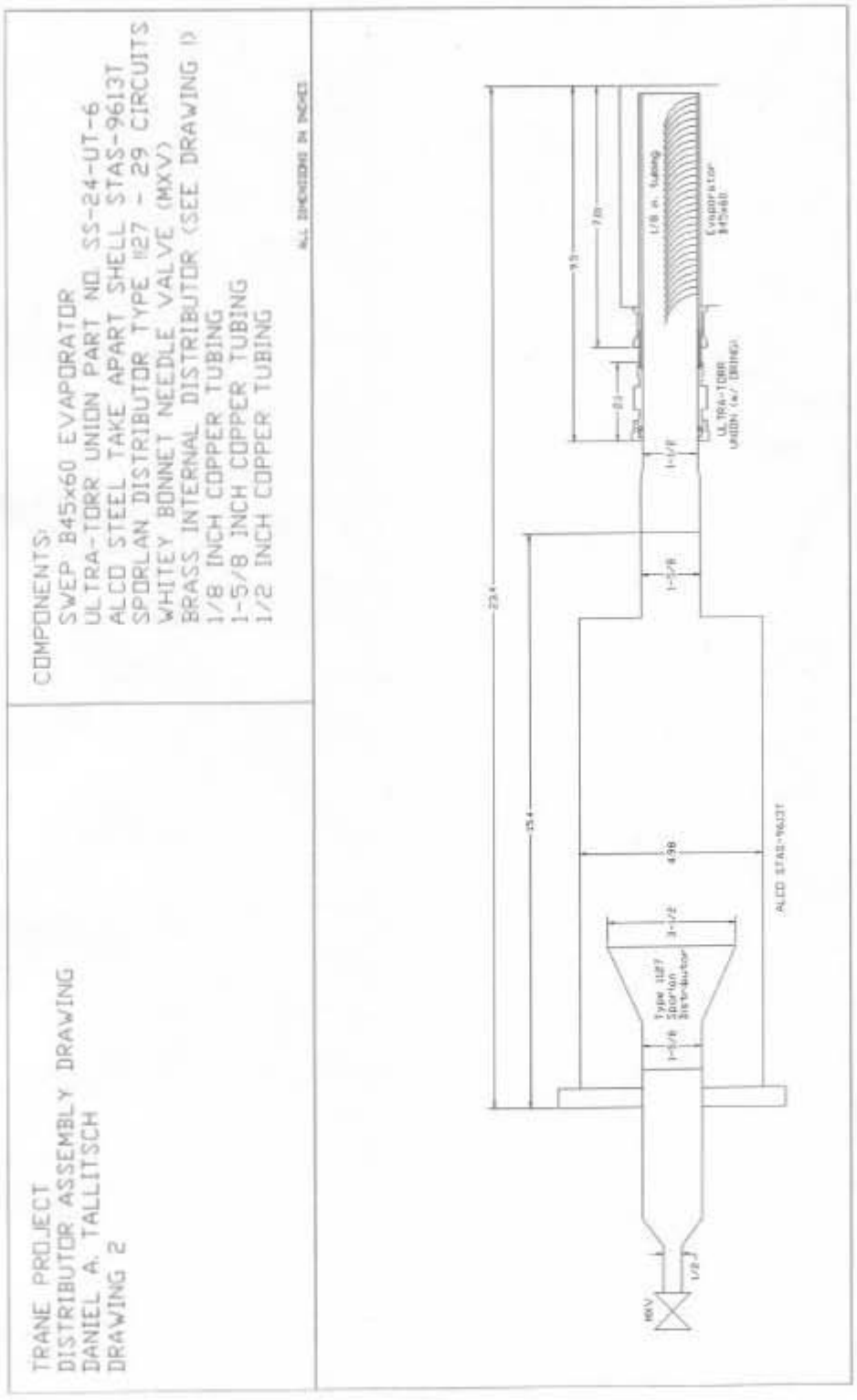

Figure 3.5 Assembly drawing of custom refrigerant distributor.

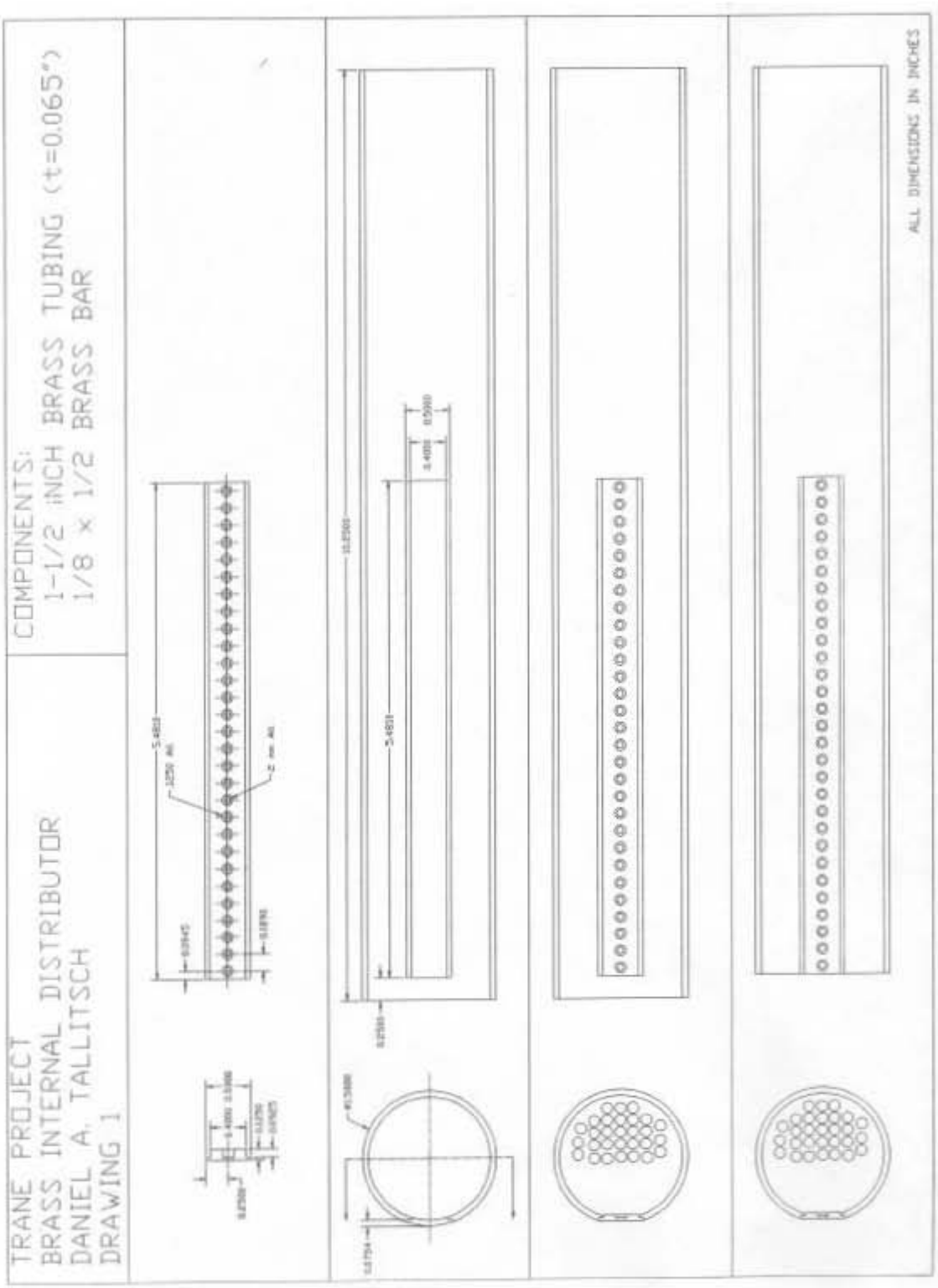

Figure 3.6 Detailed drawing of custom distributor header and orifice plate.

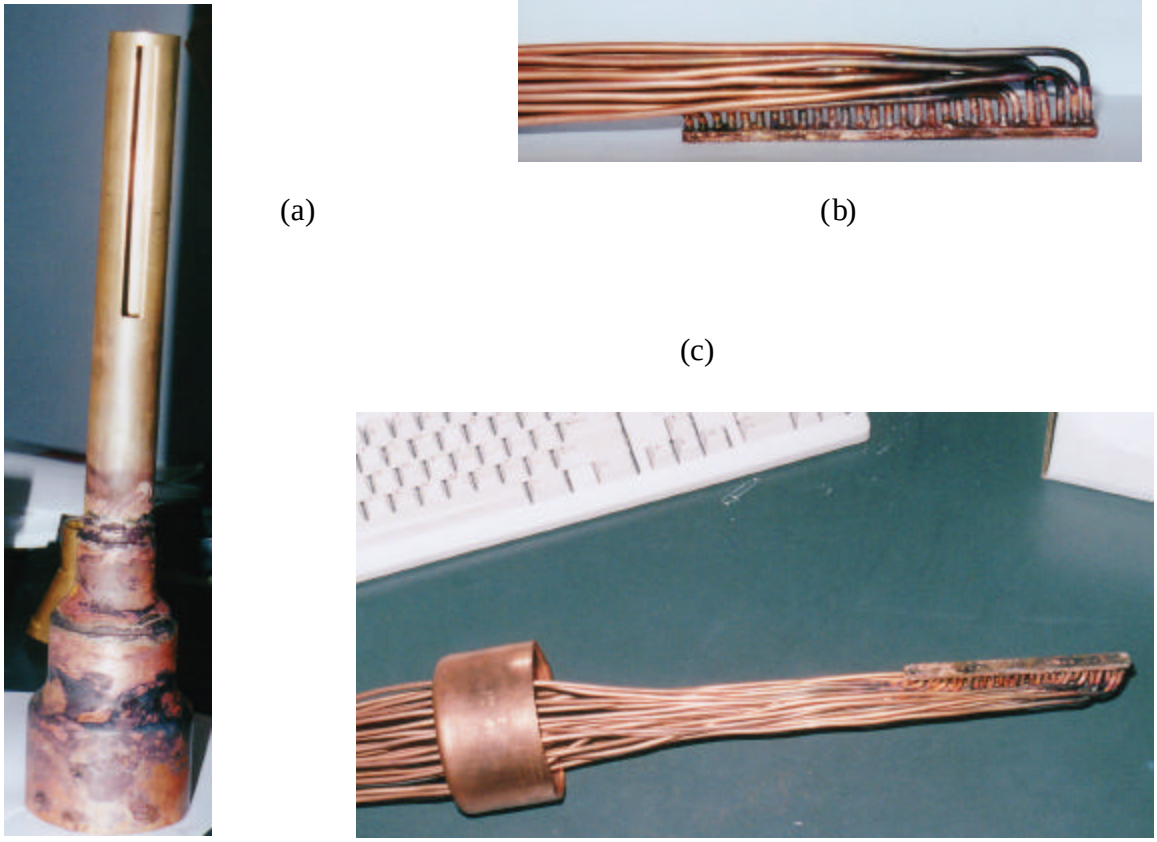

Figure 3.7 (a) Distributor header during assembly (b) Orifice plate with tubes inserted (c) Orifice plate with tubes fed through and brazed to endcap

3.2. Instrumentation and Calibration

All instrumentation shown in the following table were calibrated for this investigation. Pressure transducers and mass flow meters were new prior to use and, therefore, the manufacturers calibration was used.

All thermocouples were calibrated simultaneously using a vacuum insulated container. Three temperature regimes were used: 0°C, 23°C and 50°C. The water temperature was allowed to stabilize for approximately three hours before calibration was performed. The thermocouples were bound together such that each thermocouple would measure the temperature in the same area of the container. Data was acquired through the data acquisition system and PC for ten minutes with an interval of one second. The temperature was also measured using a calibrated thermometer once at the beginning and once at the end of the calibration period. The data acquired through the PC was averaged and plotted versus the average of the thermometer measurements. A best fit curve for these data points was obtained and used for further analysis. Through calibration, we believe the accuracy of the thermocouples to be approximately 0.1°C. Calibration curves can be found in Appendix C.

Table 3.2 List of instrumentation

Instrument	Parameter	Description
Thermocouples	Type	T copper – constantane
	Wire	special limits of error
	Accuracy	±0.5 °C or 0.4% (±0.1 after calibration)
Pressure Transducer 1	Sensotec	Model THE/3883-07TJA
(Suction Line)	Range	0-200 psia, 0-5V
	Error	±0.1% full scale
Pressure Transducer 2	Sensotec	Model THE/3883-06TJA
(Before Expansion Valve)	Range	0-500 psia, 0-5V
	Error	±0.1% full scale
Pressure Transducer 3	Setra	model C230
(dP of Evaporator)	Range	0-2 psid, 4-20 mA
	Error	±0.25% full scale
Refrigerant Mass Flow	Micro Motion	model DS025
(After Receiver)	Transmitter model no.	model RFT9712 Field-Mount
	Range	0-100g/s, 4-20 mA
	Accuracy	±0.1%
Water Mass Flow	Micro Motion	Model CMF050
(After Evaporator)	Transmitter model no.	model RFT9739
	Range	0-125 lb./min, 4-20 mA
	Accuracy	±0.1%
Watt Transducer	Ohio Semitronics	Model GW5
	Accuracy	±0.2%

3.3. Data Acquisition

The data acquisition system consists of a Gateway 386 computer, a Cambell Scientific AM416 Relay Multiplexer, and a Cambell Scientific 21X Micrologger. All data is acquired though the multiplexer and micrologger and sent to the computer via RS 232 connection.

3.4. Gas Chromatograph Description

The gas chromatograph used in this investigation was a Perkins Elmer Autosystem GC equipped with a thermal conductivity detector (TCD). This detector consisted of dual channels which measures the difference in thermal conductivity between hydrogen carrier gas flowing through a reference channel and hydrogen carrier gas plus the sample through an analytical channel. Error of the refrigerant composition measurements was experimentally determined as described in Section 9.0.

Chapter 4.0. Experimental Procedure

Three different compact brazed plate evaporators, varying in distribution method and size, were used in this study. Main dimensions of each evaporator are shown in Table 4.1. The evaporators A, B, and C were manufactured by SWEP as type B15X40, B45X60, and V45X60, nominally sized at 9, 60, and 60kW, respectively. All three evaporators are oven brazed with steel herringbone embossed plates where pattern is reversed on every other plate so that the ridges on adjacent plates intersect forming a lattice of contact points. Heat exchanger (HX) C is identical to HX B with exception to an internal distributor having 2 mm orifices directed upward in each refrigerant channel.

Table 4.1 Basic dimensions of evaporators used in study

Parameter	HX A	HX B	HX C
SWEP Model Number	B15X40	B45X60	V45X60
a [mm]	466	524	524
b [mm]	72	241	241
c [mm]	29	29	456
d [mm]	40	174	174
e [mm]	99	151	151
Total heat transfer area [m^2]	1.368	7.424	7.424
Channel volume [l]	0.969	5.452	5.452
Refrigerant channels	19	29	29
Nominal Capacity [tons]	3	20	20

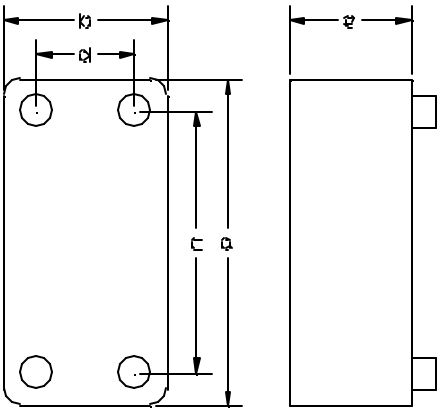

The experiment matrix and operating conditions are shown in Table 4.2. The mass flow rate was varied between 30 and 60 grams per second in all evaporators with both refrigerants. The resulting refrigerant mass flux in HX A was between 10 and 20 kg/m^2-s. In HX B and C, the mass flux was between 2 and 4 kg/m^2-s due to the greater total cross sectional area of the refrigerant channels.

The refrigerant exit temperature was set at approximately 11.5°C for experiments 1, 2, 3 and 5. This results in approximately 9°C of superheat for R-22 and 7°C for R-407c. The underlying reason for this high superheat was to obtain a stable signal at the evaporator exit. A stable signal is important in applications for the proper functioning of the thermostatic expansion valve. Furthermore, a stable signal is important during testing to obtain repeatable conditions. The stability issue is addressed in more details in Section 6.1. During Experiment 4 and 6, the refrigerant quality at the evaporator exit was maintained between 0.95 and 1.0.

Table 4.2 Experiment matrix

Experiment Series	Refrigerant	Evaporator Model	Distributor	Refrigerant Flow Direction	Refrigerant Outlet Condition
1	R-22 R-407c	HX A	No	Up	Superheated
2	R-22 R-407c	HX B	No	Up	Superheated
3	R-22 R-407c	HX C	Yes – SWEP Manufactured	Up	Superheated
4	R-22 R-407c	HX C	Yes – SWEP Manufactured	Up	Saturated Vapor
5	R-22 R-407c	HX B	Yes – See Section 3.1.4	Down	Superheated
6	R-22 R-407c	HX B	Yes – See Section 3.1.4	Down	Saturated Vapor

Experiments were taken for two refrigerant liquid subcooled temperatures: 15.6°C and 32.2°C. This corresponds to an inlet quality of 0.08 and 0.18 for R-22 and an inlet quality of 0.10 and 0.21 for R-407c. Experiments 4 through 6 were conducted only at a subcooled temperature of 32.2°C.

Refrigerant pressure at the compressor suction is held constant at 535 kPa in all experiments. It results in a slight variation of inlet refrigerant temperature for R-22 experiments and both inlet and exit temperatures for R407c experiments.

During operation with a superheated refrigerant at the evaporator exit, the inlet water temperature was held constant at 12°C. When operating with a saturated refrigerant at the evaporator exit, the inlet water temperature was varied to obtain the desired refrigerant quality. In both cases, the water flow rate was adjusted to give a water temperature difference of 5°C. Approach taken implicitly assumes that the change of refrigerant side heat transfer coefficient is proportional to the change in water side heat transfer coefficient.

The oil used in this investigation for both R-22 and R-407c was polyol-ester oil (POE) with an ISO viscosity grade of 22 (Mobil product number 60105-4). Mass concentration of oil in circulating refrigerant was measured to be between 0.2 and 1.7% for both refrigerants. Later experiments performed using HX A in ACRC at the University of Illinois with R-22 and mineral oil showed identical thermal performance, indicating that the oil does not have significant effect on R-22 thermal performance.

4.1. Composition Measurement Procedure

One of the objectives was to measure the composition of R-407c at different stages during experiments. Before experiment runs were conducted and while the system was not in operation, composition measurements were taken of liquid from the receiver and of vapor from the suction line. These were taken to insure composition changes did not occur throughout the testing period due to unforeseen reasons such as leaks in the system. During experiment runs, vapor samples were taken and analyzed from the suction line to determine the circulating composition and, when possible, liquid samples

from the bottom of the evaporator to determine the local composition of stagnating liquid. Samples were acquired from start-up to the point the system reaches desired test conditions. Composition experiments were completed at low and a high mass flux for each subcooled temperature.

4.1.1. Liquid Samples from Receiver

Liquid samples are acquired using a 300 cc cylinder as shown schematically in Figure 4.1.

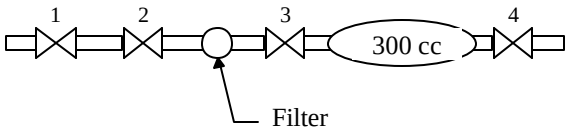

Figure 4.1 Test apparatus used to acquire refrigerant samples for composition analysis

The first step is connecting the test apparatus on the left end to a valve which supplies liquid refrigerant from the bottom of the receiver. Before a sample is taken, the sampling apparatus is evacuated using a vacuum pump connected on the right side. A sample is then acquired between valves 1 and 2. The apparatus is then removed from the chiller. Next, valve 2 is slowly opened evaporating the refrigerant. The sample flows through the filter removing the oil. At room temperature, all refrigerant will be superheated vapor. As an added measure, the entire test apparatus is heated to ensure complete evaporation of refrigerant. The final pressure in the test apparatus is approximately 60 psi providing sufficient vapor for testing with the gas chromatograph.

4.1.2. Vapor Samples from Suction Line

Vapor samples are acquired from a schrader valve on the suction line after the mixer or heater, depending on which is being used. In a manner similar to above, the test apparatus shown in Figure 4.1 is first connected to the valve and then evacuated. However, it is not necessary to trap refrigerant between valves 1 and 2 but the filter is still used to remove oil. The test apparatus is filled until reaching a pressure between 30 and 60 psi.

4.2. Oil Composition Measurement Procedure

Oil composition measurements were taken using two methods: one following ASHRAE Standard 41.4 (1984), and one using an impactor as described below. Both methods gave approximately equal results.

The apparatus shown in the following figure was used for oil composition measurements.

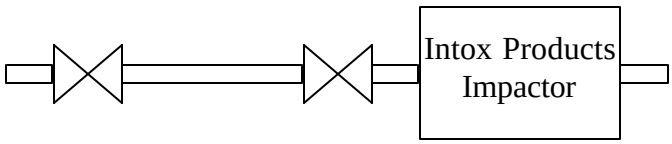

Figure 4.2 Test apparatus used to measure oil composition

First, the apparatus is connected to the compressor bypass liquid line and is evacuated using a vacuum pump. A liquid sample of circulating refrigerant-oil mixture is trapped between the two valves. The apparatus, excluding the impactor, is weighed before and after taking the sample to determine the

refrigerant-oil weight. The sample section is connected to the impactor and is heated to increase the pressure. Then, the valve is opened introducing the refrigerant to the impactor. Liquid refrigerant blows through the impactor, evaporates, and escapes to the atmosphere at the exit of the impactor. Oil is filtered out of the refrigerant by means of seven stages in the imp actor. In each stage, the oil mixture passes through a fiberglass filter and is then directed to an orifice that accelerates the mixture and also directs the refrigerant to the next filter stage. Each succeeding stage has a smaller orifice.

The impactor stages are weighed individually before and after filtering to determine the weight of the oil. Oil composition is calculated by dividing the weight of the oil by the weight of the sample.

4.3. Oil Hold-up Measurement Procedure

It was discovered during this investigation that a significant amount of oil is held up in the evaporator after shut down. It was desired to quantify the mass of oil.

After experiment runs were completed, and when possible, the evaporator was isolated with valves immediately after shut down. The evaporator was evacuated slowly, being careful not to remove any oil. After evacuation, all oil was drained from the evaporator and oil weight was measured.

Chapter 5.0. Experimental Results

5.1. Objective of Study

The objective of this investigation is to determine whether fractionation occurs in brazed plate heat exchangers (BPHE) with refrigerant R-407c especially when operating with lower mass velocities. This investigation evaluates the behavior of BPHE operating in different configurations and over a broader range of operating parameters than usual. This included operating with refrigerant flow in the upward and downward flow directions, with and without superheat, with and without refrigerant distributor and with varying evaporator inlet quality.

The approach taken in this investigation was to evaluate the thermal performance of R-407c in comparison to R-22 for the various experiment conditions and evaporator configurations discussed in detail in Section 4.0. In addition, refrigerant samples were taken for composition analysis to determine the magnitude of fractionation, relating it to the differences observed in thermal behavior.

Data collected allowed for the determination of log mean temperature difference (LMTD) and overall heat transfer coefficient (U-value). Use of U-value based on LMTD approach is associated with numerous assumptions and cannot catch the details in heat transfer differences. Comparisons are made between refrigerants based upon the calculated U-value. This approach for comparison is based from a system point of view. This investigation was not a study of local heat transfer but, rather, a study of heat exchangers. This justifies the use of LMTD and U-value to compare two different refrigerants and various evaporator configurations. Further, U-values are based upon a constant temperature difference on the water side and are not intended to be used for design.

Experiment runs in the range 50% to 100% of maximum mass flow rate were conducted with evaporator and compressor bypass. Refrigerant samples were taken for composition analysis in order to detect fractionation at two locations: the rear bottom of the evaporator inlet header (designated as "evaporator sample") and the suction line downstream of a mixer (designated as "circulating sample"). The composition of the evaporator sample is representative of stagnating liquid at the bottom of the evaporator while the circulating sample is representative of the majority of the refrigerant charge located in the suction line, receiver and liquid lines. Conclusions regarding the degree of fractionation occuring will be made based upon the circulating samples, since there is no assurance of what was sampled from the evaporator. The evaporator sample was taken from a tube inserted into the evaporator header. The tube was placed near the back bottom of the evaporator header. However, the exact location of the tube and the conditions present in the evaporator was not known. Despite this, some useful knowledge may be gained from the evaporator sample results.

5.2. Establishing the Baseline (Experiment 1)

5.2.1. Objective of Experiment 1

The objective of Experiment 1 is to evaluate the difference between R-22 and R-407c in the range 50% to 100% of typical design capacity (12 kW) using an evaporator sized for 100% capacity (HX A).

This establishes a thermal basis for comparison with other evaporator configurations and/or experiment conditions.

It was expected that fractionation and maldistribution would be minimized under these conditions allowing a fair comparison between refrigerants. This is reasonable since the high velocities and turbulence present in the heat exchanger would carry liquid upward through the evaporator refrigerant channels and prevent a liquid pool from forming in the inlet header and, thus, prevent preferential evaporation (fractionation).

5.2.2. Results of Experiment 1

Figure 5.1 compares the thermal performance of R-22 and R-407c for the baseline experiment (Experiment 1). Refrigerants R-22 and R-407c perform essentially the same under these conditions; U-values for both refrigerants are approximately equal throughout the range of mass flux (10-25 kg/m^2-s) at both subcooled temperatures. However, at a subcooled temperature of 15.6°C, U-values are slightly greater (up to ~15% greater) for R-22 than R-407c in the approximate range 50% to 75% of maximum mass flux. The thermal performance trends observed through this experiment establish the baseline for further experiments.

Figures 5.2 through 5.4 and Table 5.1 show the change in refrigerant composition of samples from the two locations from initial start-up until steady state was reached for 10 kg/m^2-s and 20 kg/m^2-s mass flux with a subcooled temperature of 32.2°C. A case was also evaluated with 20 kg/m^2-s mass flux and subcooled temperature of 15.6°C. As expected, all three figures show a greater composition of R-134a in the evaporator sample than in the circulating sample. Likewise, a greater fraction of R-32 and R-125 are found in the circulating refrigerant sample. While the changes in composition are small (R-134a composition shift is approximately 0% to -1.2% for circulating samples and 0.5% to 3.6% for evaporator samples), the preferential evaporation that characterizes fractionation is demonstrated. Unfortunately, data is not available at low mass flux with 15.6°C subcooled temperature. However, fractionation is minimal as expected for all other cases as postulated above. Refer to Table 5.1 for exact composition shift seen from initial start-up to steady state.

One may notice the appearance of greater composition shift occurring in the evaporator sample with 32.2°C subcooled temperature versus 15.6°C by comparing Figure 5.3 with 5.4. R-134a composition shift is 3.6% for subcooled temperature of 32.2°C (Figure 5.3) while composition shift is 0.5% for subcooled temperature of 15.6°C. It is known that a two-phase zeotropic mixture, such as R-407c, with a higher quality has a greater composition of the least volatile (lower pressure) component in the saturated liquid, which in this case is R-134a. Therefore, the composition of saturated liquid refrigerant R-407c entering the evaporator should have a higher composition of R-134a for higher inlet quality cases. This explains why a larger shift in composition is seen in the evaporator sample for subcooled temperature of 32.2°C (inlet quality of 0.21) than for subcooled temperature of 15.6°C (0.10). A comparison of circulating samples for these two cases show similar results (-1.2% for subcooled temperature of 32.2°C and -0.8% for 15.6°C).

An unusual result is observed by comparing Figure 5.2 with 5.3. It appears that greater composition shift occurs with greater mass flux. For example, R-134a composition shift is 0% in the circulating sample at low mass flux (Figure 5.2) while R-134a composition shift for the high mass flux case (Figure 5.3) is -1.2%. R-134a composition shift in the evaporator sample was 1.6% for the low mass flux case and 3.6% for the high mass flux case. The exact opposite was expected; i.e. composition shift was expected to be less for the high mass flux case. This effect could be related to the degree of oil hold-up seen in the evaporator at low mass flow rates, which is discussed further in Section 6.4.

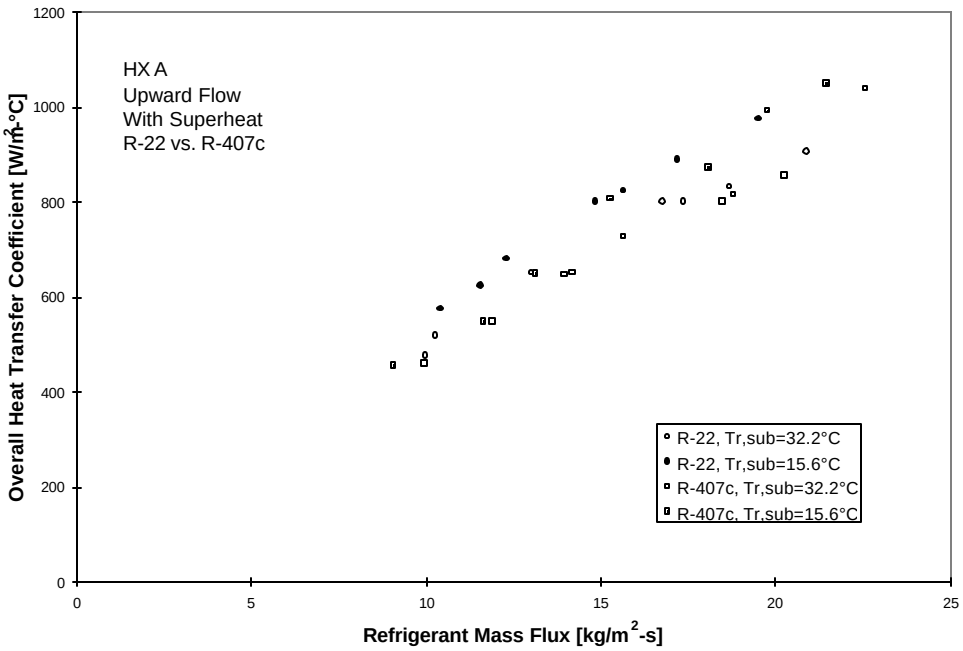

Figure 5.1 Experiment 1 - Comparison of Calculated Overall Heat Transfer Coefficient of R-22 and R-407c for Baseline Tests

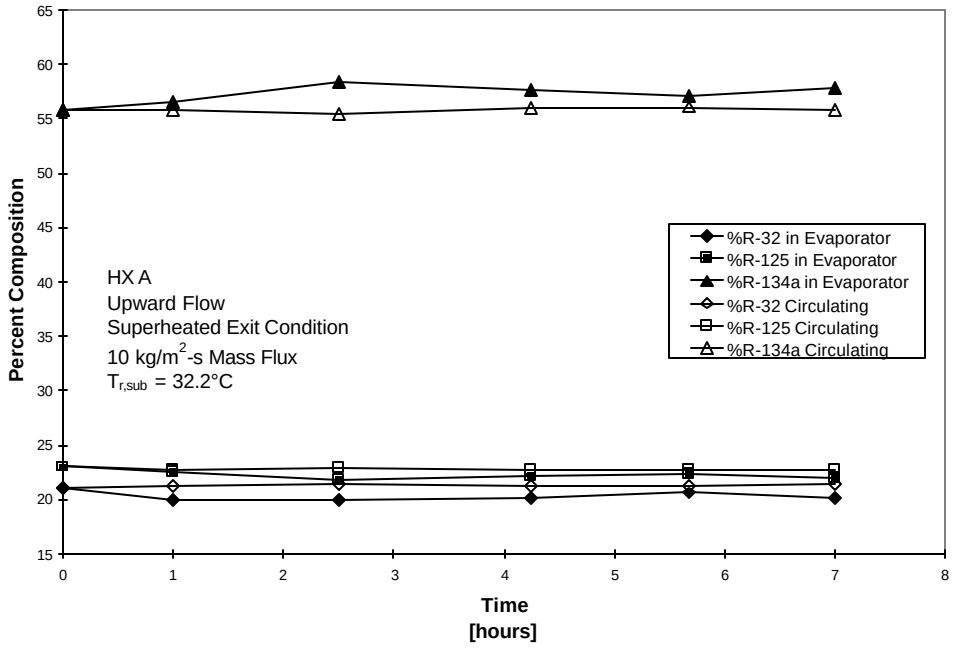

Figure 5.2 Experiment 1 - Baseline composition change of circulating and stagnating refrigerant at minimum flow rate with refrigerant subcooled to 32.2°C

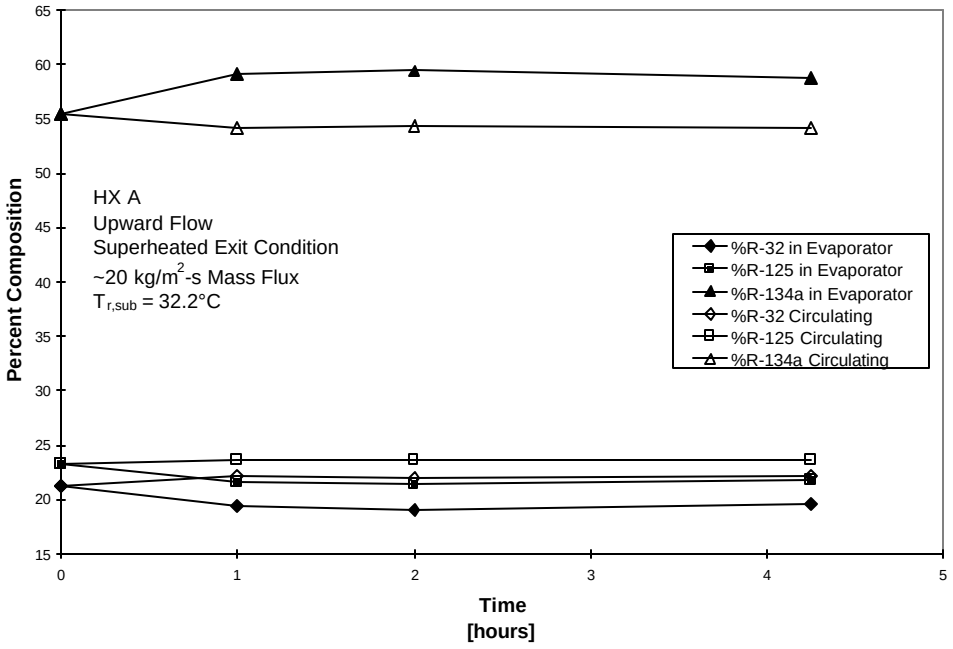

Figure 5.3 Experiment 1 - Baseline composition change of circulating and stagnating refrigerant at maximum flow rate with refrigerant subcooled to 32.2°C

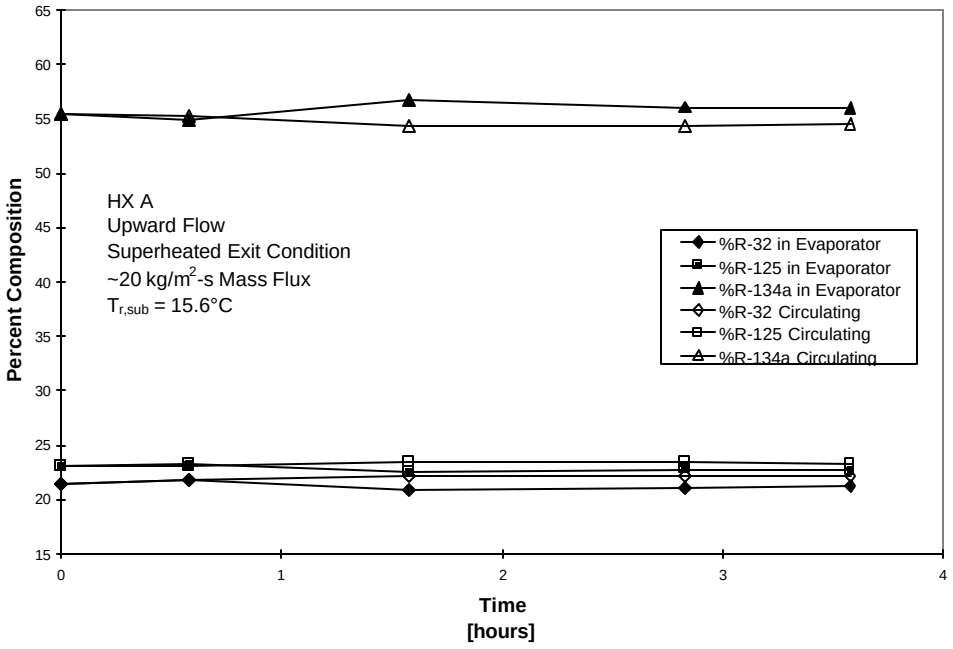

Figure 5.4 Experiment 1 - Baseline composition change of circulating and stagnating refrigerant at maximum flow rate with refrigerant subcooled to 15.6°C

5.3. In Search of Fractionation and Maldistribution (Experiment 2)

5.3.1. Objective of Experiment 2

The objective of this experiment is to explore the effect of mass flux on fractionation and maldistribution. To simulate significantly reduced compressor capacity, the evaporator used in Experiment 1 was replaced with a much larger heat exchanger, HX B. This heat exchanger is exactly the same type as HX A, just larger (design capacity of 60 kW compared to 12 kW for HX A). With the same compressor, the range of mass flow rate used in this investigation corresponds to approximately 7.5% to 15% of the heat exchanger design mass flux. The results of this experiment has some practical use since requirements for higher EER and compactness are driving technological innovation towards generously-sized heat exchangers, requiring operation with lower velocities/mass flow rates than the heat exchangers were designed for. Note, however, that the reduction in mass flux is exaggerated in this evaluation intentionally to present a worse case scenario.

With such low mass flux (~2-5 kg/m^2-s compared to ~10-20 kg/m^2-s for baseline experiment), the performance of R-407c is expected to be degraded with respect to R-22 performance when compared to Experiment 1 results due to fractionation. The large inlet header of HX B and the low inlet velocities provides an environment conductive to pooling of liquid refrigerant and preferential evaporation. Maldistribution is expected since the mass flux is significantly lower than the evaporator design. It is not known whether maldistribution has an effect on the magnitude of fractionation.

Also at issue in this experiment is the effect of inlet quality on fractionation. At 15.6°C subcooled temperature (inlet quality of 0.08 for R-22 and 0.10 for R-407c), evaporator inlet quality is significantly lower than at 32.2°C (inlet quality of 0.18 for R-22 and 0.21 for R-407c). Since two-phase fluid with lower quality is composed of a larger fraction of liquid, the fluid velocity at the inlet of the evaporator at the same mass flux is lower for the 15.6°C subcooled temperature cases increasing the likelyhood of liquid refrigerant pooling in the evaporator inlet header. It is postulated that with increased subcooling/decreased inlet quality, the reduction of R-407c performance when compared to R-22 will be of greater magnitude, i.e. fractionation is expected to be more significant at 15.6°C.

5.3.2. Results of Experiment 2

With the low mass flux present in the large evaporator HX B, U-values for R-22 are much reduced compared to higher mass fluxes seen in Experiment 1 as shown in Figure 5.5. The linear trend in U-value between HX A and B demonstrates that heat exchanger similarity was maintained between Experiment 1 and 2. R-407c U-values are significantly less than R-22 in the entire range of mass flux (2-5 kg/m^2-s) at both subcooled temperatures, as shown in Figure 5.6. Performance difference between R-407c and R-22 is approximately 15% with 15.6°C subcooled temperature and approximately 8% with 32.2°C subcooled temperature. This could indicate a slight influence of inlet quality on fractionation or could simply be related to the thermophysical differences between R-22 and R-407c.

Based upon the degradation in R-407c thermal performance, it is expected that the refrigerant composition analyses will show increased composition shift when compared to Experiment 1 results. Experiment 2 composition results for mass flux of 2 kg/m^2-s and 4 kg/m^2-s and subcooled temperatures of

32.2°C and 15.6°C are shown in Figures 5.7 through 5.10 and Table 5.1. Comparison of these figures with the corresponding figure from Experiment 1 (Figure 5.7 with 5.2, 5.8 with 5.3, etc.), shows that composition shift is slightly greater for the larger evaporator HX B (R-134a composition shift is approximately -1% to -4% for circulating refrigerant samples and 3% to 6% for evaporator samples). For example, R-134a composition shift is -1.1% in the circulating sample and 3.3% in the evaporator sample for Experiment 2 at 2 kg/m^2-s mass flux and 32.2°C subcooled temperature (Figure 5.7). In comparison, R-134a composition shift is 0% in the circulating sample and 1.6% in the evaporator sample for Experiment 1 at 10 kg/m^2-s mass flux and 32.2°C subcooled temperature (Figure 5.2). Similar conclusions are made when comparing other representative figures. However, the magnitude of composition shift is still negligible for Experiment 2; much greater fractionation was expected.

Comparison of Figures 5.7 with 5.9 and Figure 5.8 with 5.10 reveals that subcooling has a slight effect on fractionation. Composition shift of R-134a in the circulating sample is -1.1% at low mass flux and 32.2°C subcooling temperature and -1.8% at high mass flux and 32.2°C (Figure 5.7 and 5.8). In comparison, R-134a composition shift in the circulating sample is -2.2% at low mass flux and 15.6°C subcooled temperature and is -4.0% at high mass flux and 15.6°C (Figure 5.9 and 5.10). The composition shift in the circulating samples doubles with increased subcooling for the high and low mass flux cases. This is consistent with the greater degradation in R-407c performance at 15.6°C subcooled temperature versus 32.2°C, indicating that greater subcooling increases fractionation. As seen in Table 5.1, the evaporator sample shows a higher concentration shift for R-134a with 32.2°C at the same mass flux, similar to what is seen in Experiment 1. As discussed in Experiment 1, this is attributed to the inlet quality and the properties of zeotropic refrigerants.

Also seen in Experiment 1, greater composition shift is seen at higher mass flux, opposite of expectations. R-134a composition shift is -1.1% for the circulating sample and 3.3% for the evaporator sample at low mass flux (Figure 5.7) while R-134a composition shift for high mass flux is -1.8% for the circulating sample and 5.9% for the evaporator sample (Figure 5.8).

To summarize, the figures presented for Experiment 2 show that reduced mass flux does increase fractionation and does reduce R-407c performance when compared to R-22. However, the decrease in R-407c performance seen in these results does not fall to a level that could be considered degraded. Further, increased subcooling (decreased inlet quality) slightly increases fractionation and reduces R-407c performance with respect to R-22 at similar conditions.

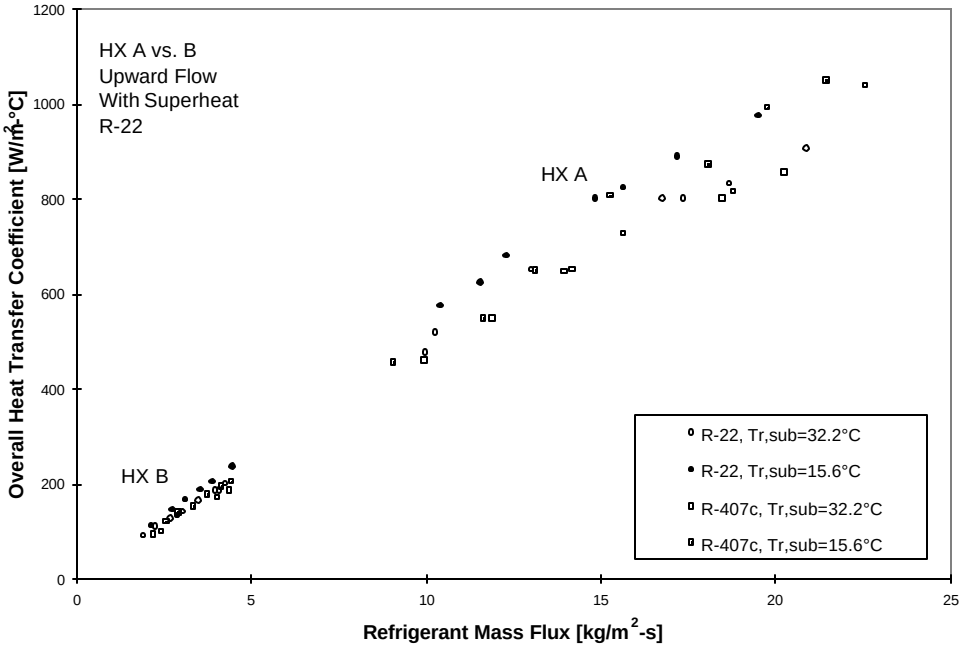

Figure 5.5 Experiment 1 vs. 2 - Comparison of Calculated Overall Heat Transfer Coefficient in large and small evaporator with R-22

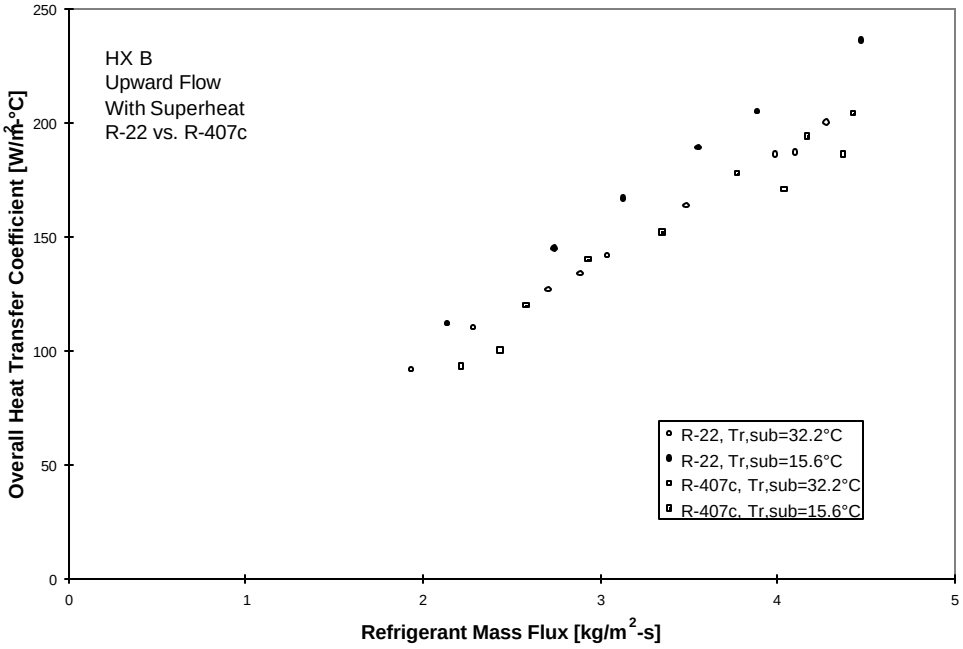

Figure 5.6 Experiment 2 - Comparison of Calculated Overall Heat Transfer Coefficient of R-22 and R-407c

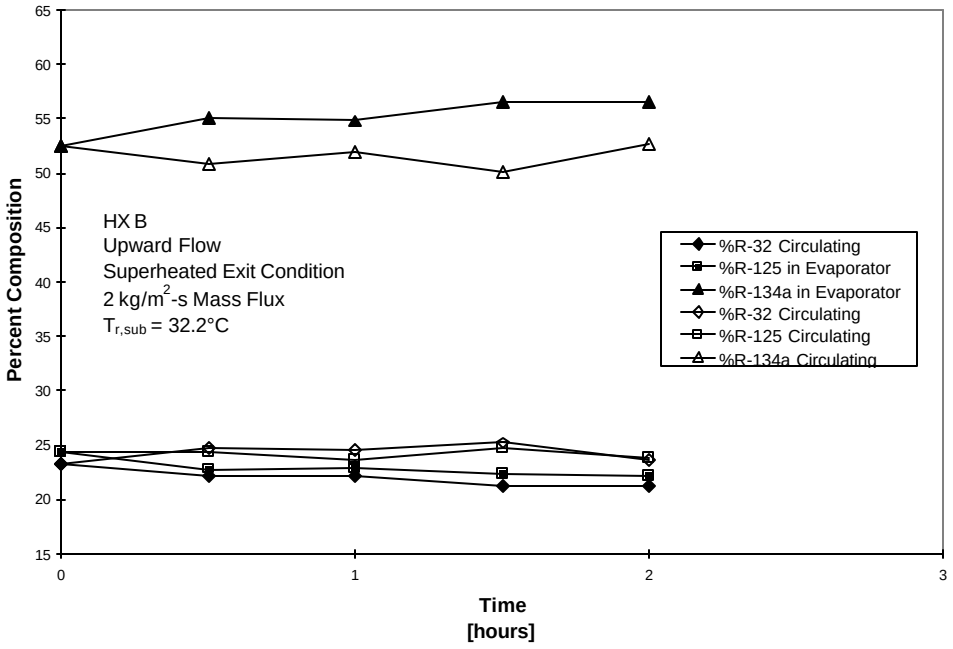

Figure 5.7 Experiment 2 - Composition change of circulating and stagnating refrigerant at minimum flow rate with refrigerant subcooled to 32.2°C

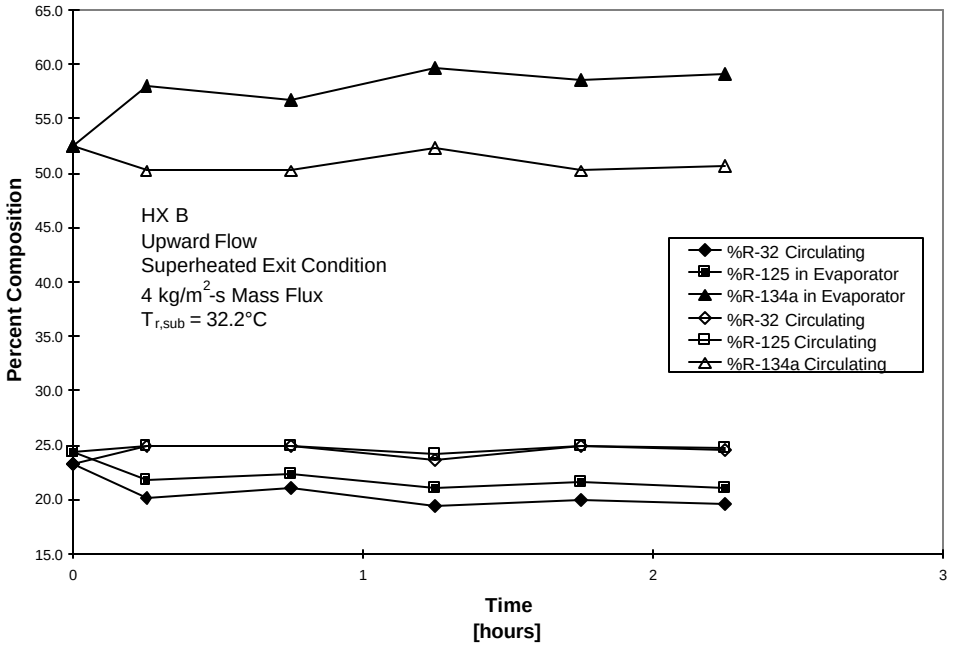

Figure 5.8 Experiment 2 - Composition change of circulating and stagnating refrigerant at maximum flow rate with refrigerant subcooled to 32.2°C

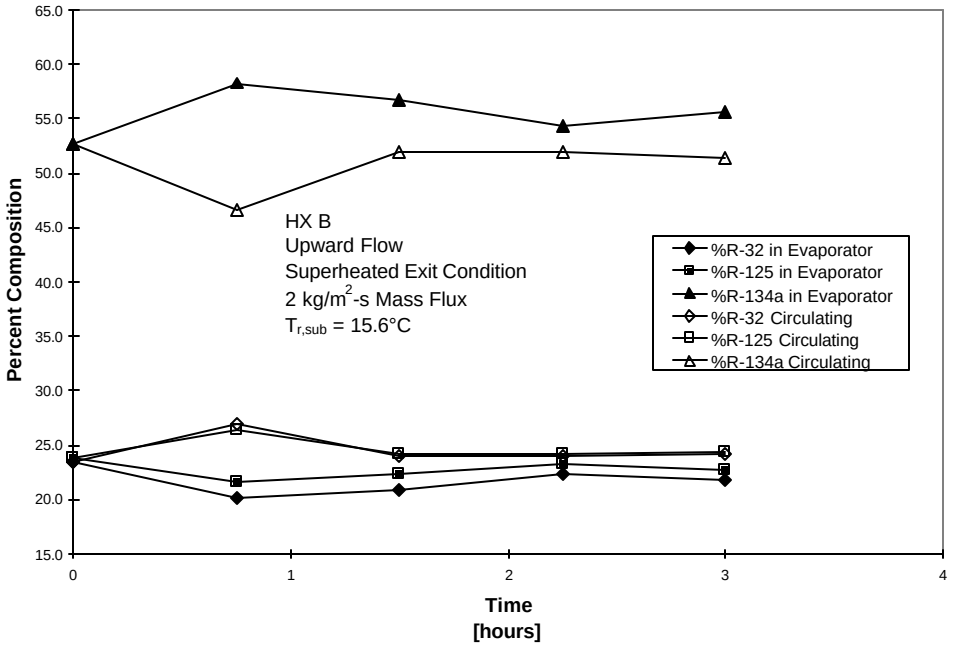

Figure 5.9 Experiment 2 - Composition change of circulating and stagnating refrigerant at minimum flow rate with refrigerant subcooled to 15.6°C

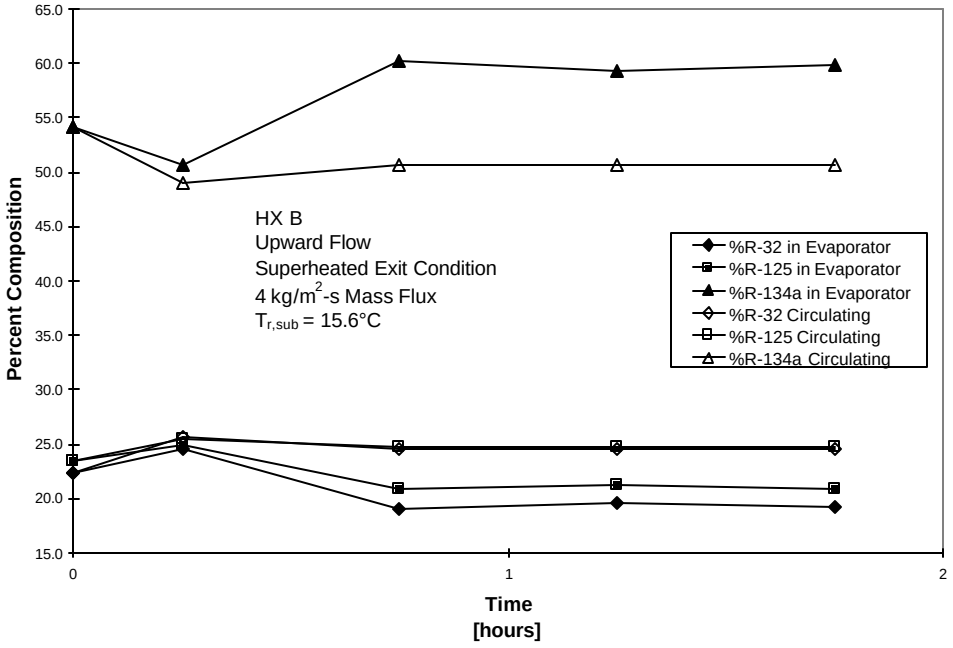

Figure 5.10 Experiment 2 - Composition change of circulating and stagnating refrigerant at maximum flow rate with refrigerant subcooled to 15.6°C

5.4. In Search of Fractionation, Reducing Potential Effects of Maldistribution (Experiment 3)

5.4.1. Objective of Experiment 3

The evaporator used in Experiment 3, HX C, incorporates a distributor internal to the refrigerant inlet header but is identical in all other respects to HX B, the evaporator used in Experiment 2. The objective of the replacement was to significantly reduce or eliminate the effects of maldistribution, if it exists, to facilitate detection of fractionation. Note that the addition of the distributor made the acquisition of refrigerant samples from the inlet header of the evaporator useless. Therefore, only circulating composition results were taken.

With the reduction or elimination of maldistribution, the performance of R-22 and R-407c should improve when compared with performance in Experiment 2 due to improved wetting of the heat exchanger surfaces. This experiment will also determine the effect maldistribution has on the magnitude of fractionation by comparing the difference between R-22 and R-407c performance of both this experiment and Experiment 2.

5.4.2. Results of Experiment 3

Figure 5.11 shows that, with the exception of a few outliers, R-22 performance in HX C is essentially the same as in HX B. This indicates that either distribution was not improved by the addition of a distributor or maldistribution is minimal in both evaporators. Observation of Figure 5.5, which compares the results of Experiment 1 and 2, shows a linear trend of U-value with mass flux. This suggests that the likely case is that maldistribution was not an issue in this investigation. However, Figure 5.12 shows a slight improvement of R-407c performance with the distributor (HX C) versus without (HX B), in the range of, perhaps, 2-3%. However, the magnitude of this difference between Experiment 2 and 3 results are within the error expected for this investigation. As such, composition analysis for this experiment is expected to produce similar results as Experiment 2.

The refrigerant R-407c composition results are presented in Figures 5.13 through 5.16 and Table 5.1 at identical conditions as Experiment 2. As expected, comparison of corresponding figures from Experiment 2 and 3 shows that the magnitude of fractionation was essentially the same for both experiments. Composition shift of R-134a in the circulating sample ranged from -1.6% to -3.1% for HX C while the composition ranged from 1.1% to 4.0% for HX B. Comparison of corresponding cases from Experiment 2 and 3 indicates greater composition shift for HX C at 32.2°C and less composition shift for HX C at 15.6°C when compared to HX B. Further, composition shift is essentially the same at 15.6°C and 32.2°C for Experiment 3. With 32.2°C subcooled temperature, R-134a composition shift is -1.6% at low mass flux and -3.1% at high mass flux. With 15.6°C, R-134a composition shift is -1.8% at low mass flux and -3.0% at high mass flux. Previous results with HX B indicated that composition shift was greater with increased subcooling (decreased inlet quality). R-134a composition shift for Experiment 2 is -1.1% (32.2°C, low mass flux), -1.8% (32.2°C, high mass flux), -2.2% (15.6°C, low mass flux) and -4.0% (15.6°C, high mass flux). However, the composition shift seen in both Experiment 2 and 3 are relatively

small and much less than expected. This leads us to believe that the distributor has no significant effects on fractionation or maldistribution.

In summary, the addition of a refrigerant distributor had negligible effects on thermal performance and fractionation. The differences in fractionation and thermal performance between Experiment 2 and 3 are much less than expected. Further, the signs that maldistribution was occurring in Experiment 2 were not detected.

5.5 Influence of Saturated Evaporator Exit Condition (Experiment 4)

5.5.1. Objective of Experiment 4

The absence of more severe fractionation in Experiments 2 and 3 was unexpected and it was postulated that, perhaps, the high degree of superheat somehow masked the effects of fractionation and that the experiment conditions had somehow overcontrained the system. This condition is discussed further in Section 6.0. To remove this constraint, this experiment allows the water side inlet temperature to float, while maintaining a constant temperature drop, in order to achieve an average 0°C of superheat at the exit of the evaporator. The evaporator with internal distributor, HX C, was used to minimize maldistribution. Since it was established in Experiment 3 that varying subcooled temperature/inlet quality with HX C does not have a significant effect on fractionation in the range of mass flux tested, experiments at a subcooled temperature of 15.6°C were eliminated hereon out.

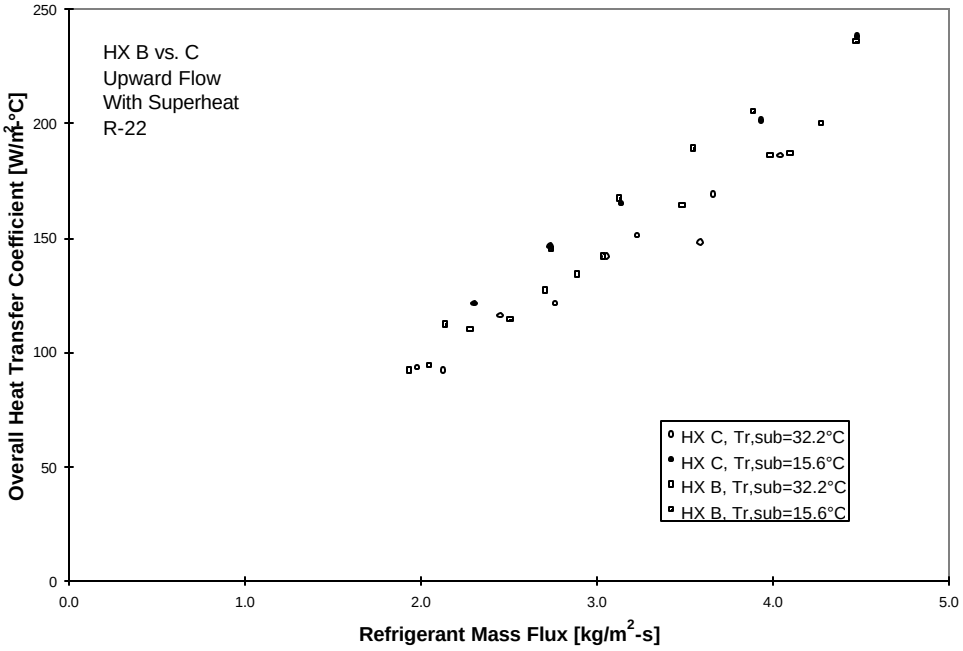

Figure 5.11 Experiment 2 vs. 3 - Comparison of Calculated Overall Heat Transfer Coefficient with and without a Distributor with R-22

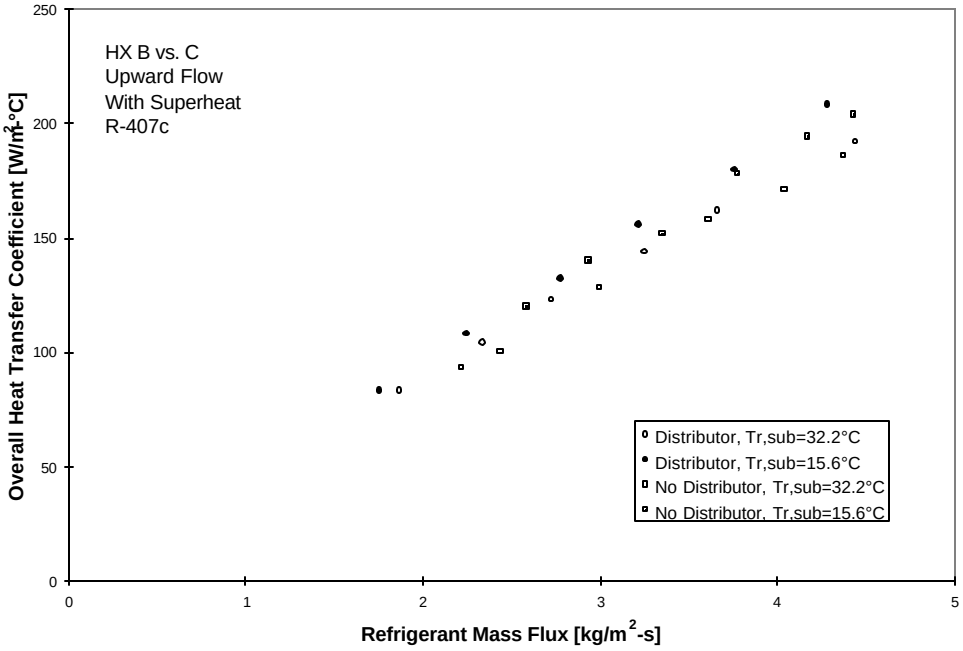

Figure 5.12 Experiment 2 vs. 3 - Comparison of Calculated Overall Heat Transfer Coefficient with and without a Distributor with R-407c

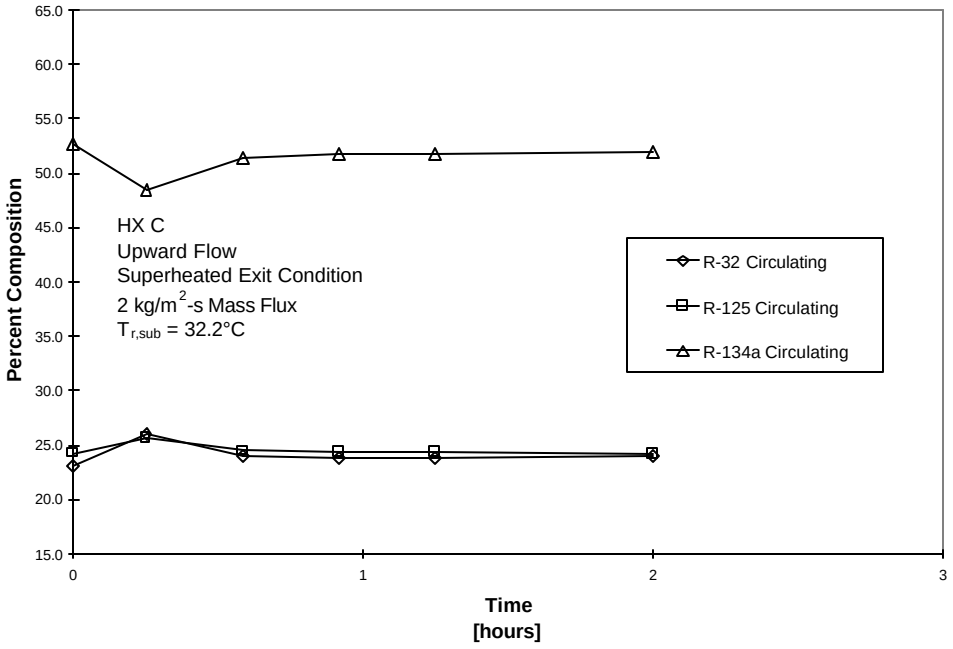

Figure 5.13 Experiment 3 - Composition change of circulating refrigerant at minimum flow rate with refrigerant subcooled to 32.2°C

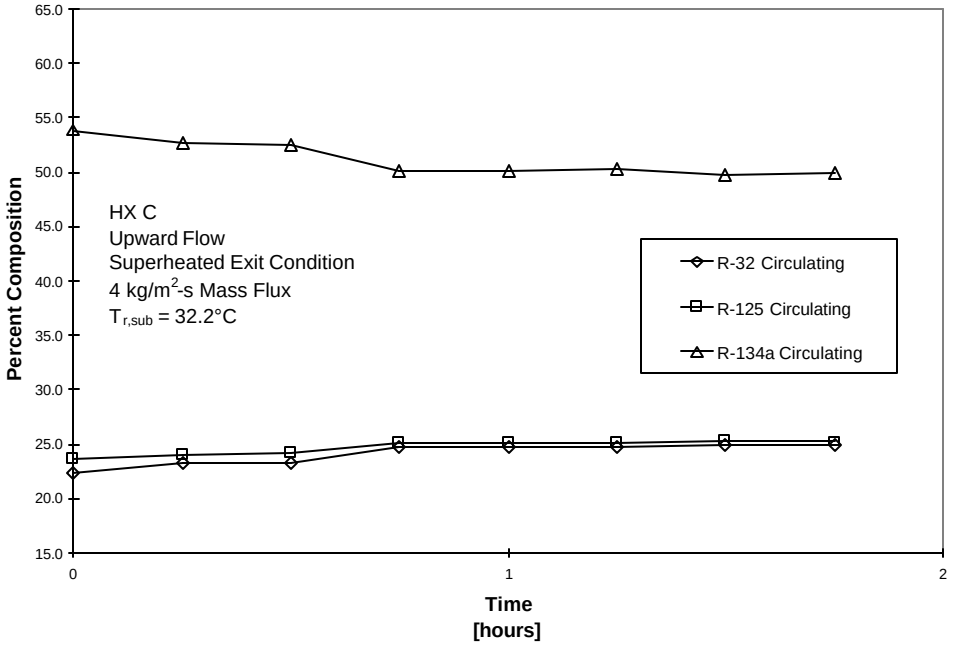

Figure 5.14 Experiment 3 - Composition change of circulating refrigerant at maximum flow rate with refrigerant subcooled to 32.2°C

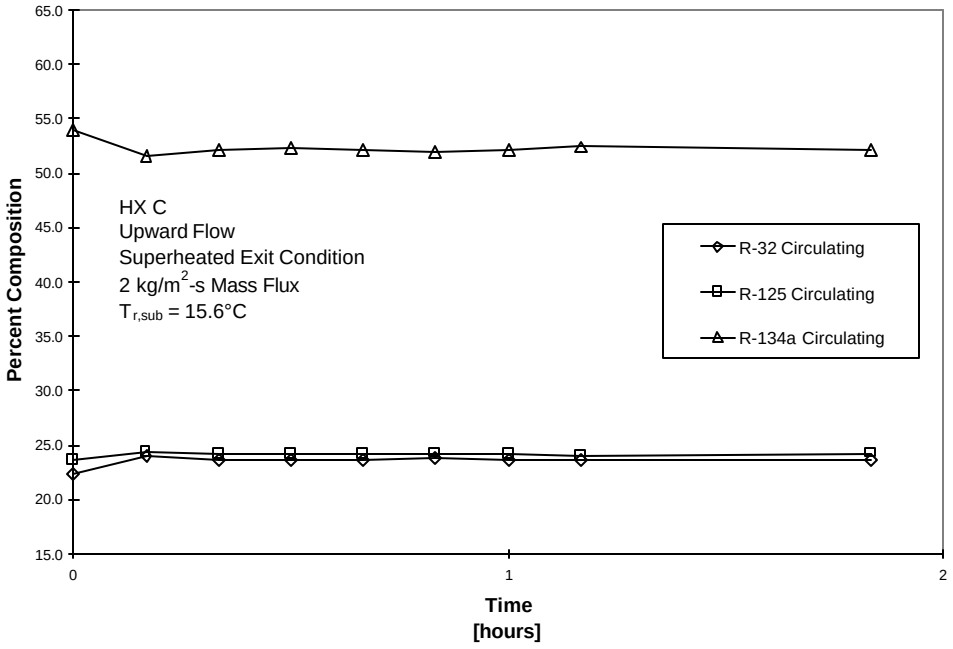

Figure 5.15 Experiment 3 - Composition change of circulating refrigerant at minimum flow rate with refrigerant subcooled to 15.6°C

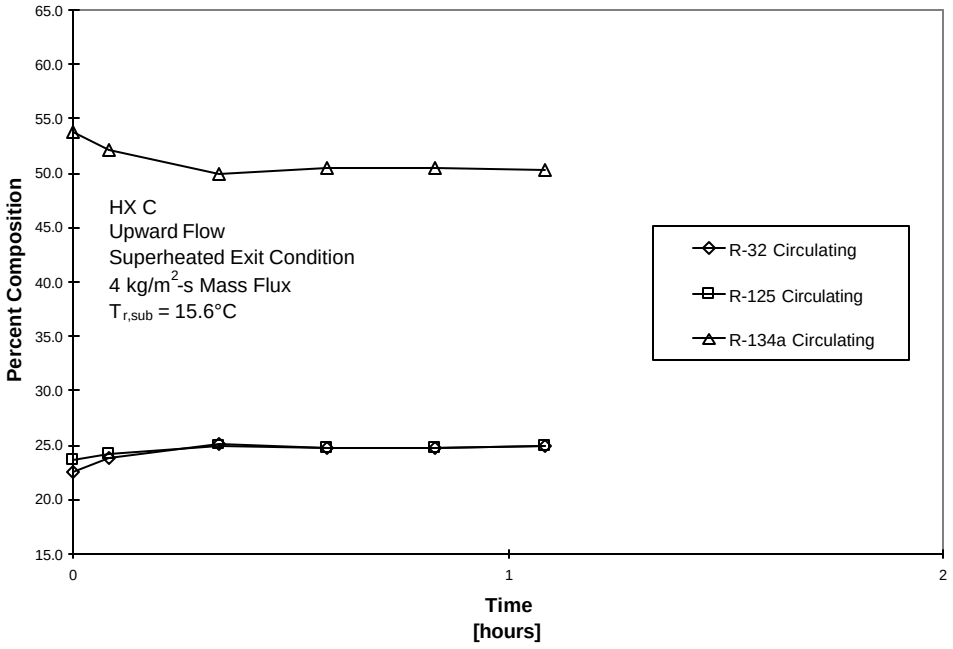

Figure 5.16 Experiment 3 - Composition change of circulating refrigerant at maximum flow rate with refrigerant subcooled to 15.6°C

It is expected that the capacity of the system will be reduced only slightly since the heat transfer associated with the superheated zone is negligible when compared to the total heat transfer. But, overall heat transfer coefficients are expected to increase for R-22 and R-407c since heat transfer in the refrigerant

channels will be, on the average, entirely two-phase. However, velocities internal to the evaporator will be lower, which could increase the likelyhood of liquid refrigerant pooling and fractionation. Further, more liquid refrigerant is present in the evaporator for this experiment since the entire evaporator is two-phase.

5.5.2. Results of Experiment 4

Figure 5.17, which compares the thermal performance of R-22 in Experiment 3 with Experiment 4, verifies expectations that U-values increase with reduction in superheat. The improvement in U-value by eliminating the superheated zone is on the order of 30% for R-22.

As discussed above, fractionation is expected to be worse with no superheat. Therefore, the increase in R-407c performance by reducing superheat is not expected to be as dramatic as R-22. However, Figure 5.18 shows that U-values for R-407c with no superheat are significantly greater (approximately 10%) than R-22, opposite of what was seen for cases with superheat (Figure 5.19). These results do not necessarily mean that fractionation has been reduced by eliminating superheat. The above results can be explained by observation refrigerant exit temperature and water inlet temperature. In Experiments 1 through 3, the refrigerant exit temperature was only slightly less than the inlet water temperature (difference of less than 1°C) indicating the presence of pinched evaporator exit conditions. Based upon this, one can conclude that R-407c two-phase heat transfer coefficient is greater than R-22, which was somehow masked in Experiments 1 through 3 due to pinched exit conditions. Since baseline Experiments were not performed with zero superheat, the composition analysis results should be used to determine the effect of superheat on fractionation.

As expected, Figures 5.20 and 5.21 and Table 5.1 show that the magnitude of fractionation increases due to the reduction in superheat. The composition shift of R-134a for this experiment is approximately -4.3% at low mass flux and -3.7% at high mass flux. Composition shift for the corresponding cases from Experiment 3 is -1.8% and -3.0%.

In Experiments 1 through 3, composition shift of R-134a in the circulating refrigerant was greater with greater mass flux, contrary to what was expected. However, this experiment shows the expected results of greater fractionation with lower mass flux.

In summary, the high degree of superheat seen in this investigation did not mask the effects of fractionation. Composition shift is still much less than expected and R-407c thermal performance degradation is not observed.

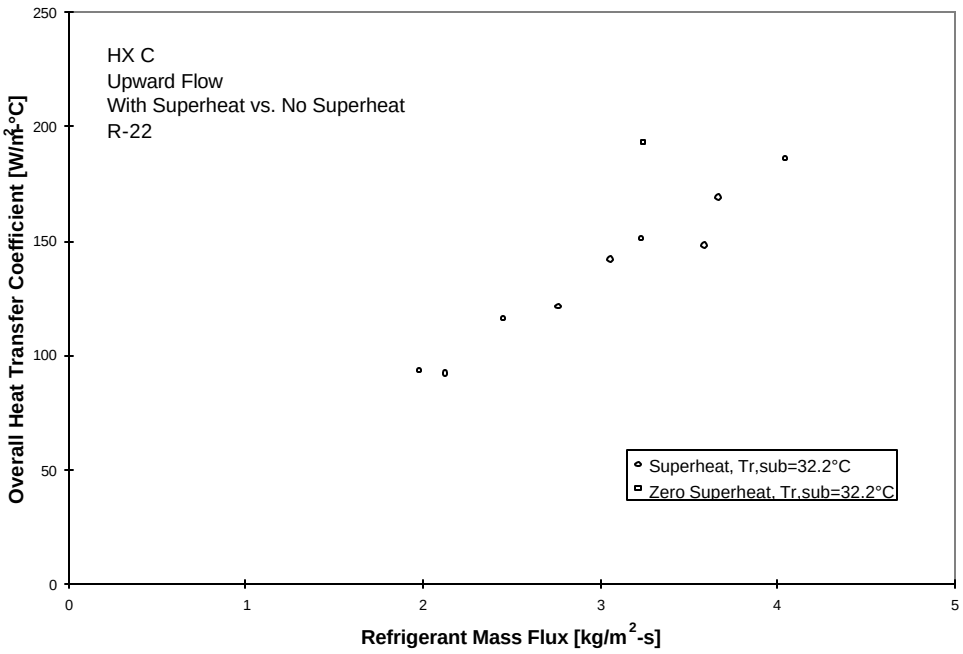

Figure 5.17 Experiment 3 vs. 4 - Comparison of Calculated Overall Heat Transfer Coefficient with and without Superheat with R-22

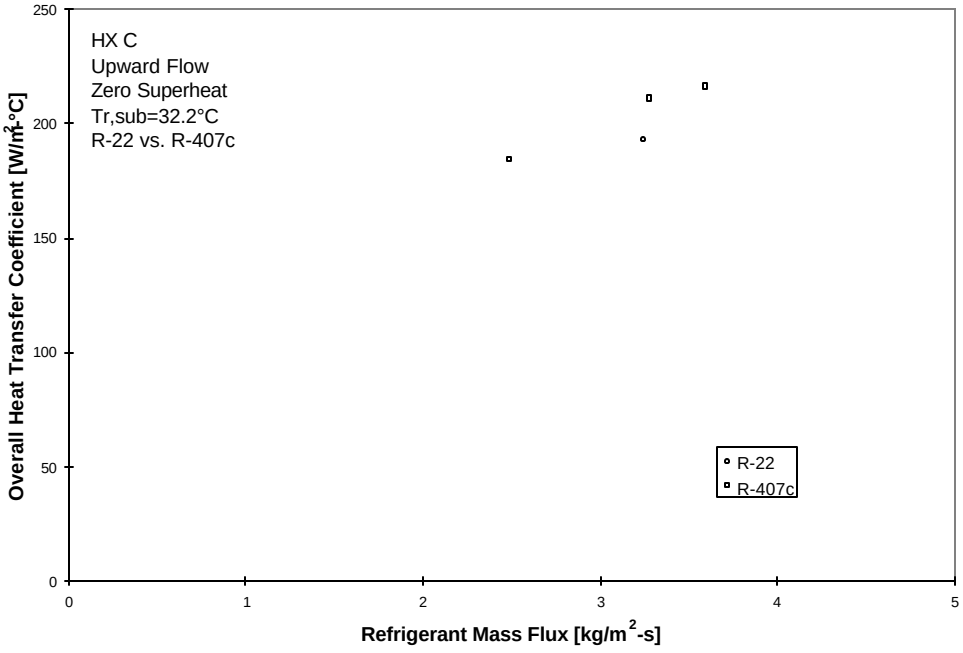

Figure 5.18 Experiment 4 - Comparison of Calculated Overall Heat Transfer Coefficient of R-22 and R-407c

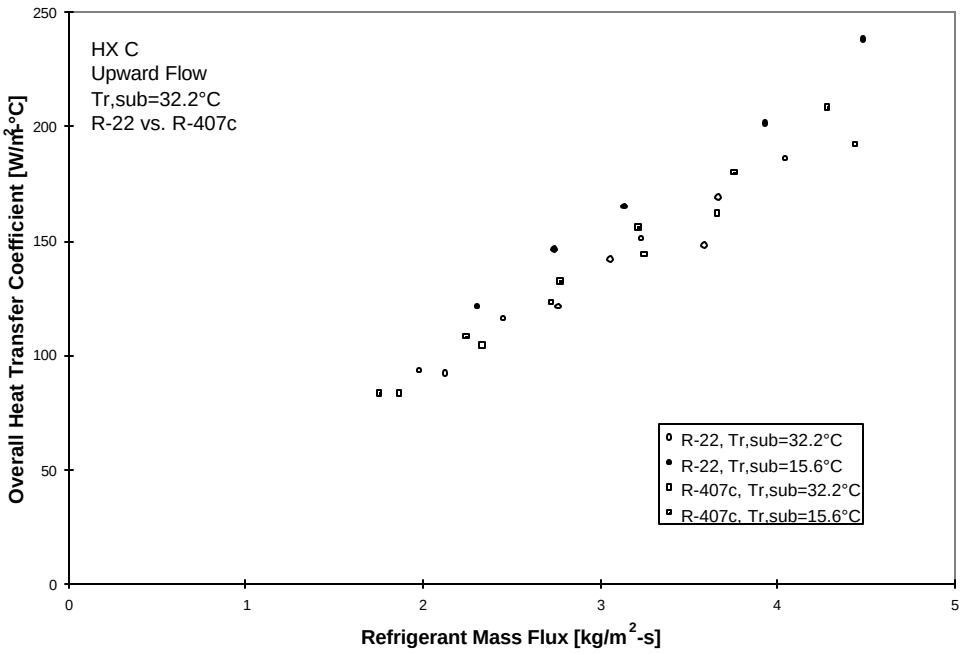

Figure 5.19 Experiment 3 - Comparison of Calculated Overall Heat Transfer Coefficient of R-22 and R-407c

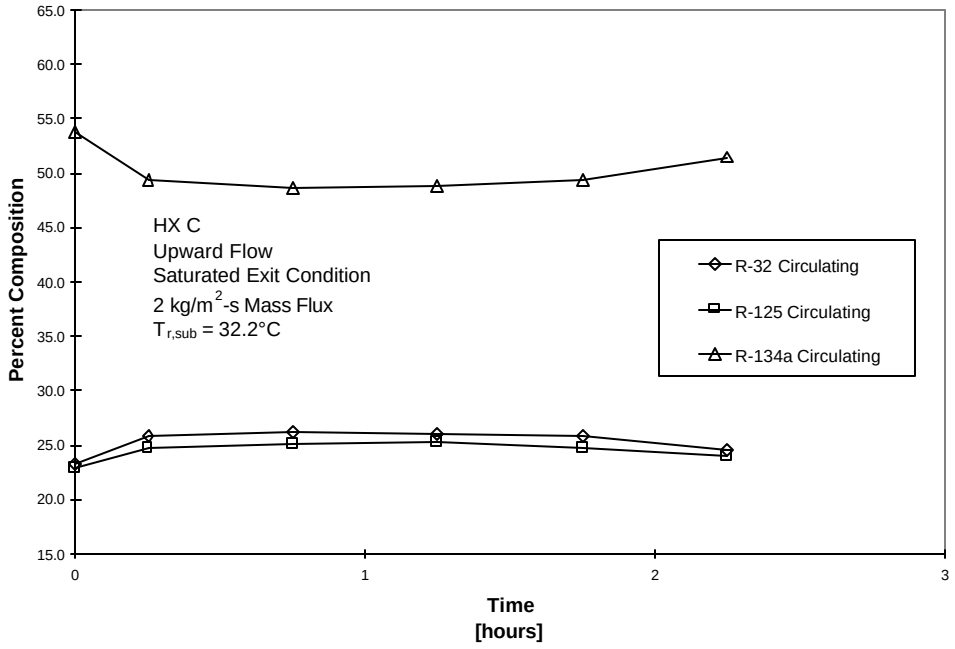

Figure 5.20 Experiment 4 - Composition change of circulating refrigerant at minimum flow rate with refrigerant subcooled to 32.2°C

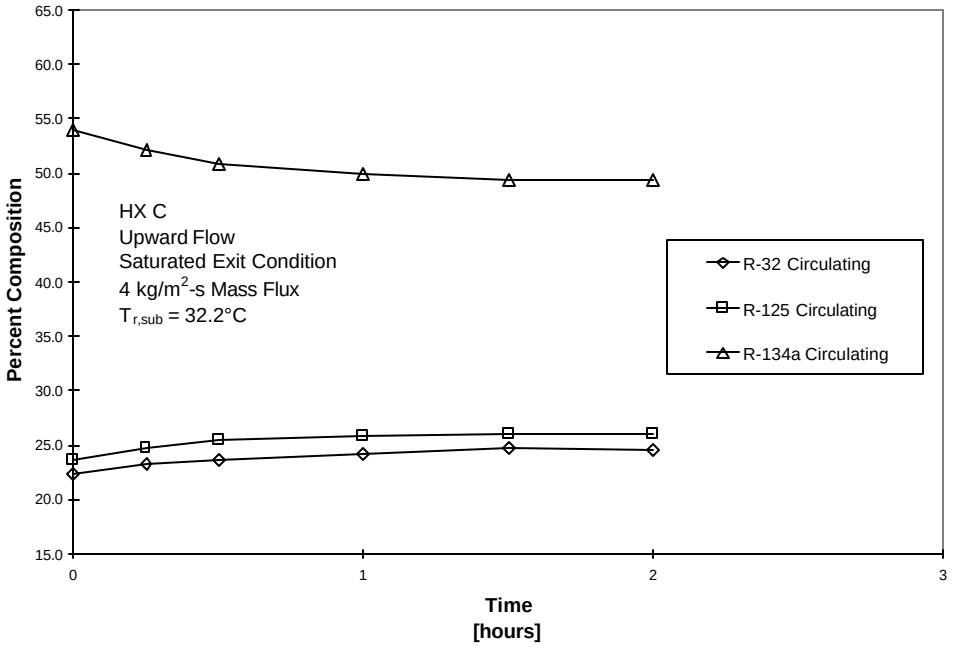

Figure 5.21 Experiment 4 - Composition change of circulating refrigerant at maximum flow rate with refrigerant subcooled to 32.2°C

5.6. Influence of Downward Flow (Experiment 5)

5.6.1. Objective of Experiment 5

The purpose of this experiment is to determine whether it is possible reduce fractionation by reversing refrigerant flow downwards. The idea of this experiment is to avoid pooling of large quantity of liquid at the bottom of the evaporator. For this investigation, it was necessary to construct a new distributor which is inserted into the inlet header of the evaporator HX B to reduce the effect of expected poor distribution. This distributor is designed to be rotated to change the angle of spray into the evaporator. It was determined through shake-down runs that the optimal spray angle was 70° from vertical (downward). Further description of the new distributor is provided in Sections 3.1.4 and shake-down experiments are summarized in Section 6.2.

The mechanism suggested in this paper for fractionation is liquid pooling in the inlet header of the evaporator. The downward refrigerant flow of this experiment eliminates this mechanism due to gravity. Composition shift is expected to be minimized by this orientation.

It is known that downward refrigerant flow is not the optimum configuration for thermal performance. Both R-22 and R-407c U-values will be penalized due to the downward refrigerant flow configuration when compared to upward flow cases. To provide a fair comparison of downward vs. upward flow (Experiment 3), water inlet temperature was increased while maintaining constant water side temperature drop such that superheat was obtained approximately equal to that of Experiment 3.

5.6.2 Results of Experiment 5

Figures 5.22 and 5.23 show a significant reduction in U-values for downward flow when compared with upward flow (Experiment 3) for both R-22 and R-407c, a penalty that was expected. U-values for R-22 and R-407c decrease by approximately the same amount, 20%. Consistent with what was seen for upward flow cases with superheat with the larger evaporators (HX B and HX C), Figure 5.24 shows R-407c U-values are less than U-values for R-22 with downward flow and superheat by approximately 15%. This was somewhat unexpected, since U-values for R-22 and R-407c were approximately equal when fractionation was assumed to be non-existent in the smaller evaporator (HX A).

Based upon the above thermal results, it appears that no reduction in fractionation was obtained by reversing refrigerant flow downwards. This is verified via observation of composition analysis results of Experiment 5 in Figures 5.25 and 5.26 and Table 5.1. R-134a composition shift is approximately -2.1% for low mass flux and -2.0% for high mass flux. The values seen in Experiment 3 fall slightly below at low mass flux (-1.6%) and slightly above at high mass flux (-3.1%). The differences in composition shift between this experiment and Experiment 3 are negligible.

In summary, this experiment shows that downward flow does not reduce fractionation in the evaporator in the range of mass flux evaluated. Further, the thermal effects of fractionation were not detected due to the small degree of fractionation witnessed in this investigation.

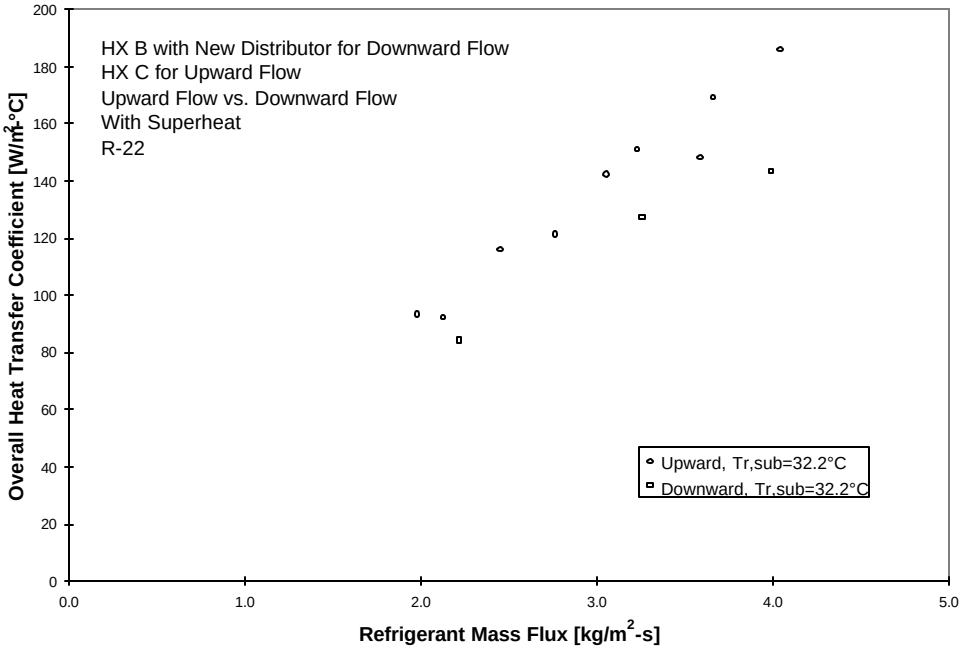

Figure 5.22 Experiment 3 vs. 5 - Comparison of Calculated Overall Heat Transfer Coefficient with Upward and Downward Flow with R-22

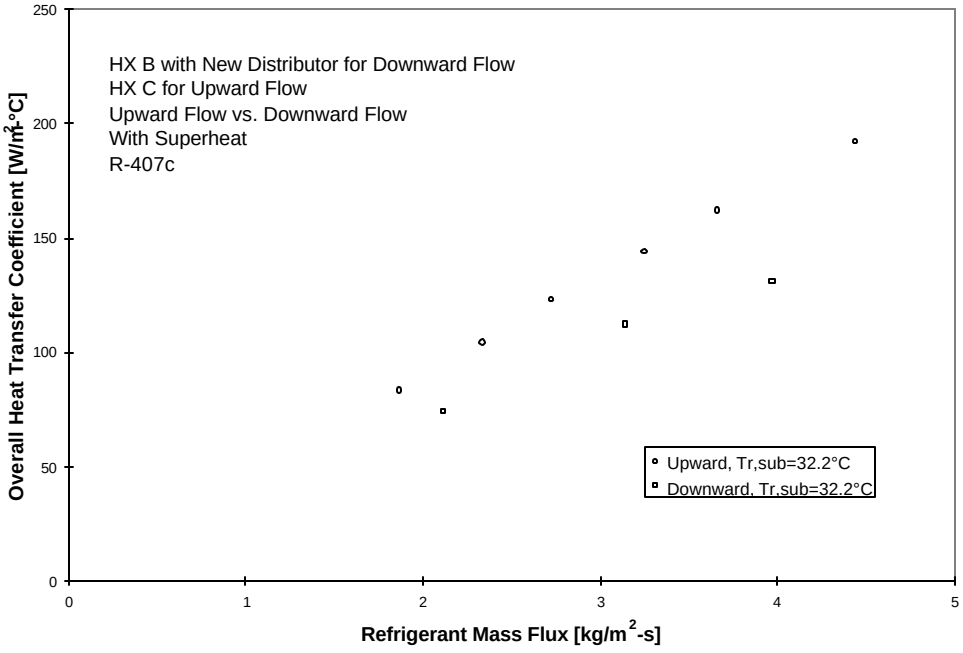

Figure 5.23 Experiment 3 vs. 5 - Comparison of Calculated Overall Heat Transfer Coefficient with Upward and Downward Flow with R-407c

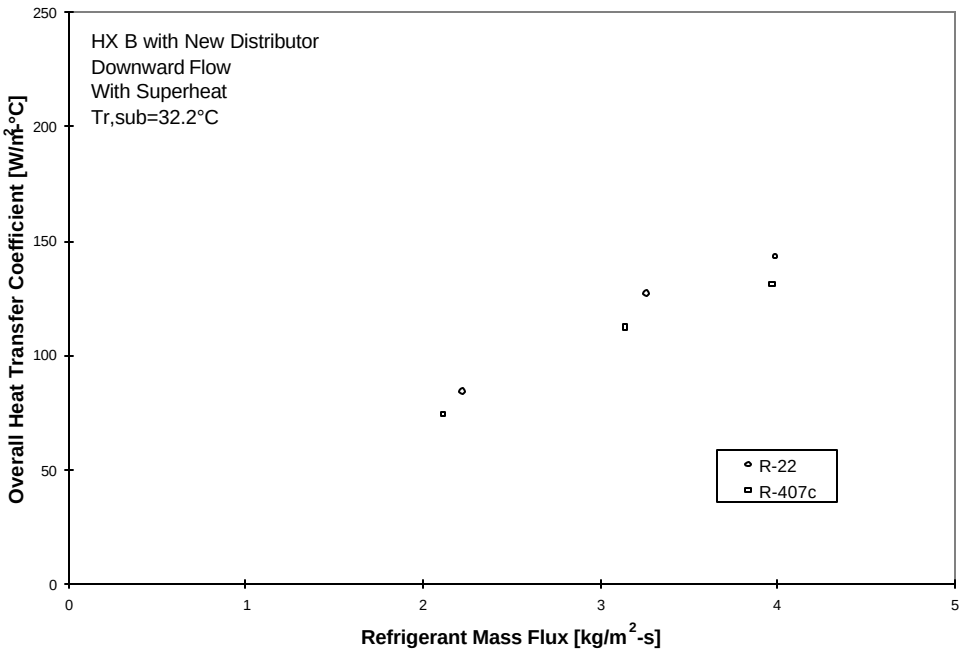

Figure 5.24 Experiment 5 - Comparison of Calculated Overall Heat Transfer Coefficient of R-22 and R-407c

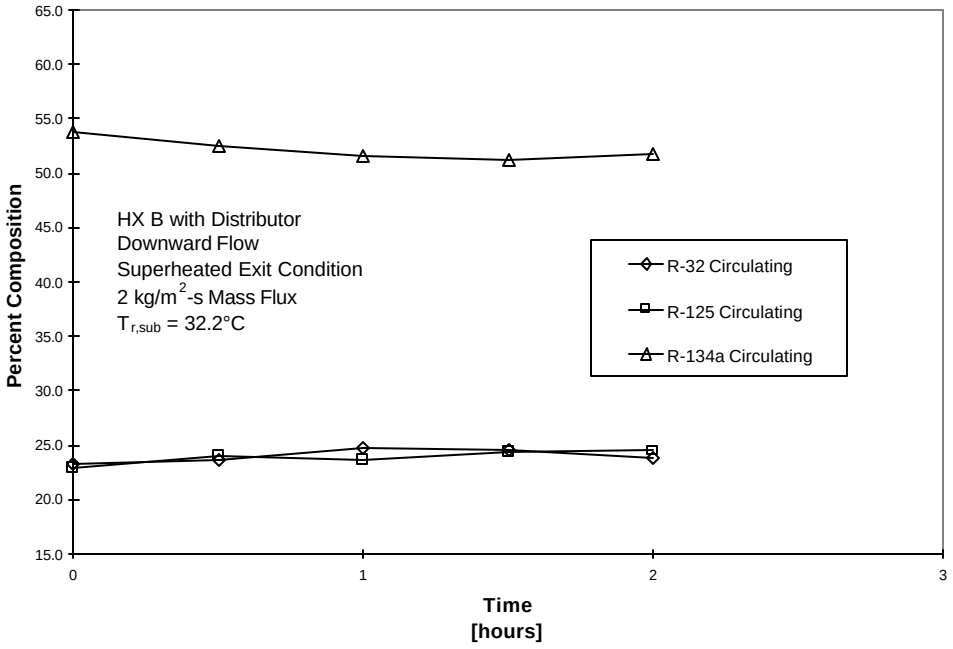

Figure 5.25 Experiment 5 - Composition change of circulating refrigerant at minimum flow rate with refrigerant subcooled to 32.2°C

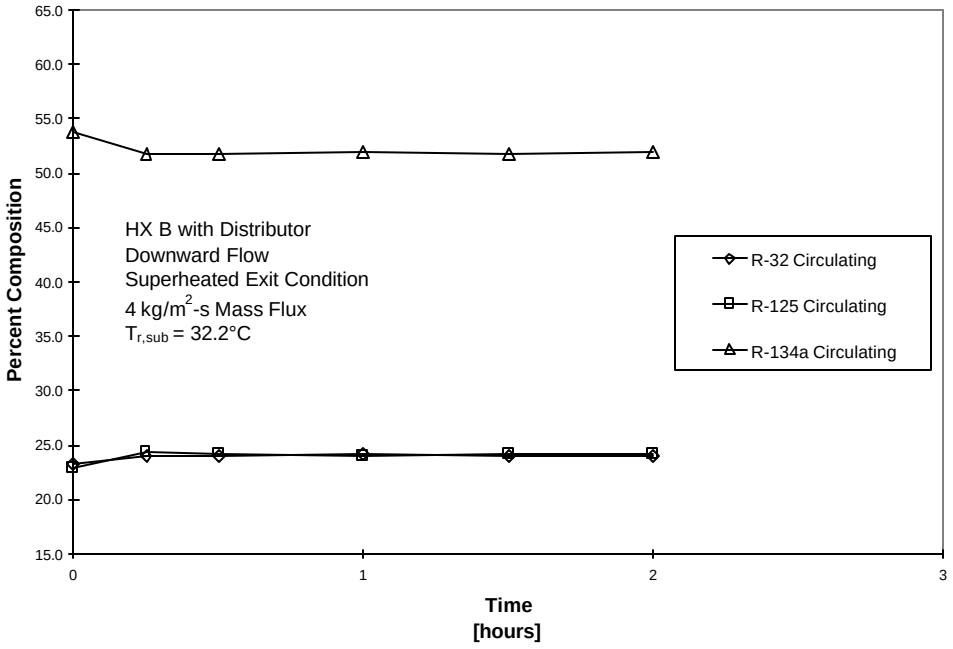

Figure 5.26 Experiment 5 - Composition change of circulating refrigerant at maximum flow rate with refrigerant subcooled to 32.2°C

5.7. Influence of Saturated Evaporator Exit Condition with Downward Flow (Experiment 6)

5.7.1. Objective of Experiment 6

Although Experiment 4 showed that the amount of superheat used in this investigation did not influence the results, experiments were performed with a saturated evaporator exit condition with downward flow as a matter of completion. Once again, the water side inlet temperature was allowed to float while maintaining constant water side temperature drop to obtain an average of 0°C superheat. Thermal performance was calculated for this experiment but composition measurements were not taken.

Results similar to that of Experiment 4 are expected where U-values are improved but fractionation is essentially unchanged.

5.7.2. Results of Experiment 6

Consistent with upward flow cases (Experiment 4), Figures 5.27 and 5.28 show considerable increase in U-value by eliminating superheat. Figure 5.29 presents a comparison of R-22 and R-407c thermal performance. Not much conclusion can be made from this figure (same comment) other than saying U-values are approximately equal, due to the data scatter. Although compositions measurements were not taken, it is safe to assume that results would be similar to that of Experiment 5.

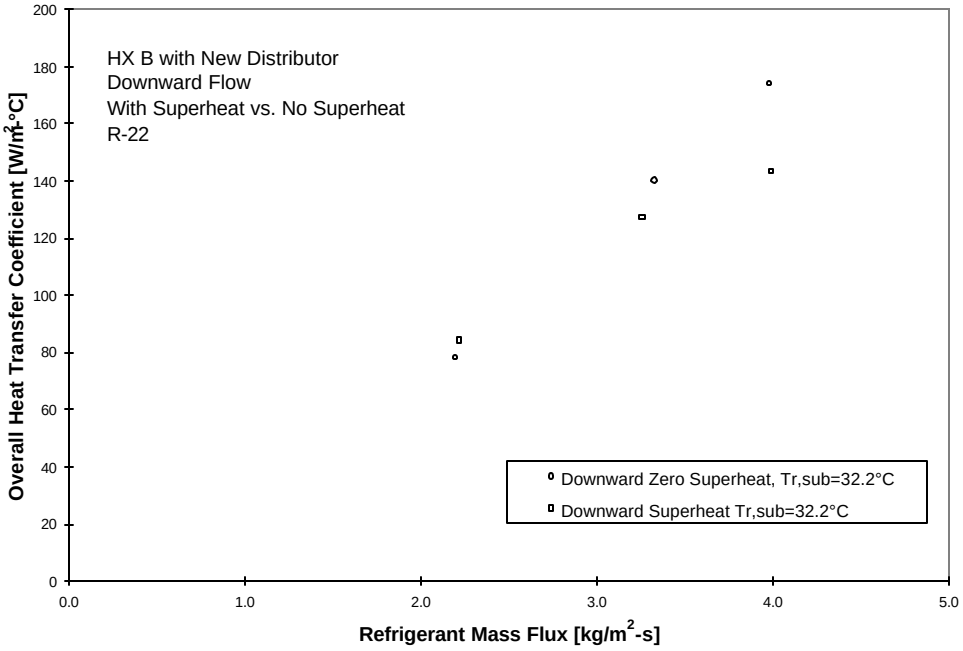

Figure 5.27 Experiment 5 vs. 6 - Comparison of Calculated Overall Heat Transfer Coefficient with and without Superheat with Downward Flow and R-22

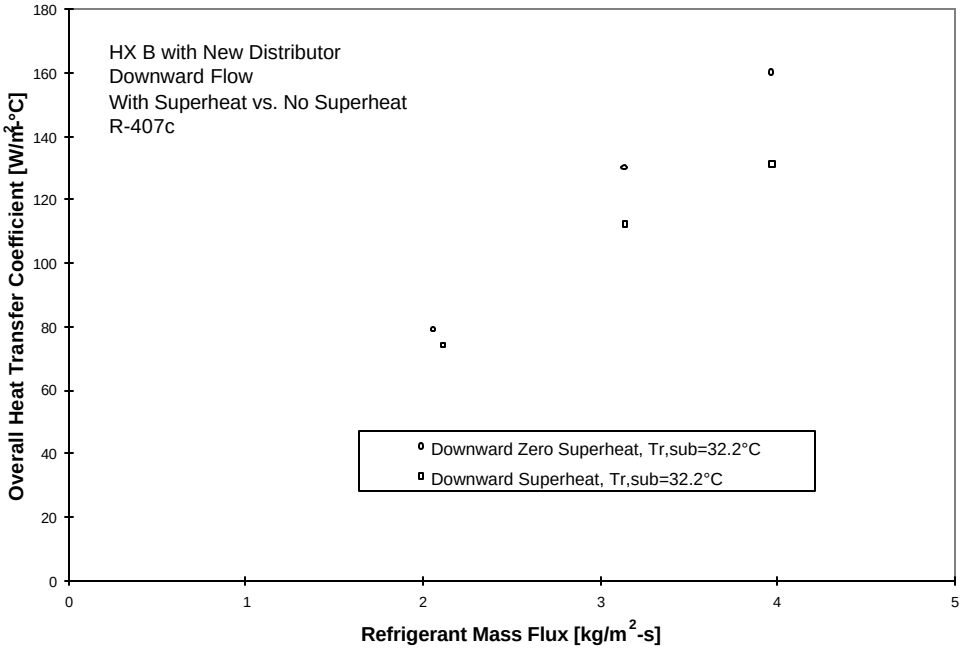

Figure 5.28 Experiment 5 vs. 6 - Comparison of Calculated Overall Heat Transfer Coefficient with and without Superheat with Downward Flow and R-407c

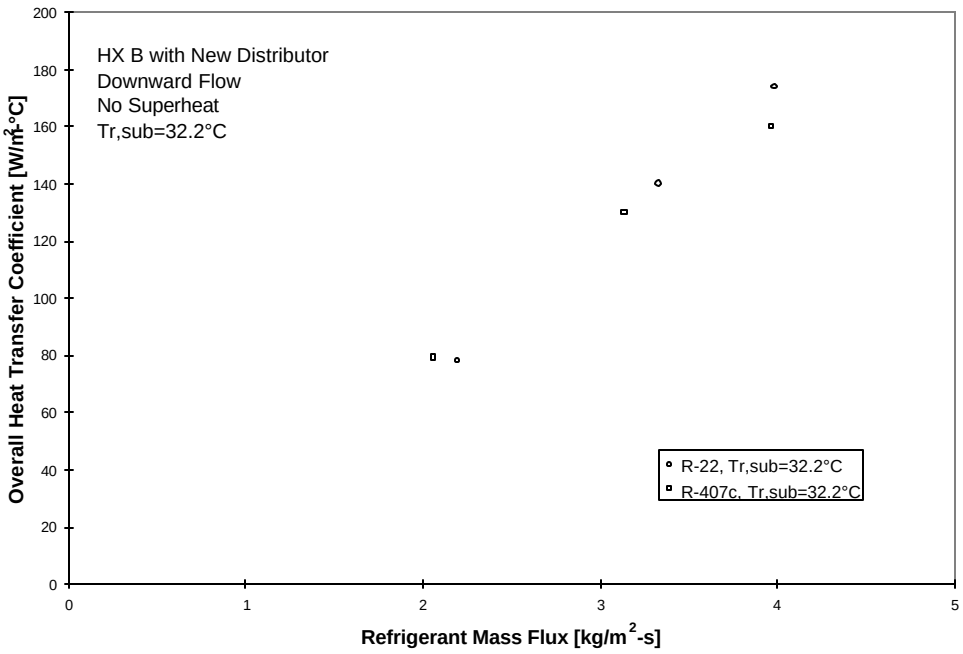

Figure 5.29 Experiment 6 - Comparison of Calculated Overall Heat Transfer Coefficient of R-22 and R-407c

Table 5.1 Change in refrigerant R-407c composition from initial start-up of chiller to steady state at two locations, the back bottom of the evaporator (evaporator sample) and from the suction line (circulating sample)

Exp. No.	Mass Flux [kg/m^2-s]	Subcooled Temp. [°C]	Evaporator Sample Shift ΔR-32 [%]	ΔR-125 [%]	ΔR-134a [%]	Circulating Sample ΔR-32 [%]	ΔR-125 [%]	ΔR-134a [%]
1	10	32.2	-1.0	-0.9	1.6	0.2	-0.2	0.0
1	20	32.2	-2.0	-1.6	3.6	0.8	0.5	-1.2
1	20	15.6	-0.3	-0.3	0.5	0.6	0.2	-0.8
2	2	32.2	-1.5	-1.8	3.3	1.3	-0.2	-1.1
2	4	32.2	-3.2	-2.7	5.9	1.4	0.4	-1.8
2	2	15.6	-2.2	-1.3	3.5	1.3	0.9	-2.2
2	4	15.6	-1.8	-1.5	3.3	2.6	1.5	-4.0
3	2	32.2	N/A	N/A	N/A	1.3	0.3	-1.6
3	4	32.2	N/A	N/A	N/A	2.0	1.1	-3.1
3	2	15.6	N/A	N/A	N/A	1.3	0.5	-1.8
3	4	15.6	N/A	N/A	N/A	2.0	1.0	-3.0
4	2	32.2	N/A	N/A	N/A	2.4	1.9	-4.3
4	4	32.2	N/A	N/A	N/A	1.7	2.0	-3.7
5	2	32.2	N/A	N/A	N/A	0.9	1.2	-2.1
5	4	32.2	N/A	N/A	N/A	0.7	1.3	-2.0

Chapter 6.0 Other Issues

6.1. Superheat Stability

During shake-down of the chiller, liquid droplets were noticed at the exit of the evaporator when operating with less than 9°C of superheat with R-22 indicating imperfect distribution (7°C with R-407c based upon difference between dew temperature at exit temperature and refrigerant outlet temperature). These droplets were observed through sight glasses and are shown graphically as downward spikes in the evaporator exit temperature reading. A static mixer was added to the suction line with the idea to allow the mixture of superheated vapor and entrained saturated liquid droplets to come to equilibrium (evaporate droplets and unify vapor temperature). This provides a mean to determine refrigerant enthalpy at the exit of the evaporator when liquid mass fraction of droplets in superheated vapor is unknown.

Existence of the temperature difference between mixer inlet and outlet indicate presence of the liquid droplets in superheated vapor (droplet carry-over). Temperatures at the inlet and at the exit are almost identical in two cases: a) inlet is pure superheated vapor or b) liquid carry over is so significant that droplets are present even at the mixer outlet. In the case when just some liquid droplets are present in the stream of superheated vapor at the evaporator exit, the inlet thermocouple reading fluctuates. Graphs in Figure 6.1 through 6.3 for R-22 and 6.4 through 6.6 for R-407c illustrate typical conditions. Flow of both refrigerants is controlled by TXV.

Figure 6.1 shows unstable operation. Temperature reading at the exit from the evaporator, $T_{r,out}$, fluctuates indicating droplets present and mass flow rate is unstable.

With increase of superheat, the system starts to stabilize. "Marginally" stable conditions are shown in Figure 6.2 with superheat of approximately 8.5^{o}C. Evaporator exit temperature and mass flow fluctuate but less than in the Figure 6.1 and exit from the static mixer is approximately 1^{o}C lower than the inlet.

With further increase of superheat evaporator-TXV loop stabilizes as shown in Figure 6.3. Superheat is raised to approximately 10^{o}C. There is no significant fluctuation of any parameter and mixer inlet and exit temperatures are on the top of each other.

The accepted criterion for stability (tolerable range of evaporator exit temperature fluctuation) is $\pm$ 0.5°C.

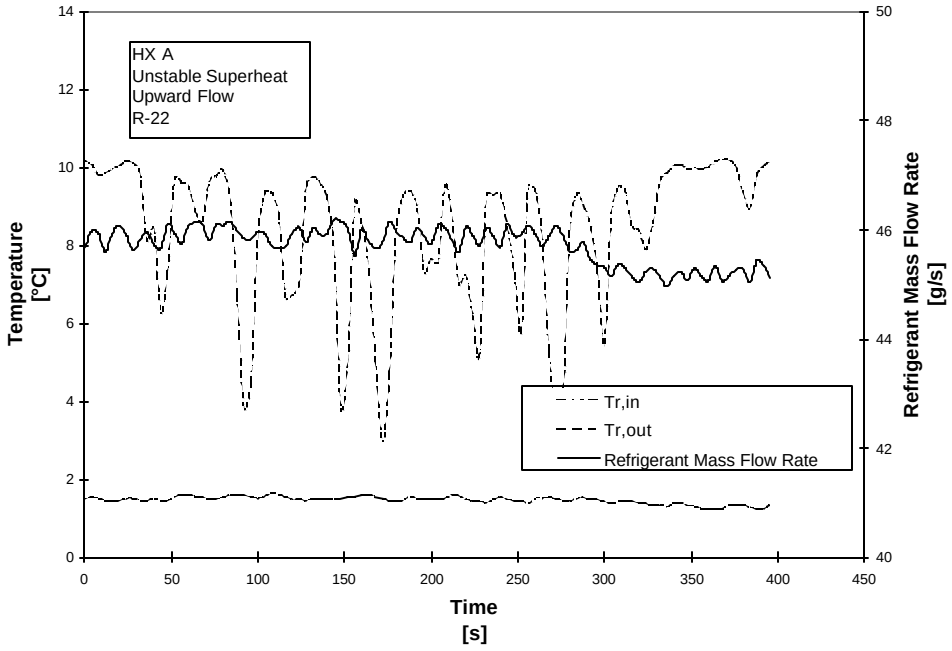

Figure 6.1 Unstable operation of evaporator (R-22)

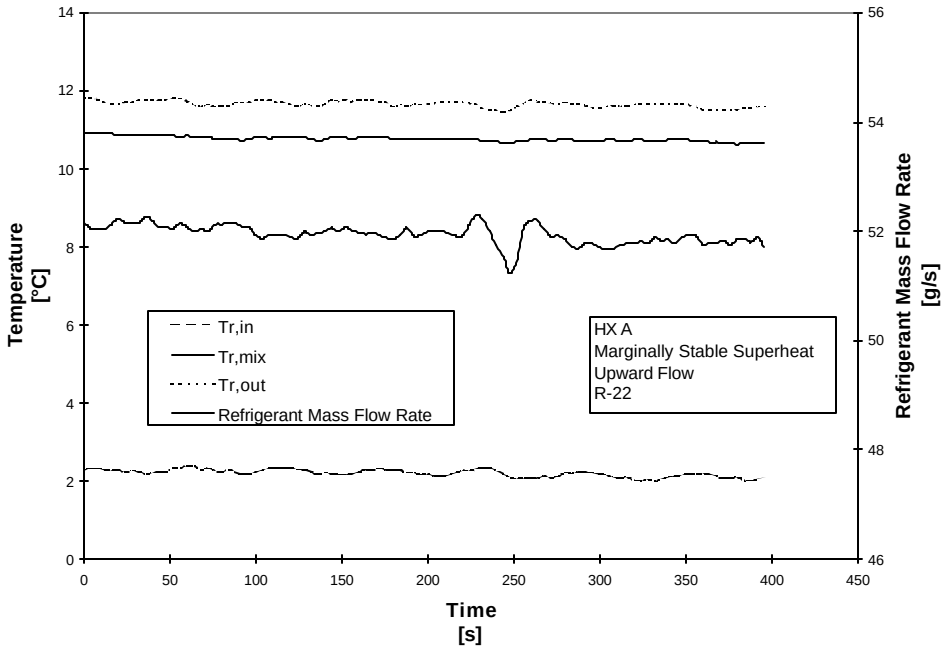

Figure 6.2 "Marginally" stable operation of evaporator (R-22)

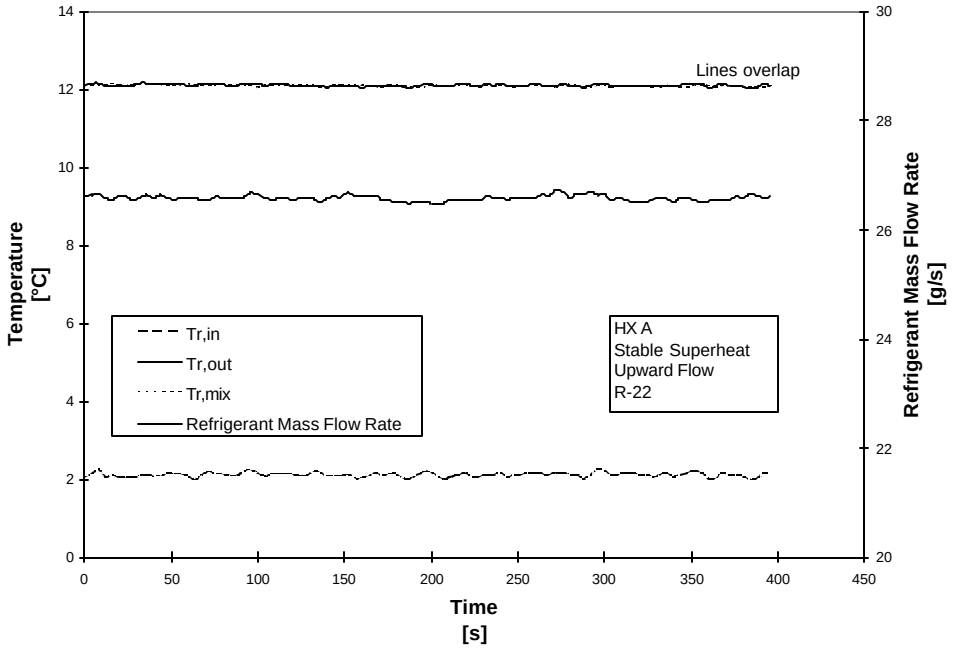

Figure 6.3 Stable operation of evaporator (R-22)

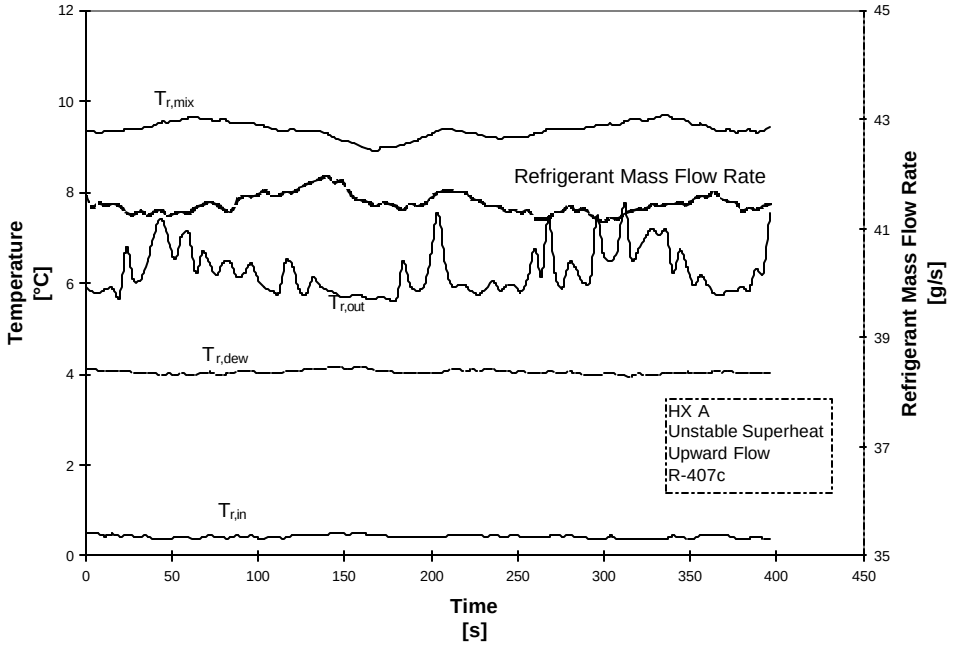

Figure 6.4 Unstable operation of evaporator (R-407c)

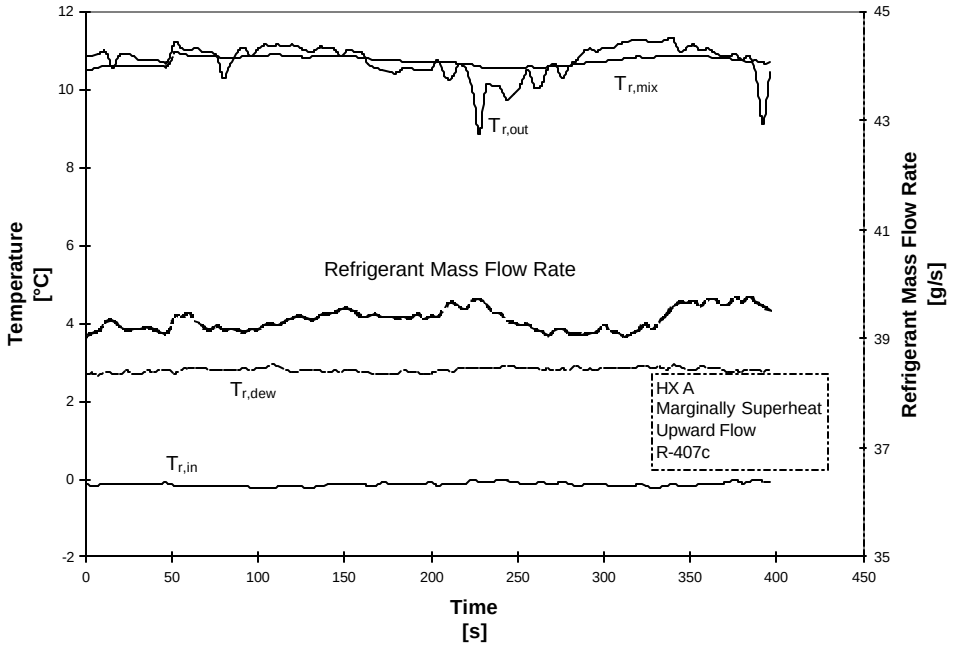

Figure 6.5 Marginally Stable operation of evaporator (R-407c)

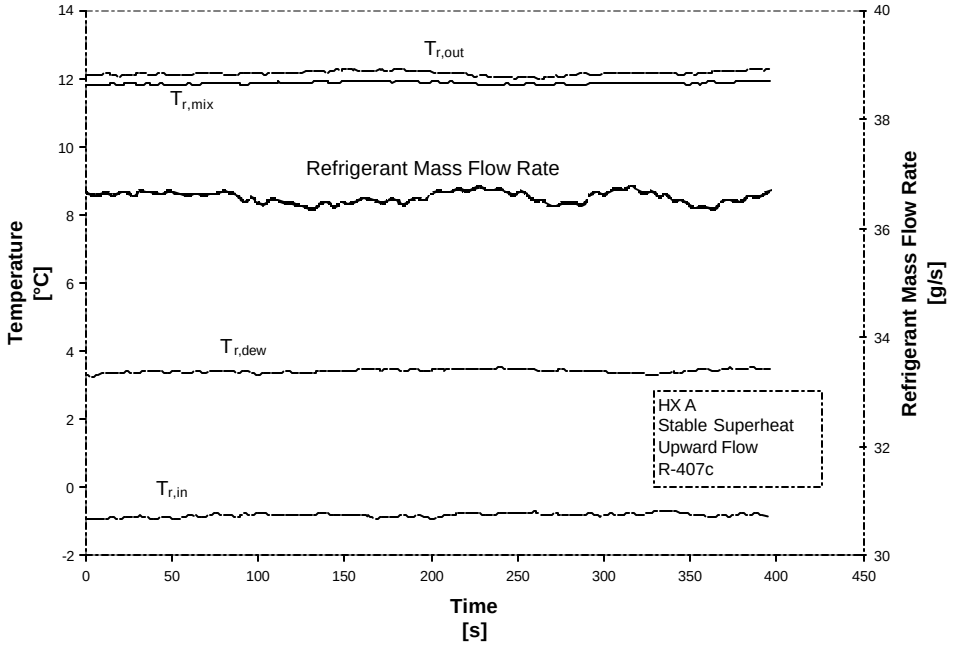

Figure 6.6 Stable operation of evaporator (R-407c)

6.2. Downward Flow Distributor Optimum Angle

Shake-down experiments were conducted with R-22 to optimize the angle of spray into the evaporator prior to conducting Experiment 5. The chart in Figure 6.7 shows results of these experiments and indicates that the optimal angle is approximately 70° for all three mass fluxes. Notice some scatter of

data with operation at 45 g/s. This can be attributed to hitting some internal obstruction at that particular angle. Care was taken in this investigation to insure that the angle was identical for all tests and that the distributor was not pointed at an internal obstruction for fair comparison.

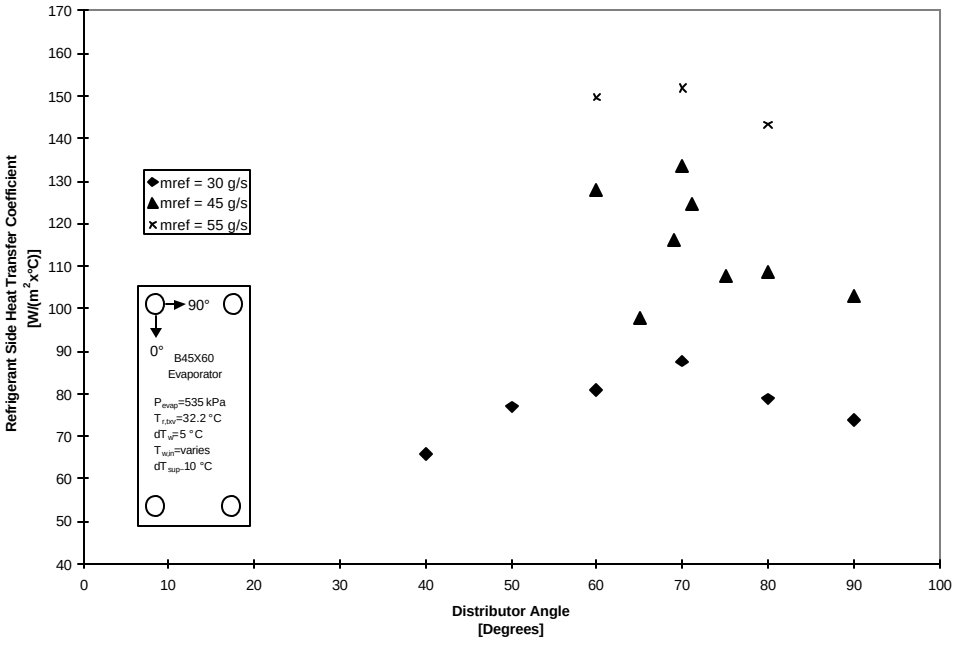

Figure 6.7 Optimization of distributor angle

6.3. Refrigerant and Oil Mixture Composition

The facility described in Chapter 3 uses a scroll compressor which requires the use of a lubricant which circulates throughout the system. For refrigerant compatibility reasons, polyol ester oil was for use with both R-22 and R-407c experiments.

It was identified by Martz and Jacobi (1994) that system performance could be reduced by oil "adsorbing refrigerant that could otherwise be used to transfer heat." Since mineral oil is typically used with R-22, the oil concentration circulating through the system was measured to ensure a fair comparison between refrigerants. In addition, samples were taken from the bottom back of the refrigerant inlet header as this was identified as a possible location for oil and liquid refrigerant hold-up. This location is labeled "refrigerant liquid sample point" in Figure 4.2. Data was acquired using the procedure described in Section 3.2 and plotted in Figure 6.8.

The circulating oil composition ranges between 0.24 and 1.71% by mass for R-22 and between 0.24 and 0.87% by mass for R-407c.

There is a noticeable trend for measurements of oil composition in the back bottom of HX B. As mass flux is reduced, the mass concentration of oil increases significantly.

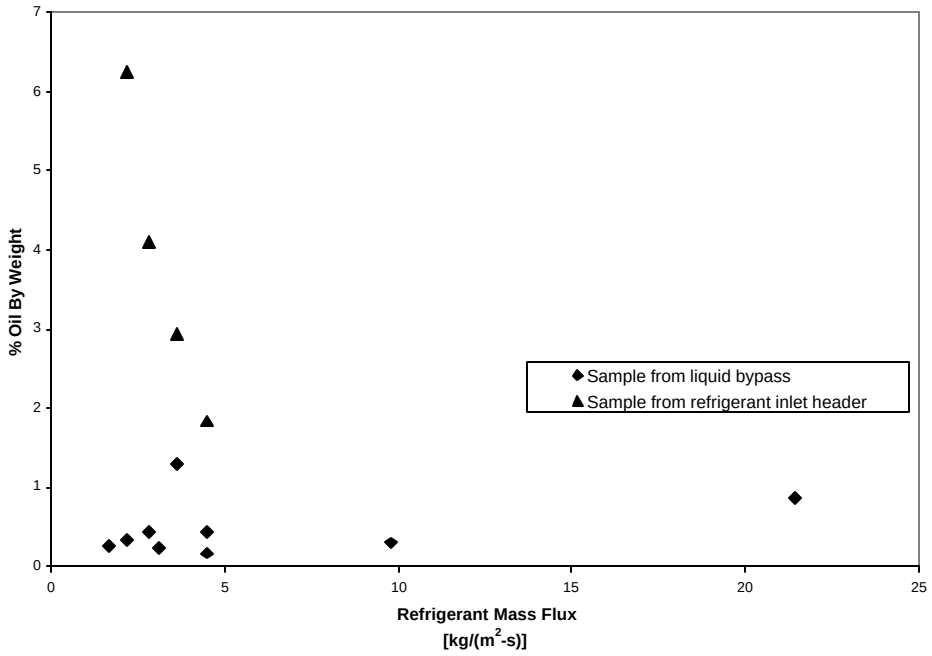

Figure 6.8 Circulating oil concentration (liquid bypass sample) and oil composition in refrigerant inlet header of evaporator

6.4. Evaporator Oil Hold-up

Sight glasses were installed at the refrigerant inlet and outlet header to allow visualization of flow quality. Through the sight glasses, it was discovered that a significant amount of oil drained out of the evaporator into the inlet header after shutdown of the system. As a result, isolation valves were installed at the inlet and outlet of the evaporator. These valves were closed immediately after shutdown to contain all oil in the evaporator for measurement. Measurements were acquired following the procedure described in Section 4.3.

The oil hold-up was quantified in HX A, B and C during operation with upward flow and is shown graphically below in Figure 6.9. The diamond and triangle represent oil hold-up with R-407c in evaporators HX A and B, respectively. The square and circle represent oil hold-up with R-22 in evaporator HX B and C, respectively. An additional data point was acquired in HX A with R-22 at an unknown mass flux. This data point is identified on the graph as a horizontal line, the length of which spans the range of possible mass flux in HX A.

At first view, Figure 6.9 below indicates oil hold-up is dependent on mass flux. This is expected since there is more vapor momentum at higher mass flux which will carry the oil up and out of the evaporator. Also, evaporator flow is expected to be more turbulent at higher mass flux reducing dead zones in the evaporator where oil could build up.

Since there is a limited number of data points, it cannot be determined whether the type of refrigerant affects oil hold-up. However, it appears that R-22 and R-407c follow the same trend in HX B

(squares for R-22 and Triangles for R-22) indicating that oil hold-up is similar for both refrigerants. Table 6.1 is presented, showing that approximately 6% to 35% of the refrigerant channel volume was full of oil.

The quantity of oil hold-up with R-22 is significantly greater in HX C than in HX B. This can be attributed to a dead zone between the refrigerant inlet and water outlet header created by the distributor.

Table 6.1 Pecent of Evaporator Refrigerant Channels filled with oil

Evaporator	Refrigerant	Mass Flux (kg/m^2-s)	Oil Quantity (g)	Oil Volume (m^3)	Evaporator Volume (m^3)	%Oil (by volume)
HX A	R-22	N/A	340	3.44E-04	9.68E-04	35.5%
HX A	R-407c	22	63	6.34E-05	9.68E-04	6.5%
HX B	R-22	4.5	335	3.39E-04	5.42E-03	6.3%
HX B	R-22	3.5	514	5.20E-04	5.42E-03	9.6%
HX B	R-407c	3	1046	1.06E-03	5.42E-03	19.5%
HX B	R-22	4.2	879	8.89E-04	5.42E-03	16.4%
HX C	R-22	2	1211	1.23E-03	5.42E-03	22.6%

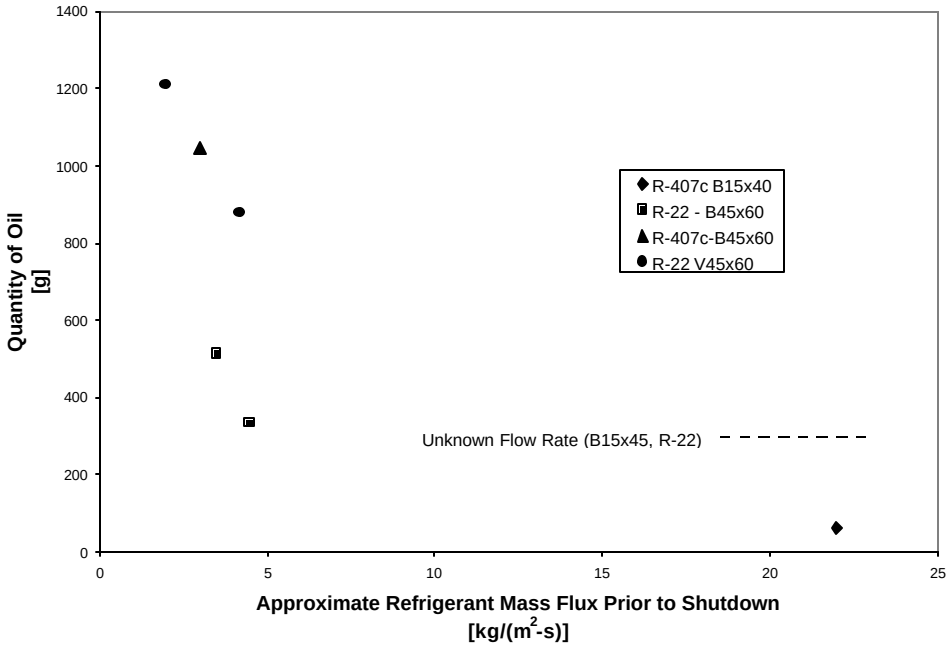

Figure 6.9 Oil holdup in evaporator with upward flow

6.5. Imperfect exit conditions

The following four figures (Figures 6.10 through 6.13) illustrate the variation of the superheat at the exit of the evaporator while changing the refrigerant mass flow rate. It is presented for experiments with HX A. It was originally intended to maintain constant superheat and constant compressor suction pressure for all tests. Further, water side inlet temperature and temperature rise were also desired to be held constant. Baseline results shown in Figures 6.10 through 6.13 present the change in superheat to maintain constant compressor suction pressure, which indicated the need to relax constraint on refrigerant side outlet temperature. Consequence is some effect on overall heat transfer coefficient due to decrese in length of superheated zone at higher refrigerant flow rates.

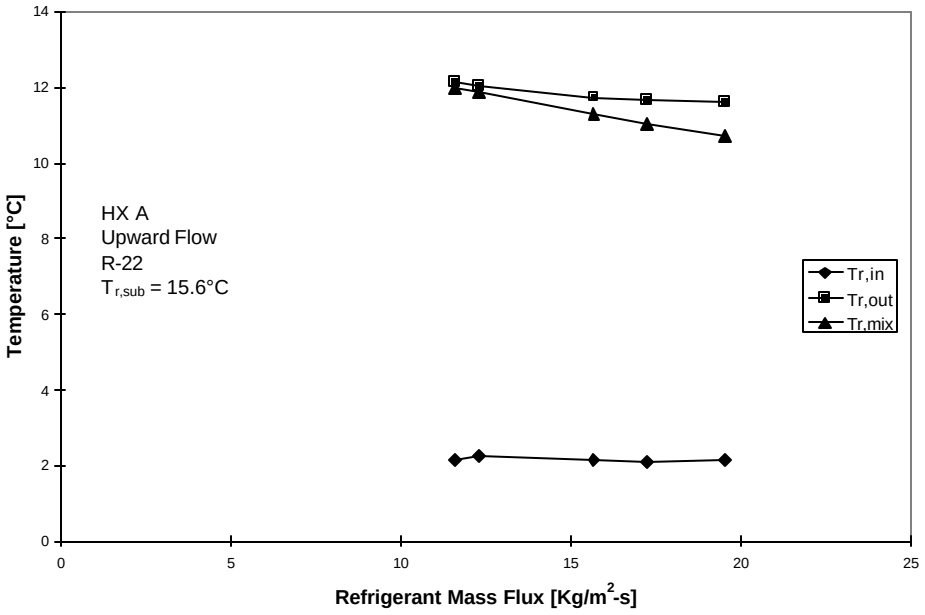

Figure 6.10 Experiment 1, Change in evaporator refrigerant outlet temperature for R-22 with 15.6°C subcooled temperature

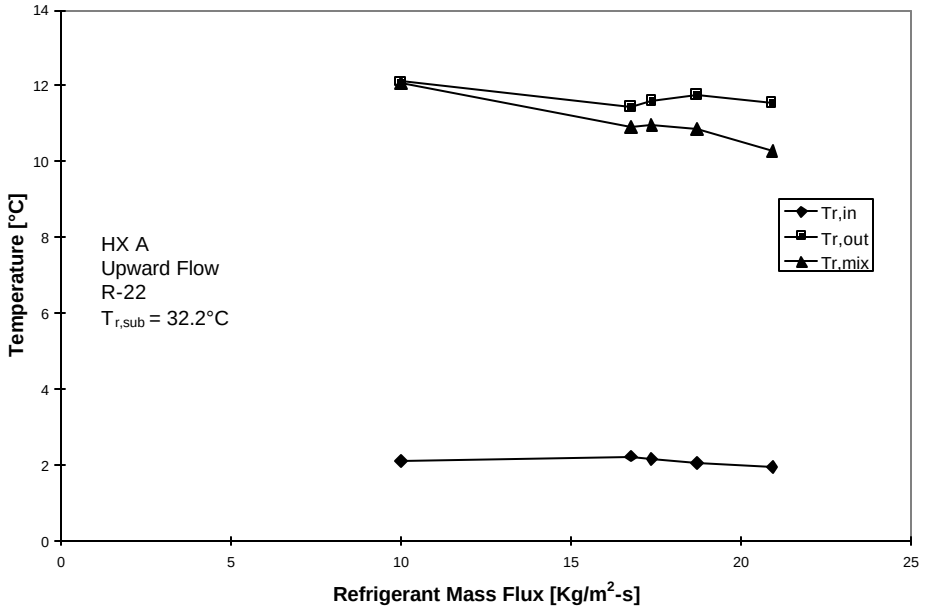

Figure 6.11 Experiment 1, Change in evaporator refrigerant outlet temperature for R-22 with 32.2°C subcooled temperature

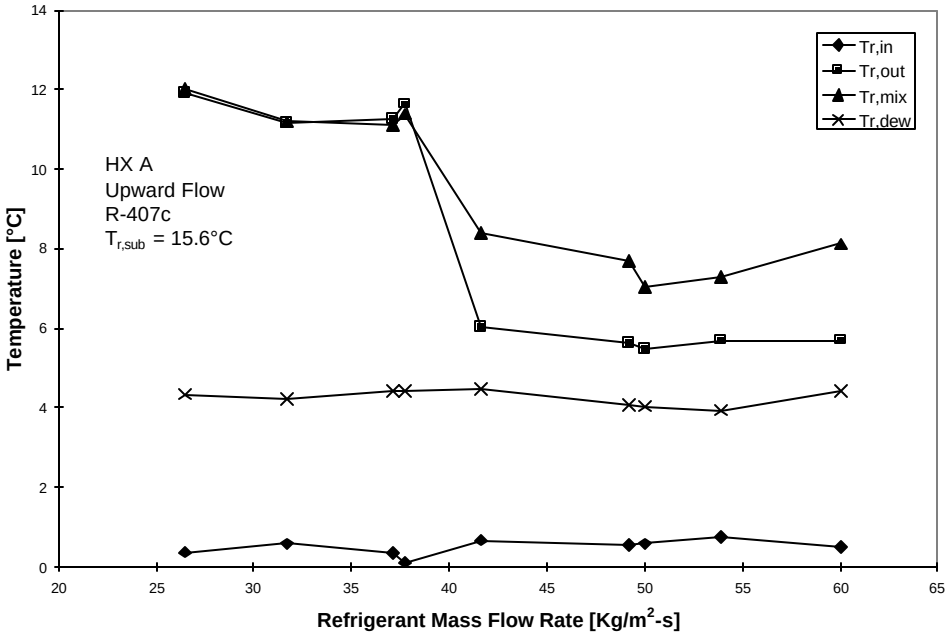

Figure 6.12 Experiment 1, Change in evaporator refrigerant outlet temperature for R-407c at 15.6°C subcooled temperature

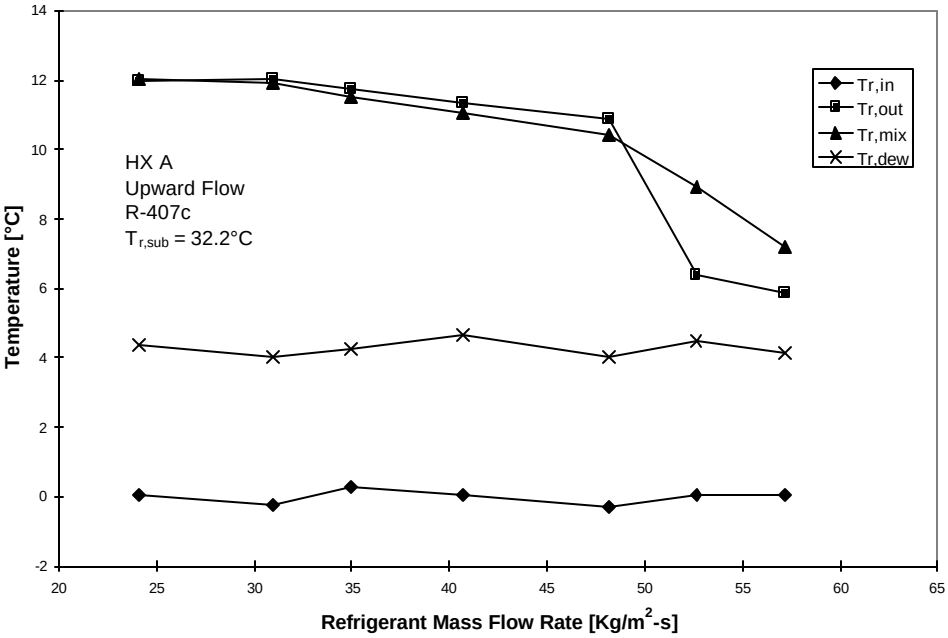

Figure 6.13 Experiment 1, Change in evaporator refrigerant outlet temperature for R-407c at 32.2°C subcooled temperature

Chapter 7.0: Summary, Conclusions and Recommendations

This investigation explored the effects of fractionation and distribution of R-407c in brazed plate evaporators especially when operating with low refrigerant mass flux. The results presented are based upon a study of an evaporator in a system not of local heat transfer. Fractionation was detected by means of analyzing the composition of refrigerant samples from the suction line and from the back bottom of the evaporator. Thermal performance was represented by calculation of the overall heat transfer coefficient from measured parameters.

Intention was to relate the magnitude of fractionation with differences observed in thermal behavior with respect to a baseline experiments with R22. Experiments were performed with R-22 in parallel with R-407c so that the thermal consequences of fractionation can be singled out. The study consisted of six experiments to highlight the effects of low mass flux, improved refrigerant distribution, varied evaporator exit quality/superheat and downward refrigerant flow. Also evaluated was the effect of subcooling (inlet quality). This investigation was purposefully set up such that recommendations could be made with respect to future design of systems that will use R-407c or other zeotropic refrigerant.

Since it is well accepted that R-407c will fractionate severely in shell and tube heat exchangers, significant fractionation was expected. On the contrary, only slight fractionation (up to 5%) was observed for all experiments, as shown in Table 5.1, indicating that the configuration of the plate evaporator does not significantly influence the magnitude of fractionation. However, much information was gathered with respect to fractionation. Fractionation doubled with lowering inlet quality although the magnitude of composition shift with low inlet quality was still small. This is attributed to lower velocity in the inlet header allowing liquid refrigerant to pool and preferential evaporation to occur. Unexpectedly, fractionation increased with increased mass flux when operating with upward flow in Experiment 1, 2 and 3. This phenomena did not occur with downward flow or when operating with upward flow and saturated exit condition. Increased fractionation may be related to significant oil hold-up in the evaporator occurring at low mass flux which displaces liquid refrigerant.

Overall heat transfer coefficients for R-407c were essentially equal to that of R-22 when operating at nominal conditions. U-values for R-407c at low mass flux were up to 15% less than R-22. However, R-407c U-values were approximately 10% greater than R-22 when operating with a saturated refrigerant outlet condition.

Operation of a plate evaporator with downward refrigerant flow was tried using a custom distributor. This orientation prevents pooling of liquid refrigerant at the bottom of the evaporator, removing the mechanism for fractionation. There was no significant change in composition shift but the thermal performance was significantly reduced, as expected. Reduced heat transfer performance is consequence of the design that did not wet entire surface but just a limited part affected by narrow jet. The benefits of such a device with improved jet may be useful for other applications where more severe fractionation is seen.

In the course of the investigation, various anomalies were noticed. Some data was acquired but it is recommended that more research be performed to fully understand the issues.

One of these issues was superheat instability. Liquid droplets were present at the evaporator outlet when operating with less than 9°C of superheat for R-22 (7°C for R-407c). These droplets were also seen graphically as spikes in the evaporator exit temperature reading. It is postulated that this phenomena could be due to maldistribution.

The other problem which surfaced during this investigation is oil hold-up in the evaporator at very low mass flux. This condition may starve the compressor of needed lubrication, not to mention that this condition penalizes thermal performance due to loss of heat transfer area. This problem could be related to the two compressor failures of this investigation. The mass of oil held-up in the evaporator corresponded to up to 35% of the volume of refrigerant channels for some cases.

Effect of fractionation (and maldistribution in some cases) are expressed through UA value. It is imperfect because it is affected by temperature glide and sometime unequal superheated zones. More precise measurement might be change in heat transfer coefficient in two phase region.

Chapter 8.0 Data Reduction

8.1. Determination of Mass Fractions using the Gas Chromatograph

Samples were analyzed using a Perkin Elmer Autosystem Gas Chromatograph utilizing a thermal conductivity detector (TCD). Carrier gas was zero grade hydrogen, at least 99.995% pure. The gas chromatograph was allowed to warm up and carrier gas flow was allowed to equilibriate for at least 45 minutes prior to calibration.

Calibration was completed by analyzing pure components of R-32, R-125, and R-134a. The test chamber was bled with the refrigerant being sampled and allowed to reach atmospheric pressure before samples were taken. Since the sample volume, test chamber temperature, and the atmospheric pressure were known, the weight of the smaple taken was easily determined. The gas chromatograph outputs the results as an area for each component corresponding to differences in conductivity between the carrier gas and the sample gas. This area is directly related to the weight of the sample taken. Because the weight of the sample is known, a weight factor is determined for each component which is used when analyzing R-407c samples. The weight factors are determined using the formulas below where w is the weight factor, ρ is the density, V is the volume of the test chamber, and A is the result output by the gas chromatograph.

$$w_{R-32} = \frac{r_{R-32} \cdot V}{A_{R-32}}$$

$$w_{R-125} = \frac{r_{R-125} \cdot V}{A_{R-125}}$$

$$w_{R-134a} = \frac{r_{R-134a} \cdot V}{A_{R-134a}}$$

When R-407c samples are analyzed, three areas will be output by the gas chromatograph. The areas are converted to mass fraction, denoted by x, by using the following equations.

$$x_{R-32} = \frac{w_{R-32} \cdot A_{R-32}}{w_{R-32} \cdot A_{R-32} + w_{R-125} \cdot A_{R-125} + w_{R-134a} \cdot A_{R-134a}}$$

$$x_{R-125} = \frac{w_{R-125} \cdot A_{R-125}}{w_{R-32} \cdot A_{R-32} + w_{R-125} \cdot A_{R-125} + w_{R-134a} \cdot A_{R-134a}}$$

$$x_{R-134a} = \frac{w_{R-134a} \cdot A_{R-134a}}{w_{R-32} \cdot A_{R-32} + w_{R-125} \cdot A_{R-125} + w_{R-134a} \cdot A_{R-134a}}$$

8.2. Determination of Heat Exchanged

Heat exchanged is determined on both the water and refrigerant side using the following equations:

$$Q_w = M_w c_p \left(T_{w,in} - T_{w,out}\right) \qquad \text{Equation 1}$$

$$Q_r = M_r \left(h_{r,out} - h_{r,in} \right)$$ Equation 2

Mass flow rates are acquired using coriolis type mass flow meters on both the water and refrigerant side. The water specific heat is calculated at the average of the inlet and outlet water temperatures, which are acquired with thermocouples. The enthapy at the outlet of the evaporator is calculated for data with superheat differently than data without superheat. With superheat, the evaporator outlet enthalpy is a function of the temperature and pressure after the mixer. For data without superheat, the enthalpy at the outlet of the heater is determined first as a function of temperature and pressure. The heat exchanged in the heater is measured using a watt transducer which allows the enthalpy at the outlet of the evaporator to be determined as follows:

$$h_{evap,out} = \frac{\left(Q_{heat} - M_r h_{heat,out} \right)}{M_r}$$ Equation 3

The evaporator inlet enthalpy is calculated as a function of the temperature and pressure at the inlet to the expansion valve. All pressures and temperatures are aquired with pressure transducers and thermocouples, respectively.

8.3. Determination of the Overall Heat Transfer Coefficient

The overall heat transfer coefficient is determined by the following formula:

$$U = \frac{Q_w}{A_{evap} LMTD}$$ Equation 4

The water side heat exchanged was used in the calculation of the overall heat transfer coefficient due to a uncertainty in the R-407c refrigerant composition.

The log mean temperature difference, or LMTD, is calculated as a function of the inlet and outlet water temperatures, inlet refrigerant temperature, and saturated refrigerant outlet temperature.

$$LMTD = \frac{\left(T_{w,in} - T_{r,out,sat} \right) - \left(T_{w,out} - T_{r,in} \right)}{\ln\left[\left(T_{w,in} - T_{r,out,sat} \right) \Big/ \left(T_{w,out} - T_{r,in} \right) \right]}$$ Equation 5

It was decided to use the saturated outlet temperature calculated as a function of the evaporator outlet pressure. The refrigerant inlet temperature is determined as a function of the inlet pressure and enthalpy. The inlet and outlet water temperatures are directly measured with thermocouples.

8.4. Determination of the Water Side Heat Transfer Coefficient

The single phase correlation shown below was provided by SWEP to determine water side heat transfer coefficient.

$$\mathrm{Pr} = \frac{mCp}{k}$$ Equation 6

$$y = 0.333\exp\left(\frac{6.4}{\mathrm{Pr}+30}\right)$$ Equation 7

$$\mathrm{Re} = \frac{M_r C_{\mathrm{Re}}}{m n_{pi}}$$ Equation 8

$$\mathrm{Nu} = C\,\mathrm{Re}^{n}\,\mathrm{Pr}^{y}$$ Equation 9

$$h = \mathrm{Nu}k / d_h$$ Equation 10

The coefficients in the Nusselt number calculation are shown in the table below.

Table 8.1 Coefficients in single phase heat transfer coefficient correlation used for water

	C	n
Re<10	0.61649	0.33
10<Re<20	0.38305	0.54
20<Re<40	0.04995	1.22
40<Re<80	0.63676	0.53
Re>80	0.330	0.68

Trane, Co., conducted experiments to determine the validity of this correlation. They determined that this correlation predicted heat transfer coefficients within 3.5% of their lab results.

8.5. Kedzierski's Method

An alternative method of calculating LMTD, as used by Kedzierski (1997), was evaluated and compared to the method in Section 8.3. His method is as follows:

$$\Delta T = \frac{q_v \Delta T_v + q_{2f} \Delta T_{2f}}{q_T}$$ Equation 11

Where,

ΔT Average temperature difference

ΔT_v Log mean temperature difference for the superheated zone

ΔT_{2f} Log mean temperature difference for the two phase zone

q_T Total heat transfer

q_v Heat transfer associated with the superheated zone

q_{2f} Heat transfer associated with the two phase zone

Kedzierski's method does not provide significantly different results than using the method of Section 8.3.

Chapter 9.0 Error Analysis

9.1. Fractionation Determination

There are many possible sources of error encountered when measuring the composition of ternary mixtures. To begin with, it is essential that the system was maintained leak-proof since R-407c is a zeotropic mixture. Vapor leaks of zeotropic mixtures can have significant effects on overall system composition and performance. Thus, composition measurements of vapor and liquid R-407c were taken prior to operation and data acquisition to ensure that composition shifts due to vapor leaks had not occurred (see figures in Attachment C). Other error could be introduced during sampling of refrigerant, especially if sampling liquid refrigerant. To reduce sampling error, vapor samples were taken when possible.

The final source of error is instrument uncertainty. A Perkin Elmer Autosystem GC was used to measure composition. Per the instrument specification sheet, error in measurements for this instrument is on the order of 0.5%. It was desired to verify this uncertainty by measuring the composition of a known mixture (33.1% R-32, 50.4% R-125 and 16.5% R-134a). Three measurements were made in a 1 hour time span, the results of which are shown in the following table:

Table 9.1 Measurement of composition of known mixture

Sample	R-32 Composition	R-125 Composition	R-134a Composition
Known Mixture	33.1	50.4	16.5
1	33.1	50.9	15.9
2	33.1	50.9	16.0
3	33.1	50.9	16.0

The results shown in Table 9.1 indicate that the gas chromatograph measurements are repeatable and measurements are within 0.5%. Therefore, this investigation will consider composition measurements to be accurate to within 0.5%.

9.2. Thermal Performance Calculations

The “uncertainty propagation” feature in EES was used to determine instrument propagation error for the calculated U-values presented in this investigation. EES uses a method for determining this uncertainty propagation as described in NIST Technical Note 1297 (Taylor and Kuyatt, 1994). Instrument propagation error for U-value is presented in Appendix A and is typically in the range from 3% to 4%.

List of References

1. DuPont, Transport Properties of AC9000 Refrigerants.
2. DuPont, Thermodynamic Properties of SUVA AC9000 Refrigerant.
3. Kedzierski, Mark A., "Effect of Inclination on the Performance of a Compact Brazed Plate Condenser and Evaporator," Heat Transfer Engineering, vol. 18, no. 3, 1997.
4. Martz, W. L. and Jacobi, A. M., "Refrigerant-Oil Mixtures and Local Composition Modeling," 1994.
5. SWEP International AB, Compact Brazed Heat Exchangers for Refrigerant Applications, Technical Handbook, 1992.
6. Taylor B.N. and Kuyatt, C.E., Guidelines for Evaluating and Expressing the Uncertainty of NIST Measurement Results, National Institute of Standards and Technology Technical Note 1297, 1994.
7. Autosystem XL Gas Chromatograph Specification Sheet, Perkin Elmer Instruments, 2000.

For further reading:

8. Bayani, A., "Online Measurement of Oil Concentrations of R-134a/Oil Mixtures with a Density Flowmeter," HVAC&R Research, vol. 1, no. 3, July 1995.
9. Biancardi, F., "Investigation into the Fractionation of Refrigerant Blends," Presented at 1996 International Compressor Engineering Conference at Purdue, July 1996.
10. Biancardi, F., "Modeling and Testing of Fractionation Effects with Refrigerant Blends in an Actual Residential Heat Pump System," ASHRAETransactions: Symposia.
11. Bivens, Donald B., "HCFC-22 Alternative for Air Conditioners and Heat Pumps," ASHRAE Transactions: Symposia.
12. Bivens, Donald B., "Performance of R-32/R-125/R-134a Mixtures in Systems with Accumulators or Flooded Evaporators," ASHRAE Transactions: Symposia.
13. Corr, Stuart, "Composition Shifts of Zeotropic HFC Refrigerants in Service," ASHRAE Transactions: Symposia.
14. Judge, John, "A Heat Exchanger Model for Mixtures and Pure Refrigerant Cycle Simulations," International Journal of Refrigeration, vol. 20, no. 4, 1997.
15. Kandlikar, S. G., "A General Correlation for Saturated Two-Phase Flow Boiling Heat Transfer Inside Horizontal and Vertical Tubes," Journal of Heat Transfer, vol. 112, 1990.
16. Kim, Minn Soo, "Simulation of a Leak/Recharge Process of Refrigerant Mixtures," HVAC&R Research, vol. 1, no. 3, July 1995.
17. Kruse, Horst, "Concentration Shift When Using Refrigerant Mixtures," ASHRAE Transactions: Symposia.
18. Wei, Chung-szu, "System Performance of a Split-Type Unit having R-22 and R-407c as Working Fluids," ASHRAE Transactions: Symposia.

Appendix A: Heat Transfer Data

All of the heat transfer data collected in this study are listed in Appendix A. Also included are the parameters calculated for analysis.

Table A.1 Thermal performance data summary for Experiment 1 (R-22)

Experiment 1 - R-22

HX A: Three Ton Evaporator

Measured Values										Calculated Values					
M_r	M_w	$P_{r,txv}$	$P_{r,out}$	$T_{r,txv}$	$T_{r,in}$	$T_{r,out}$	$T_{r,mix}$	$T_{w,in}$	$T_{w,out}$	$T_{r,sat,out}$	Q_r	Q_w	h_w	U	
[g/s]	[g/s]	[kPa]	[kPa]	[°C]	[°C]	[°C]	[°C]	[°C]	[°C]	[°C]	[kW]	[kW]	[W/(m^2-°C)]	[W/(m^2-°C)]	
27.7	N/A	1536	532.1	15.6	2.0	11.8	N/A	12.0	7.0	2.1	5.4	N/A	5314	576	±19
30.8	275.8	1487	529.0	15.7	2.2	12.1	12.0	12.1	6.9	1.9	6.0	6.1	5592	624	±20
32.7	291.9	1583	530.7	15.2	2.3	12.0	11.9	12.1	6.8	2.0	6.4	6.5	5808	681	±22
39.5	N/A	1444	529.4	15.8	2.0	11.6	N/A	11.9	7.1	1.9	7.7	N/A	6914	802	±27
41.7	391.1	1441	523.3	15.4	2.1	11.7	11.3	11.9	6.8	1.6	8.1	8.3	7080	824	±27
45.8	435.0	1409	521.5	15.5	2.1	11.7	11.1	11.9	6.9	1.5	8.9	9.1	7613	890	±30
51.9	484.5	1376	519.2	15.6	2.2	11.6	10.7	12.1	7.0	1.3	10.0	10.3	8204	976	±32
26.6	225.8	1575	529.3	32.4	2.1	12.1	12.1	12.1	7.0	1.9	4.6	4.8	4882	477	±16
27.4	N/A	1544	535.8	32.4	2.3	11.9	N/A	12.1	7.0	2.3	4.7	N/A	4805	518	±17
34.6	N/A	1482	532.2	32.1	2.1	10.4	N/A	12.0	6.9	2.1	6.0	N/A	5648	651	±21
44.6	372.5	1418	525.1	32.3	2.2	11.5	10.9	11.9	6.8	1.7	7.7	7.9	6849	802	±27
46.2	389.5	1405	522.7	32.3	2.2	11.6	11.0	12.0	6.9	1.5	8.0	8.2	7068	802	±27
49.7	414.8	1380	520.0	32.2	2.1	11.8	10.9	12.1	7.0	1.4	8.6	8.9	7387	832	±27
55.6	478.5	1352	515.6	32.4	2.0	11.6	10.3	12.0	7.1	1.1	9.6	9.8	8134	905	±30

Table A.2 Thermal performance data summary for Experiment 1 (R-407c)

Experiment 1 - R-407c
HX A: 3 Ton Evaporator

Measured Values											Calculated Values					
M_r [g/s]	M_w [g/s]	$P_{r,txv}$ [kPa]	$P_{r,in}$ [kPa]	$P_{r,out}$ [kPa]	$T_{r,txv}$ [°C]	$T_{r,in}$ [°C]	$T_{r,out}$ [°C]	$T_{r,mix}$ [°C]	$T_{w,in}$ [°C]	$T_{w,out}$ [°C]	$T_{r,sat,out}$ [°C]	Q_r [kW]	Q_w [kW]	h_w [W/(m2-°C)]	U [W/(m2-°C)]	
24.1	232.0	1708	N/A	530.1	15.6	0.06	12.0	12.0	12.0	7.0	4.4	4.8	4.8	5106	456	±14
31.0	301.3	1635	N/A	523.8	15.6	-0.24	12.0	11.9	12.1	7.2	4.0	6.2	6.2	6107	548	±16
35.0	324.2	1642	N/A	528.2	15.7	0.27	11.8	11.5	12.2	7.0	4.3	7.0	7.0	6420	650	±19
40.7	387.9	1660	543.2	534.8	15.6	0.04	11.3	11.1	12.1	7.0	4.6	8.1	8.2	7246	807	±24
48.2	477.6	1617	533.0	523.4	15.6	-0.32	10.9	10.4	11.9	7.1	4.0	9.5	9.7	8336	872	±27
52.6	484.1	1646	542.1	531.9	15.6	0.04	6.4	8.9	12.1	7.0	4.5	10.4	10.5	8430	993	±29
57.1	527.2	1636	N/A	525.5	15.6	0.04	5.9	7.2	12.0	6.9	4.1	11.2	11.3	8921	1049	±31
26.5	222.6	1697	536.6	529.5	32.2	0.37	11.9	12.0	12.0	7.0	4.3	4.6	4.7	4966	460	±14
31.7	272.9	1632	N/A	527.3	32.2	0.58	11.2	11.2	11.9	7.0	4.2	5.5	5.6	5694	548	±17
37.2	311.9	1466	N/A	531.0	32.3	0.36	11.3	11.1	12.1	7.1	4.4	6.4	6.5	6246	647	±19
37.7	318.9	1440	539.3	530.7	32.3	0.12	11.6	11.4	12.0	7.1	4.4	6.5	6.6	6341	651	±20
41.6	347.7	1699	540.8	532.0	32.2	0.67	6.0	8.4	11.9	7.0	4.5	7.1	7.2	6717	728	±22
49.2	392.0	1687	534.7	524.7	32.2	0.55	5.6	7.7	12.1	7.0	4.1	8.3	8.4	7298	802	±27
50.0	405.1	1838	534.7	524.1	32.3	0.58	5.5	7.0	12.0	7.0	4.0	8.4	8.4	7457	815	±25
53.9	436.0	1703	N/A	522.3	32.2	0.75	5.7	7.3	12.1	7.1	3.9	9.1	9.1	7846	856	±26
60.1	488.2	1645	543.2	530.9	32.3	0.50	5.7	8.1	12.0	7.0	4.4	10.2	10.2	8465	1039	±32

Table A.3 Thermal performance data summary for Experiment 2 (R-22)

Experiment 2 - R-22

HX B: 20 Ton Evaporator w/o Distributor

Measured Values											Calculated Values				
M_r [g/s]	M_w [g/s]	$P_{r,txv}$ [kPa]	$P_{r,in}$ [kPa]	$P_{r,out}$ [kPa]	$T_{r,txv}$ [°C]	$T_{r,in}$ [°C]	$T_{r,out}$ [°C]	$T_{r,mix}$ [°C]	$T_{w,in}$ [°C]	$T_{w,out}$ [°C]	$T_{r,sat,out}$ [°C]	Q_r [kW]	Q_w [kW]	h_w [W/(m2-°C)]	U [W/(m2-°C)]
29.6	272.9	1548	536.1	534.9	15.6	2.20	11.8	11.8	12.0	7.0	2.25	5.7	5.7	1955	112 ±4
37.9	352.8	1462	537.6	536.4	15.5	2.25	12.1	11.7	12.0	7.0	2.34	7.4	7.4	2241	145 ±5
43.2	404.7	1414	537.8	536.6	15.6	2.25	12.1	11.6	11.9	7.0	2.35	8.4	8.4	2460	167 ±6
49.1	446.5	1376	537.1	535.9	15.6	2.24	12.1	11.4	12.0	6.9	2.31	9.5	9.5	2631	189 ±6
53.7	496.0	1352	536.9	535.7	15.7	2.21	12.0	11.2	11.9	7.0	2.29	10.4	10.3	2825	205 ±7
61.8	561.9	1316	536.6	535.4	15.6	2.23	12.1	10.8	12.0	6.9	2.28	11.9	11.9	3076	236 ±8
26.8	221.0	1739	538.5	537.3	32.2	2.35	11.6	11.8	12.0	7.0	2.39	4.6	4.6	1749	92 ±3
31.6	255.4	1704	538.8	537.6	32.3	2.37	11.9	11.9	12.0	6.9	2.41	5.5	5.5	1888	110 ±4
37.4	314.5	1660	536.1	534.9	32.2	2.19	12.1	11.8	11.9	7.0	2.25	6.5	6.5	2107	127 ±4
39.9	333.1	1595	536.5	535.3	32.3	2.20	12.2	11.8	12.0	7.1	2.27	6.9	6.9	2174	134 ±4
42.0	339.1	1658	535.1	533.9	32.3	2.21	11.9	11.5	12.0	6.9	2.19	7.3	7.2	2194	142 ±4
48.2	405.3	1547	536.5	535.3	32.2	2.19	12.1	11.4	11.9	7.0	2.27	8.3	8.3	2462	164 ±5
55.1	453.2	1567	536.4	535.2	32.1	2.23	12.2	11.2	12.0	7.0	2.27	9.5	9.5	2660	186 ±6
56.6	469.6	1674	535.6	534.4	32.2	2.23	12.1	11.1	12.1	7.1	2.22	9.8	9.8	2725	187 ±6
59.1	481.9	1504	537.6	536.3	32.3	2.31	12.2	11.0	12.1	7.0	2.33	10.2	10.2	2774	200 ±7

Table A.4 Thermal performance data summary for Experiment 2 (R-407c)

Experiment 2 - R-407c
HX B: 20 Ton Evaporator w/o Distributor

Measured Values											Calculated Values					
M_r [g/s]	M_w [g/s]	$P_{r,txv}$ [kPa]	$P_{r,in}$ [kPa]	$P_{r,out}$ [kPa]	$T_{r,txv}$ [°C]	$T_{r,in}$ [°C]	$T_{r,out}$ [°C]	$T_{r,mix}$ [°C]	$T_{w,in}$ [°C]	$T_{w,out}$ [°C]	$T_{r,sat,out}$ [°C]	Q_r [kW]	Q_w [kW]	h_w [W/(m2-°C)]	U [W/(m2-°C)]	
35.7	332.1	1527	534.9	532.8	15.57	-1.31	12.2	11.9	11.97	6.96	4.5	7.1	7.0	2170	120	±4
40.6	376.1	1488	538.6	536.6	15.55	-1.14	12.1	11.7	11.99	6.93	4.7	8.1	8.0	2341	140	±4
46.2	432.4	1443	535.0	532.9	15.57	-1.48	12.1	11.2	12.05	7.05	4.5	9.2	9.1	2576	152	±5
52.1	492.3	1417	537.7	535.6	15.61	-1.22	12.1	11.2	12.01	7.03	4.7	10.4	10.3	2813	178	±5
57.6	542.7	1389	535.0	532.9	15.64	-1.44	12.0	10.6	11.91	6.93	4.5	11.4	11.3	3002	194	±6
61.2	561.4	1374	534.6	532.6	15.60	-1.54	12.1	10.7	12.01	6.88	4.5	12.1	12.1	3075	204	±6
30.6	248.8	1700	537.3	535.3	32.26	-0.76	12.0	11.0	11.96	6.97	4.7	5.3	5.2	1861	93	±3
33.7	273.1	1605	535.1	533.1	32.25	-0.95	12.0	9.2	12.00	7.01	4.5	5.7	5.7	1956	100	±3
55.8	457.0	1742	538.6	536.5	32.22	-0.76	12.0	9.8	11.97	6.99	4.7	9.5	9.5	2673	171	±5
60.4	496.4	1739	536.6	534.5	32.27	-0.74	12.1	10.7	12.02	7.01	4.6	10.4	10.4	2829	186	±6

Table A.5 Thermal performance data summary for Experiment 3 (R-22)

Experiment 3 - R-22

HX C: 20 Ton Evaporator w/ Distributor

Measured Values											Calculated Values							
M_r [g/s]	M_w [g/s]	$P_{r,txv}$ [kPa]	$P_{r,in}$ [kPa]	$P_{r,out}$ [kPa]	$T_{r,txv}$ [°C]	$T_{r,in}$ [°C]	$T_{r,out}$ [°C]	$T_{r,mix}$ [°C]	$T_{w,in}$ [°C]	$T_{w,out}$ [°C]	$T_{r,sat,out}$ [°C]	$T_{r,dist}$ [°C]	$P_{r,dist}$ [kPa]	Q_r [kW]	Q_w [kW]	h_w [W/(m2-°C)]	U [W/(m2-°C)]	
31.9	291.8	1749	537.4	536.2	15.5	2.6	12.0	12.0	12.1	7.0	2.3	2.4	537.4	6.2	6.2	2027	121	±4
37.9	346.7	1696	537.4	536.2	15.6	2.7	11.8	11.6	12.0	6.9	2.3	2.4	537.4	7.3	7.4	2220	146	±5
43.4	397.9	1635	537.1	535.3	15.5	2.7	10.7	10.7	11.9	7.0	2.3	2.3	536.5	8.4	8.2	2431	165	±5
54.4	499.3	1538	536.1	534.8	15.5	2.9	11.7	11.1	12.2	7.1	2.2	2.3	536.0	10.5	10.7	2845	201	±7
61.9	546.1	1497	538.7	536.9	15.7	3.2	11.4	10.4	12.1	6.9	2.4	2.4	538.1	11.9	11.9	3021	238	±8
27.4	224.7	1677	538.6	536.5	32.2	2.6	11.8	11.9	12.1	7.0	2.3	2.4	537.7	4.7	4.8	1765	93	±3
29.4	240.8	1609	528.2	526.1	32.1	2.1	11.9	11.9	12.0	7.1	1.7	1.8	527.3	5.1	4.9	1830	92	±3
33.9	283.3	1583	538.9	536.7	32.2	2.7	11.6	11.5	12.0	7.0	2.4	2.4	537.9	5.9	5.9	1995	116	±4
38.2	315.6	1413	530.8	528.6	32.2	2.3	11.9	11.7	12.1	7.1	1.9	2.0	529.9	6.6	6.6	2113	121	±4
42.2	357.8	1513	537.7	535.6	32.2	2.8	11.7	11.4	12.0	7.1	2.3	2.4	536.8	7.3	7.3	2264	142	±5
44.6	372.4	1624	537.7	536.5	32.3	3.0	11.5	11.2	12.0	7.1	2.3	2.4	537.7	7.7	7.6	2326	151	±5
49.6	410.7	1396	522.3	520.2	32.2	2.2	11.7	11.2	12.0	7.0	1.4	1.5	521.4	8.6	8.6	2486	148	±5
50.6	420.3	1713	536.0	534.7	32.2	3.1	11.4	10.8	12.1	7.0	2.2	2.3	535.9	8.7	9.0	2528	169	±6
55.9	463.2	1833	536.5	535.2	32.2	3.2	11.6	10.8	12.1	7.1	2.3	2.3	536.5	9.6	9.7	2701	186	±6

Table A.6 Thermal performance data summary for Experiment 3 (R-407c)

Experiment 3 - R-407c
HX C: 20 Ton Evaporator w/ Distributor

Measured Values											Calculated Values						
M_r [g/s]	M_w [g/s]	$P_{r,txv}$ [kPa]	$P_{r,in}$ [kPa]	$P_{r,out}$ [kPa]	$T_{r,txv}$ [°C]	$T_{r,in}$ [°C]	$T_{r,out}$ [°C]	$T_{r,mix}$ [°C]	$T_{w,in}$ [°C]	$T_{w,out}$ [°C]	$T_{r,sat,out}$ [°C]	$T_{r,dist}$ [°C]	$P_{r,dist}$ [kPa]	Q_r [kW]	Q_w [kW]	h_w [W/(m2-°C)]	U [W/(m2-°C)]
24.3	229.1	1707	N/A	533.6	15.7	0.18	12.0	12.0	12.0	7.0	4.6	-1.03	534.8	4.8	4.8	1783	83 ±2
31.0	283.9	1688	549.3	536.2	15.8	-0.28	11.9	12.0	12.0	6.9	4.7	-0.88	537.4	6.2	6.1	1997	108 ±3
38.3	371.4	1699	545.4	534.5	15.7	-0.56	11.8	11.7	12.0	7.1	4.6	-0.98	535.7	7.6	7.6	2321	132 ±4
44.4	421.2	1664	548.4	536.2	15.6	-0.34	11.7	11.5	12.0	7.0	4.7	-0.89	537.4	8.8	8.8	2529	156 ±5
51.9	480.6	1634	549.3	534.7	15.7	-0.12	11.7	11.2	12.0	6.9	4.6	-0.97	535.9	10.3	10.2	2766	180 ±5
59.2	539.9	1584	554.0	537.3	15.7	0.15	11.4	10.7	12.1	6.9	4.8	-0.83	538.5	11.7	11.6	2997	208 ±6
25.8	209.5	1720	535.7	534.4	32.2	-0.55	11.8	11.9	11.9	6.9	4.6	-0.21	535.7	4.5	4.4	1699	83 ±2
32.3	262.7	1708	536.0	534.7	32.2	-0.31	11.9	11.9	12.0	6.9	4.6	-0.20	535.9	5.6	5.6	1916	104 ±3
37.7	303.8	1653	538.0	536.7	32.2	-0.26	11.7	10.5	12.0	6.9	4.7	-0.09	537.9	6.5	6.5	2070	123 ±4
44.9	363.2	1601	538.5	537.3	32.3	-0.24	11.5	10.5	12.0	7.0	4.8	-0.05	538.5	7.7	7.6	2286	144 ±4
50.6	405.8	1582	536.9	535.6	32.2	-0.05	11.6	9.8	12.0	6.9	4.7	-0.15	536.9	8.7	8.7	2467	162 ±5
61.3	490.2	1717	N/A	533.7	32.3	1.40	10.8	10.0	12.0	6.9	4.6	-0.25	534.9	10.5	10.4	2804	192 ±6

Table A.7 Thermal performance data summary for Experiment 4 (R-22)

Experiment 4 - R-22
HX C: 20 Ton Evaporator w/ Distributor

Measured Values												Calculated Values								
M_r	M_w	$P_{r,txv}$	$P_{r,in}$	$P_{r,out}$	dP_{heat}	$T_{r,txv}$	$T_{r,in}$	$T_{r,out}$	$T_{r,heat}$	$T_{w,in}$	$T_{w,out}$	$T_{r,sat,out}$	$T_{r,dist}$	$P_{r,dist}$	x_{out}	Q_{heat}	Q_r	Q_w	h_w	U
[g/s]	[g/s]	[kPa]	[kPa]	[kPa]	[kPa]	[°C]	[°C]	[°C]	[°C]	[°C]	[°C]	[°C]	[°C]	[kPa]	[%]	[W]	[kW]	[kW]	[W/(m2-°C)]	[W/(m2-°C)]
44.8	338.7	1345	538.1	536.7	58.5	32.2	3.03	2.8	20.4	10.3	5.3	2.4	2.43	535.5	96.6	805	7.3	7.2	2170	193 ±7

Table A.8 Thermal performance data summary for Experiment 4 (R-407c)

Experiment 4 - R-407c
HX C: 20 Ton Evaporator w/ Distributor

Measured Values												Calculated Values								
M_r	M_w	$P_{r,txv}$	$P_{r,in}$	$P_{r,out}$	dP_{heat}	$T_{r,txv}$	$T_{r,in}$	$T_{r,out}$	$T_{r,heat}$	$T_{w,in}$	$T_{w,out}$	$T_{r,sat,out}$	$T_{r,dist}$	$P_{r,dist}$	x_{out}	Q_{heat}	Q_r	Q_w	h_w	U
[g/s]	[g/s]	[kPa]	[kPa]	[kPa]	[kPa]	[°C]	[°C]	[°C]	[°C]	[°C]	[°C]	[°C]	[°C]	[kPa]	[%]	[W]	[kW]	[kW]	[W/(m2-°C)]	[W/(m2-°C)]
34.4	272.4	1667	546.3	536.6	38.5	32.1	-0.79	4.6	22.5	9.0	4.0	4.7	-0.10	535.4	99.7	430	5.8	5.7	1916	184 ±6
45.3	356.5	N/A		534.5	63.4	32.3	-0.01		11.6	9.5	4.5	4.6	-0.21	533.2	99.9	180	7.7	7.5	2217	211 ±7
49.6	409.4	1562	548.5	536.1	76.0	32.1	0.25	9.1	22.3	9.9	5.0	4.7	-0.13	534.9	99.9	514	8.6	8.3	2425	216 ±7

Table A.9 Thermal performance data summary for Experiment 5 (R-22)

Experiment 5 - R-22
HX B: 20 Ton Evaporator w/ Custom Distributor

Measured Values										Calculated Values							
M_r [g/s]	M_w [g/s]	$P_{r,txv}$ [kPa]	$P_{r,out}$ [kPa]	$T_{r,txv}$ [°C]	$P_{r,in}$ [kPa]	$T_{r,out}$ [°C]	$T_{r,mix}$ [°C]	$T_{w,in}$ [°C]	$T_{w,out}$ [°C]	$T_{r,sat,out}$ [°C]	$T_{r,dist}$ [°C]	$P_{r,dist}$ [kPa]	Q_r [kW]	Q_w [kW]	h_w [W/(m2-°C)]	U [W/(m2-°C)]	
30.7	254.3	1532.0	536.4	32.1	537.2	12.03	12.50	13.76	8.74	2.33	2.41	537.6	5.36	5.36	1904.4	84	±3
45.1	374.1	1411.8	533.8	32.2	534.7	12.70	11.94	13.44	8.40	2.18	2.26	535.0	7.88	7.89	2368.1	127	±4
55.1	486.0	1341.7	536.0	32.2	536.9	11.09	9.94	13.60	9.22	2.31	2.38	537.2	9.60	9.62	2843.7	143	±5

Table A.10 Thermal performance data summary for Experiment 5 (R-407c)

Experiment 5 - R-407c
HX B: 20 Ton Evaporator w/ Custom Distributor

Measured Values										Calculated Values							
M_r [g/s]	M_w [g/s]	$P_{r,txv}$ [kPa]	$P_{r,out}$ [kPa]	$T_{r,txv}$ [°C]	$P_{r,in}$ [kPa]	$T_{r,out}$ [°C]	$T_{r,mix}$ [°C]	$T_{w,in}$ [°C]	$T_{w,out}$ [°C]	$T_{r,sat,out}$ [°C]	$T_{r,dist}$ [°C]	$P_{r,dist}$ [kPa]	Q_r [kW]	Q_w [kW]	h_w [W/(m2-°C)]	U [W/(m2-°C)]	
29.2	237.6	1505.1	533.0	32.3	534.0	4.76	8.88	13.55	8.63	4.54	-0.29	534.2	4.99	4.91	1834.9	74	±2
43.4	367.5	1517.4	533.2	32.3	534.2	8.80	10.85	13.70	8.79	4.55	-0.28	534.4	7.50	7.54	2345.4	112	±3
54.9	447.8	1486.6	537.2	32.0	538.1	5.17	8.87	14.59	9.54	4.77	-0.07	538.4	9.43	9.46	2707.2	131	±4

Table A.11 Thermal performance data summary for Experiment 6 (R-22)

Experiment 6 - R-22
HX B: 20 Ton Evaporator w/ Custom Distributor

Measured Values											Calculated Values								
M_r	M_w	$P_{r,txv}$	$P_{r,in}$	$P_{r,out}$	dP_{heat}	$T_{r,txv}$	$T_{r,out}$	$T_{r,heat}$	$T_{w,in}$	$T_{w,out}$	$T_{r,sat,out}$	$T_{r,dist}$	$P_{r,dist}$	x_{out}	Q_{heat}	Q_r	Q_w	h_w	U
[g/s]	[g/s]	[kPa]	[kPa]	[kPa]	[kPa]	[°C]	[°C]	[°C]	[°C]	[°C]	[°C]	[°C]	[kPa]	[%]	[W]	[kW]	[kW]	[W/(m2-°C)]	[W/(m2-°C)]
30.4	234.7	1490.2	535.7	534.8	33.0	32.3	2.53	12.76	13.56	8.57	2.24	2.315	533.59	98.4	348.1	4.96	4.90	1823.1	78 ±2
46.0	367.2	1353.0	537.0	536.2	66.9	32.2	2.61	15.11	12.50	7.57	2.32	2.395	534.99	100.0	484.9	7.66	7.59	2315.8	140 ±4
55.0	443.8	1341.5	534.9	534.0	84.5	32.2	2.44	14.40	12.00	7.14	2.20	2.266	532.79	99.7	614.3	9.13	9.03	2620.5	174 ±6

Table A.12 Thermal performance data summary for Experiment 6 (R-407c)

Experiment 6 - R-407c
HX B: 20 Ton Evaporator w/ Custom Distributor

Measured Values											Calculated Values								
M_r	M_w	$P_{r,txv}$	$P_{r,in}$	$P_{r,out}$	dP_{heat}	$T_{r,txv}$	$T_{r,out}$	$T_{r,heat}$	$T_{w,in}$	$T_{w,out}$	$T_{r,sat,out}$	$T_{r,dist}$	$P_{r,dist}$	x_{out}	Q_{heat}	Q_r	Q_w	h_w	U
[g/s]	[g/s]	[kPa]	[kPa]	[kPa]	[kPa]	[°C]	[°C]	[°C]	[°C]	[°C]	[°C]	[°C]	[kPa]	[%]	[W]	[kW]	[kW]	[W/(m2-°C)]	[W/(m2-°C)]
28.4	227.0	1511.2	533.6	532.6	26.0	32.2	4.27	12.02	12.17	7.42	4.52	-0.314	533.81	96.4	364.0	4.57	4.52	1775.5	79 ±2
43.3	349.5	1515.5	535.4	534.5	57.0	32.2	4.76	15.80	11.93	7.10	4.62	-0.207	535.71	98.3	567.0	7.10	7.06	2228.5	130 ±4
54.8	427.5	1486.6	536.5	535.6	86.9	32.3	4.41	11.83	12.10	7.20	4.69	-0.143	536.81	97.1	732.0	8.80	8.77	2557.6	160 ±5

Appendix B: Composition Data

All of the composition data collected in this study are listed in Appendix B.

Table B. Composition measurement summary for Experiment 1

Experiment 1 - Baseline R-407c Fractionation Data

HX A: 3 Ton Evaporator

Daily Composition - Before Running System							
Day		Liquid			Vapor		
Actual	Plot	%R-32	%R-125	%R134a	%R-32	%R-125	%R134a
12/3/96	0	21.5	23.0	55.5	30.6	29.3	40.1
12/6/96	3	22.4	23.9	53.7	33.7	30.4	35.9
12/9/96	6	21.1	23.0	55.9	30.7	29.1	40.2
12/10/96	7	21.5	23.9	54.6	31.8	30.7	37.5
12/11/96	8	21.3	23.2	55.5	30.7	29.5	39.8
12/12/96	9	21.5	23.1	55.4	31.4	29.7	38.9
AVERAGE		21.6	23.4	55.1	31.5	29.8	38.7

m_r = 27 $T_{r,txv}$ = 32.2°C							
12/9/96		Evaporator			Circulating		
Actual Time	Time (hours)	%R-32	%R-125	%R134a	%R-32	%R-125	%R134a
10:30	0.00	21.1	23.0	55.9	21.1	23.0	55.9
11:30	1.00	20.0	22.6	56.5	21.3	22.8	55.9
1:00	2.50	19.9	21.7	58.4	21.5	22.9	55.5
2:45	4.25	20.1	22.2	57.7	21.3	22.7	56.0
4:10	5.67	20.6	22.3	57.1	21.2	22.7	56.1
5:30	7.00	20.1	21.9	57.9	21.4	22.7	55.9

m_r = 56 $T_{r,txv}$ = 32.2°C							
12/11/96		Evaporator			Circulating		
Actual Time	Time (hours)	%R-32	%R-125	%R134a	%R-32	%R-125	%R134a
9:30	0.00	21.3	23.2	55.5	21.3	23.2	55.5
10:30	1.00	19.3	21.6	59.1	22.1	23.7	54.2
11:30	2.00	19.1	21.5	59.4	22.0	23.6	54.4
1:45	4.25	19.5	21.7	58.8	22.1	23.7	54.2

m_r = 57 $T_{r,txv}$ = 15.6°C							
12/13/96		Evaporator			Circulating		
Actual Time	Time (hours)	%R-32	%R-125	%R134a	%R-32	%R-125	%R134a
11:10	0.00	21.5	23.1	55.4	21.5	23.1	55.4
11:45	0.58	21.8	23.3	54.9	21.7	23.0	55.3
12:45	1.58	20.8	22.5	56.7	22.2	23.4	54.4
2:00	2.83	21.1	22.8	56.1	22.2	23.4	54.4
2:45	3.58	21.2	22.7	56.0	22.2	23.3	54.5

Table B.2 Composition measurement summary for Experiment 2

Experiment 2 - Reduced Mass Flux

HX B - 20 Ton Evaporator w/o Distributor

Daily Composition - Before Running System							
Day		Liquid			Vapor		
Actual	Plot	%R-32	%R-125	%R134a	%R-32	%R-125	%R134a
3/6/97	0	23.1	24.0	52.9	30.0	30.0	40.0
3/7/97	1	23.2	24.3	52.5	35.0	31.1	33.9
3/9/97	3				34.3	30.5	35.2
3/17/97	11	22.3	23.4	54.2	34.6	30.9	34.5
3/20/97	14	23.5	23.8	52.7	27.2	26.6	46.3
AVERAGE		23.0	23.9	53.1	32.2	29.8	38.0

m_r = 30 $T_{r,txv}$ = 32.2°C							
3/9/97		Evaporator			Circulating		
Actual Time	Time (hours)	%R-32	%R-125	%R134a	%R-32	%R-125	%R134a
4:00	0	23.2	24.3	52.5	23.2	24.3	52.5
4:30	0.5	22.1	22.8	55.1	24.7	24.4	50.9
5:00	1	22.2	22.9	54.8	24.5	23.6	51.9
5:30	1.5	21.2	22.3	56.5	25.2	24.8	50.1
6:00	2	21.3	22.1	56.6	23.6	23.8	52.7

m_r = 60 $T_{r,txv}$ = 32.2°C							
3/12/97		Evaporator			Circulating		
Actual Time	Time (hours)	%R-32	%R-125	%R134a	%R-32	%R-125	%R134a
4:45	0.00	23.2	24.3	52.5	23.2	24.3	52.5
5:00	0.25	20.2	21.8	58.0	24.9	24.9	50.2
5:30	0.75	21.0	22.4	56.7	24.9	24.9	50.2
6:00	1.25	19.3	21.1	59.6	23.6	24.1	52.3
6:30	1.75	19.9	21.6	58.6	24.9	24.9	50.2
7:00	2.25	19.6	21.1	59.2	24.5	24.8	50.7

m_r = 30 $T_{r,txv}$ = 15.6°C							
3/20/97		Evaporator			Circulating		
Actual Time	Time (hours)	%R-32	%R-125	%R134a	%R-32	%R-125	%R134a
8:00	0	23.5	23.8	52.7	23.5	23.8	52.7
8:45	0.75	20.1	21.6	58.3	27.0	26.3	46.7
9:30	1.5	20.9	22.3	56.7	23.9	24.1	51.9
10:15	2.25	22.4	23.3	54.4	23.9	24.1	51.9
11:00	3	21.7	22.7	55.6	24.2	24.4	51.4

m_r = 60 $T_{r,txv}$ = 15.6°C							
3/17/97		Evaporator			Circulating		
Actual Time	Time (hours)	%R-32	%R-125	%R134a	%R-32	%R-125	%R134a
4:30	0.00	22.3	23.4	54.2	22.3	23.4	54.2
5:00	0.25	24.5	24.9	50.6	25.6	25.4	49.0
6:00	0.75	19.0	20.8	60.2	24.6	24.8	50.6
6:45	1.25	19.5	21.2	59.3	24.6	24.7	50.7
7:15	1.75	19.2	20.9	59.9	24.6	24.7	50.7

Table B.3 Composition measurement summary for Experiment 3

Experiment 3 - Effect of Distributor

HX C -20 Ton Evaporator w/ Distributor

Daily Composition - Before Running System							
Day		Liquid			Vapor		
Actual	Plot	%R-32	%R-125	%R134a	%R-32	%R-125	%R134a
5/30/97	1	24.7	24.8	50.4	37.5	32.6	29.9
6/2/97	4	24.0	24.4	51.6	36.1	31.6	32.3
6/4/97	6	24.3	25.0	50.8	35.4	31.5	33.1
6/12/97	14	22.6	23.7	53.7	35.7	31.8	32.5
6/13/97	15	22.4	23.7	53.9	36.0	32.3	31.7
6/16/97	18	20.4	24.1	55.5	36.1	31.4	32.5
AVERAGE		23.1	24.3	52.7	36.1	31.9	32.0

m_r = 30 $T_{r,txv}$ = 32.2°C				
6/16/97		Circulating		
Actual Time	Time (hours)	%R-32	%R-125	%R134a
10:45	0.00	23.1	24.3	52.7
11:00	0.25	25.9	25.7	48.4
11:20	0.58	24.1	24.4	51.5
11:40	0.92	23.9	24.4	51.7
12:00	1.25	23.8	24.4	51.8
12:45	2.00	24.0	24.1	51.9

m_r = 60 $T_{r,txv}$ = 32.2°C				
6/4/97		Circulating		
Actual Time	Time (hours)	%R-32	%R-125	%R134a
11:00	0.00	22.4	23.7	53.9
11:15	0.25	23.3	24.1	52.6
11:30	0.50	23.3	24.1	52.6
11:45	0.75	24.7	25.1	50.2
12:00	1.00	24.8	25.1	50.1
12:15	1.25	24.6	25.0	50.3
12:30	1.50	24.9	25.3	49.8
12:45	1.75	24.8	25.2	50.0

m_r = 30 $T_{r,txv}$ = 15.6°C				
6/4/97		Circulating		
Actual Time	Time (hours)	%R-32	%R-125	%R134a
10:00	0	22.4	23.7	53.9
10:10	0.17	23.9	24.4	51.7
10:20	0.33	23.6	24.2	52.1
10:30	0.50	23.6	24.1	52.3
10:40	0.67	23.7	24.2	52.1
10:50	0.83	23.8	24.3	52.0
11:00	1.00	23.7	24.2	52.1
11:10	1.17	23.6	24.0	52.4
11:50	1.83	23.6	24.3	52.1

m_r = 60 $T_{r,txv}$ = 15.6°C				
6/12/97		Circulating		
Actual Time	Time (hours)	%R-32	%R-125	%R134a
11:25	0.00	22.6	23.7	53.7
11:30	0.08	23.8	24.1	52.1
11:45	0.33	25.1	25.0	49.9
12:00	0.58	24.8	24.8	50.5
12:15	0.83	24.7	24.8	50.5
12:30	1.08	24.8	24.8	50.3

Table B.4 Composition measurement summary for Experiment 4

Experiment 4 - Effect of Superheat

HX C -20 Ton Evaporator w/ Distributor, dT_{sup} = 0°C

Daily Composition - Before Running System							
Day		Liquid			Vapor		
Actual	Plot	%R-32	%R-125	%R134a	%R-32	%R-125	%R134a
7/30/97	1	23.3	22.9	53.8	34.1	31.5	34.3
10/10/97	2	21.4	24.4	54.2	31.9	32.4	35.7
AVERAGE		22.3	23.6	54.0	33.0	31.9	35.0

m_r = 25 $T_{r,txv}$ = 32.2°C				
7/30/97		Circulating		
Actual Time	Time (hours)	%R-32	%R-125	%R134a
9:45	0	23.3	22.9	53.8
10:00	0.25	25.9	24.7	49.3
10:30	0.75	26.2	25.1	48.7
11:00	1.25	26.0	25.3	48.8
11:30	1.75	25.8	24.8	49.4
12:00	2.25	24.5	24.0	51.5

m_r = 55 $T_{r,txv}$ = 32.2°C				
10/10/97		Circulating		
Actual Time	Time (hours)	%R-32	%R-125	%R134a
12:45	0.00	22.3	23.6	54.0
1:00	0.25	23.2	24.7	52.1
1:15	0.50	23.7	25.4	50.9
1:45	1.00	24.2	25.9	50.0
2:15	1.50	24.7	26.0	49.3
2:45	2.00	24.6	26.0	49.4

Table B.5 Composition measurement summary for Experiment 5

Experiment 5 - Effect of Downward Flow

HX B - 20 Ton Evaporator w/ Custom Distributor

Daily Composition - Before Running System							
Day		Liquid			Vapor		
Actual	Plot	%R-32	%R-125	%R134a	%R-32	%R-125	%R134a
1/8/98	0	25.1	25.0	49.9	30.3	28.9	40.8
1/9/98	1	23.3	22.9	53.8	31.3	28.8	39.9
AVERAGE		24.2	24.0	51.9	30.8	28.9	40.3

m_r = 30 $T_{r,txv}$ = 32.2°C				
1/8/98		Circulating		
Actual Time	Time (hours)	%R-32	%R-125	%R134a
6:30	0.00	23.3	22.9	53.8
7:00	0.50	23.6	23.9	52.4
7:30	1.00	24.7	23.7	51.6
8:00	1.50	24.5	24.3	51.1
8:30	2.00	23.9	24.4	51.7

m_r = 55 $T_{r,txv}$ = 32.2°C				
1/9/98		Circulating		
Actual Time	Time (hours)	%R-32	%R-125	%R134a
10:30	0.00	23.3	22.9	53.8
10:45	0.25	23.9	24.3	51.7
11:00	0.50	23.9	24.3	51.8
11:30	1.00	24.1	24.0	51.9
12:00	1.50	24.0	24.2	51.8
12:30	2.00	23.9	24.2	51.9

Appendix C: Miscellaneous Figures

Miscellaneous figures not discussed in the main body, but relevant to this study, are presented in this Appendix.

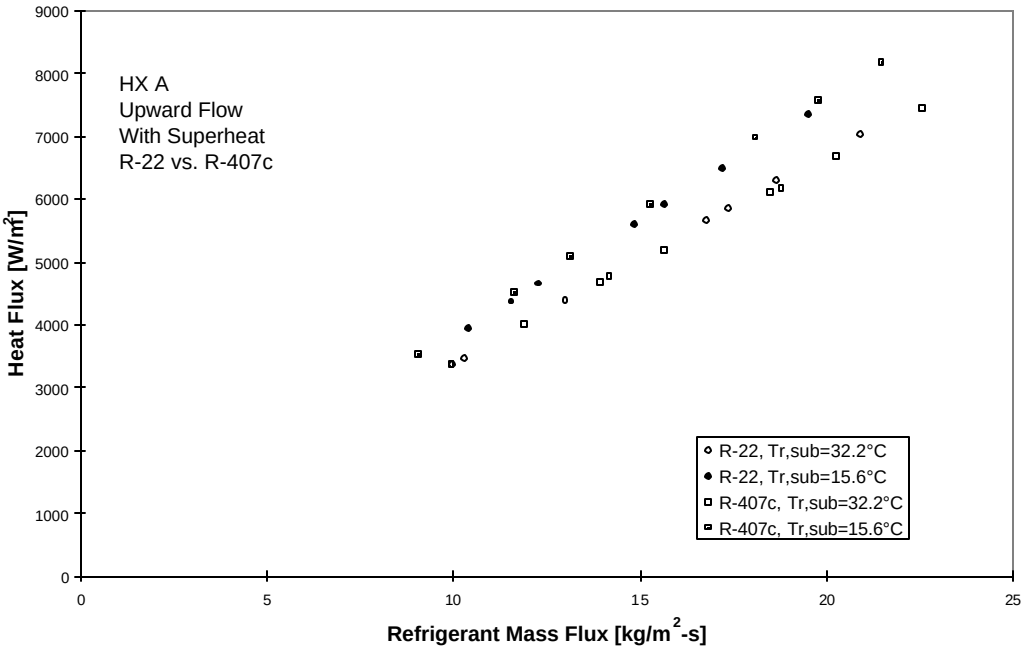

Figure C.1 Heat Flux for Experiment 1

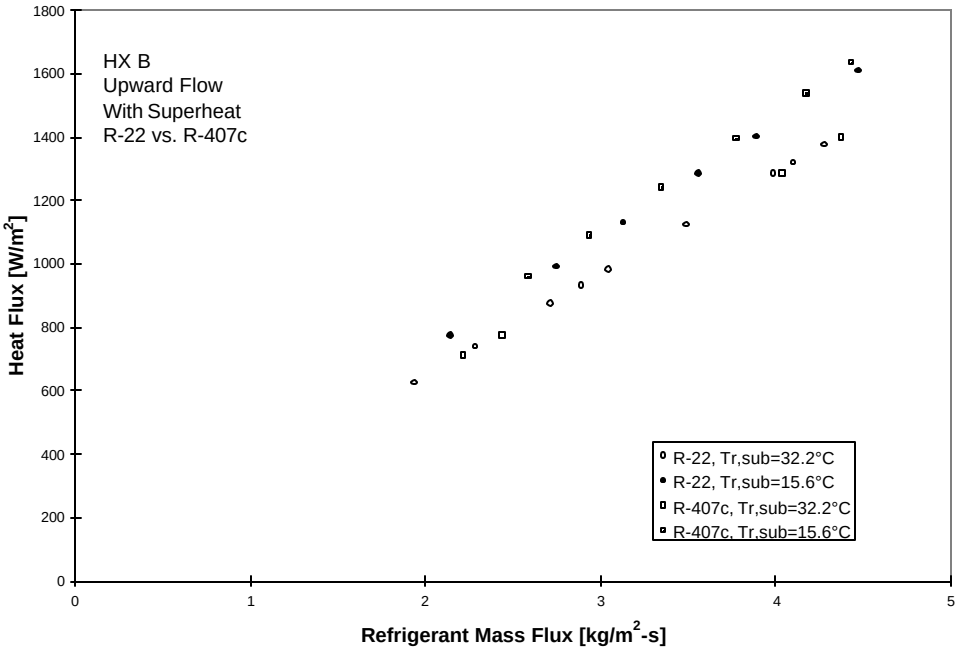

Figure C.2 Heat Flux for Experiment 2

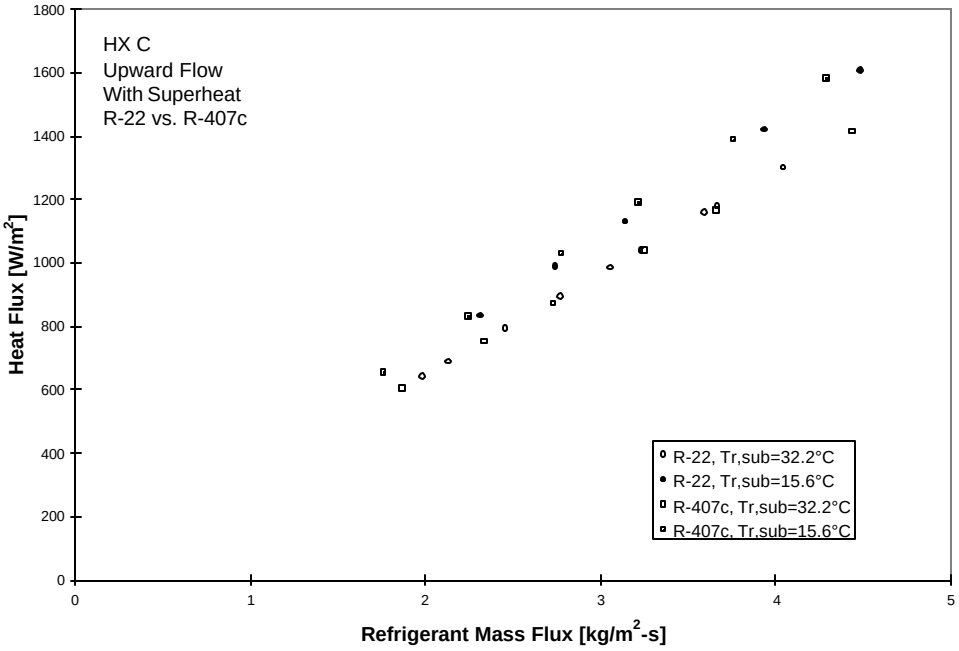

Figure C.3 Heat Flux for Experiment 3

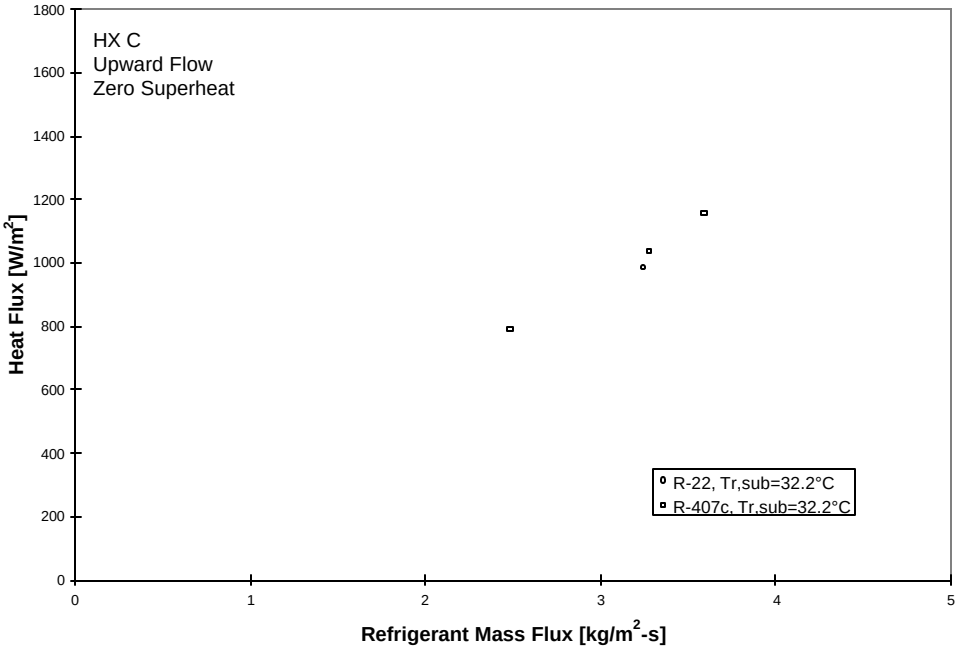

Figure C.4 Heat Flux for Experiment 4

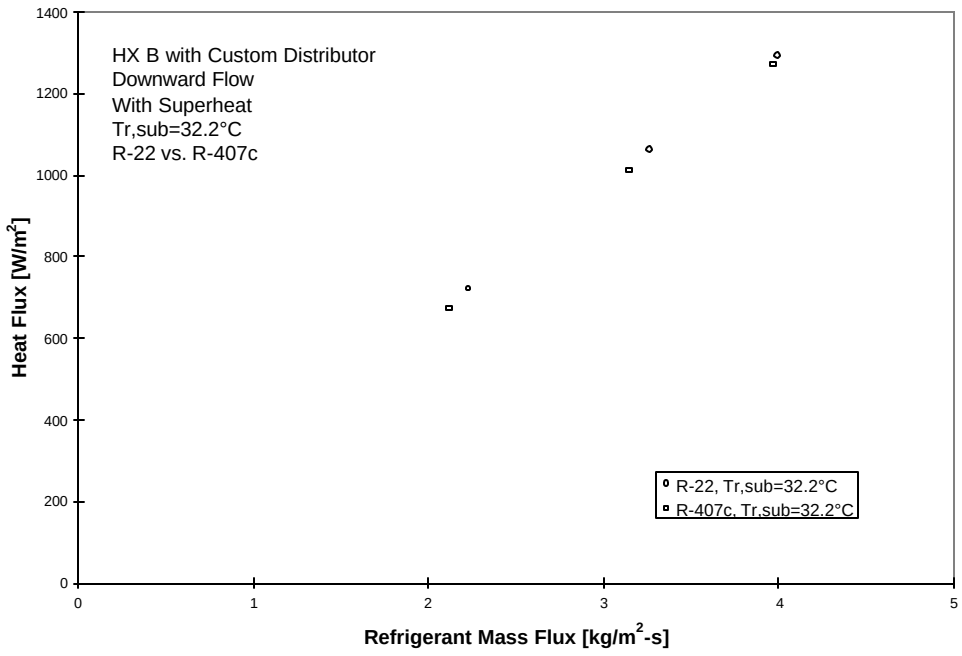

Figure C.5 Heat Flux for Experiment 5

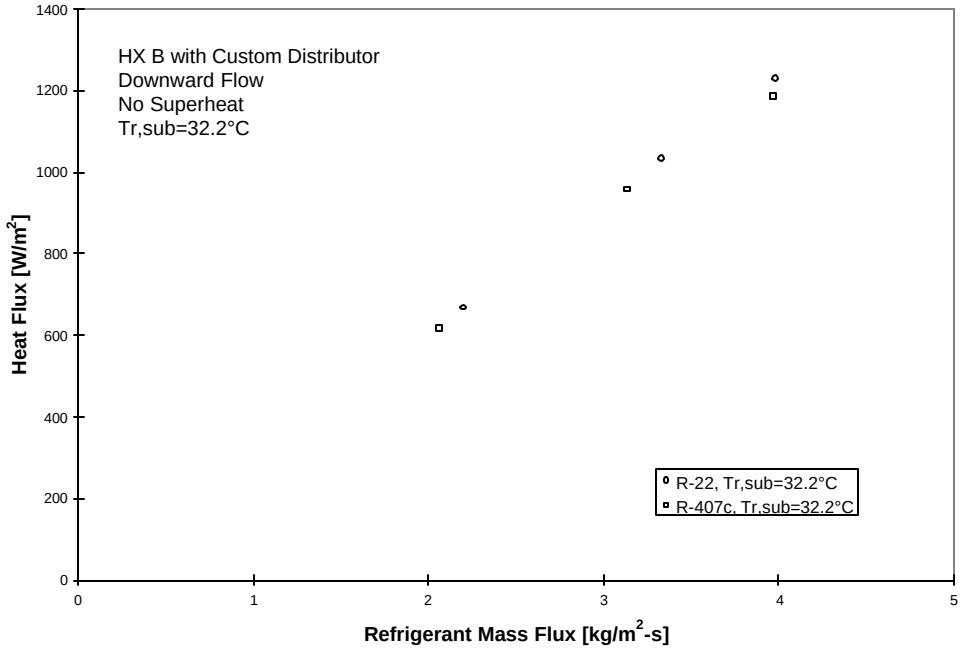

Figure C.6 Heat Flux for Experiment 6

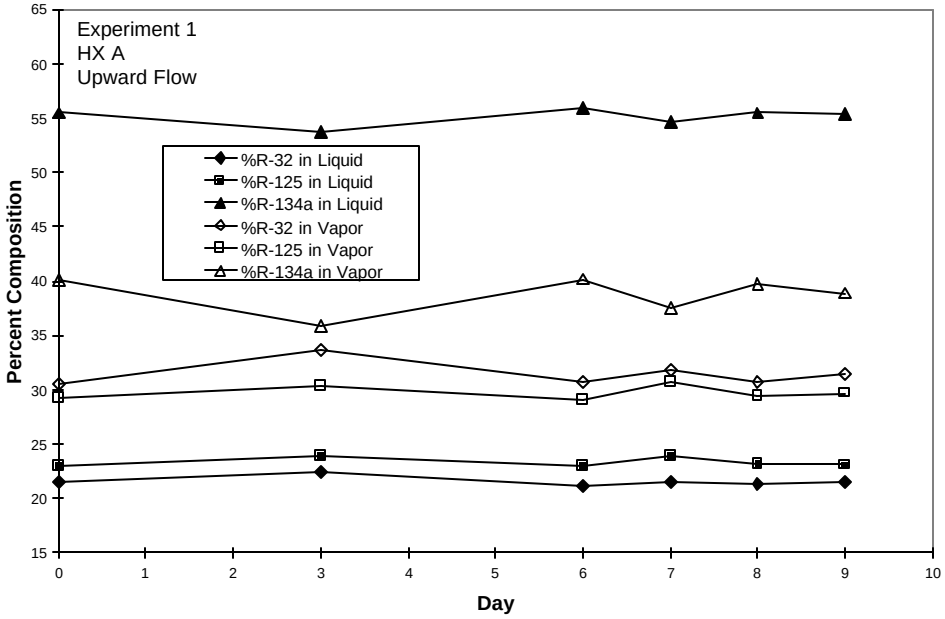

Figure C.7 Daily system composition (system not in operation) for Experiment 1

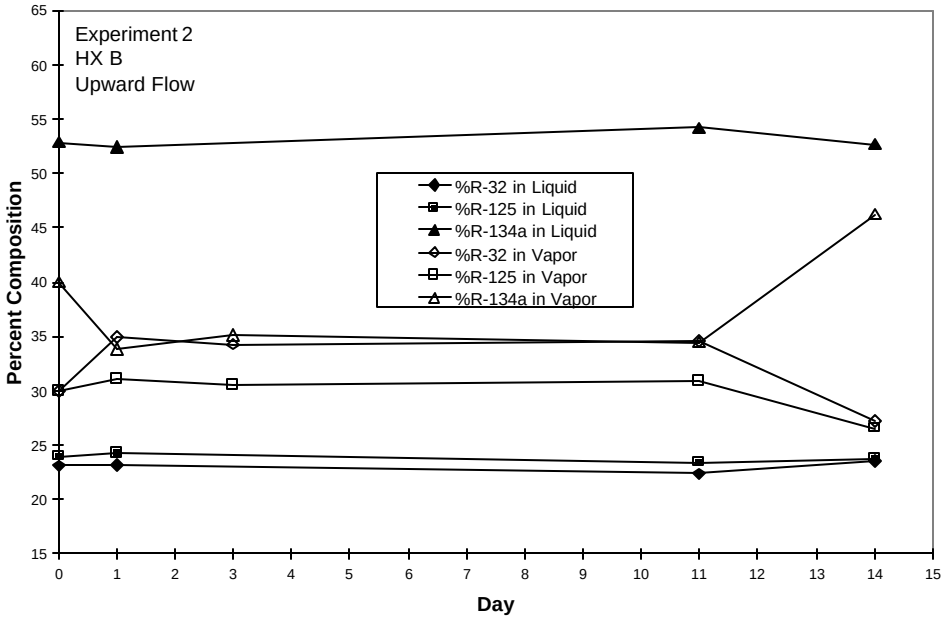

Figure C.8 Daily system composition (system not in operation) for Experiment 2

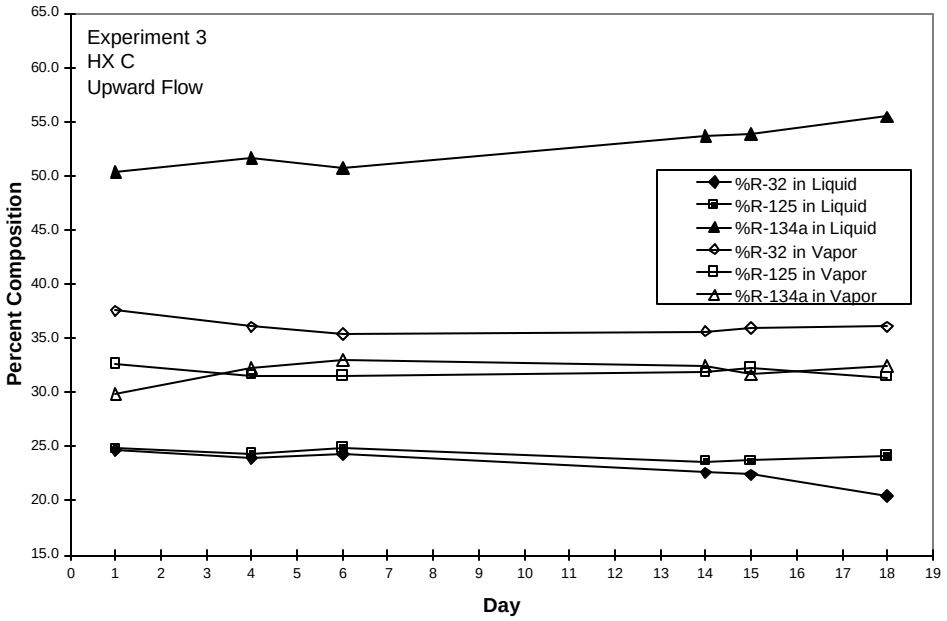

Figure C.9 Daily system composition (system not in operation) for Experiment 3

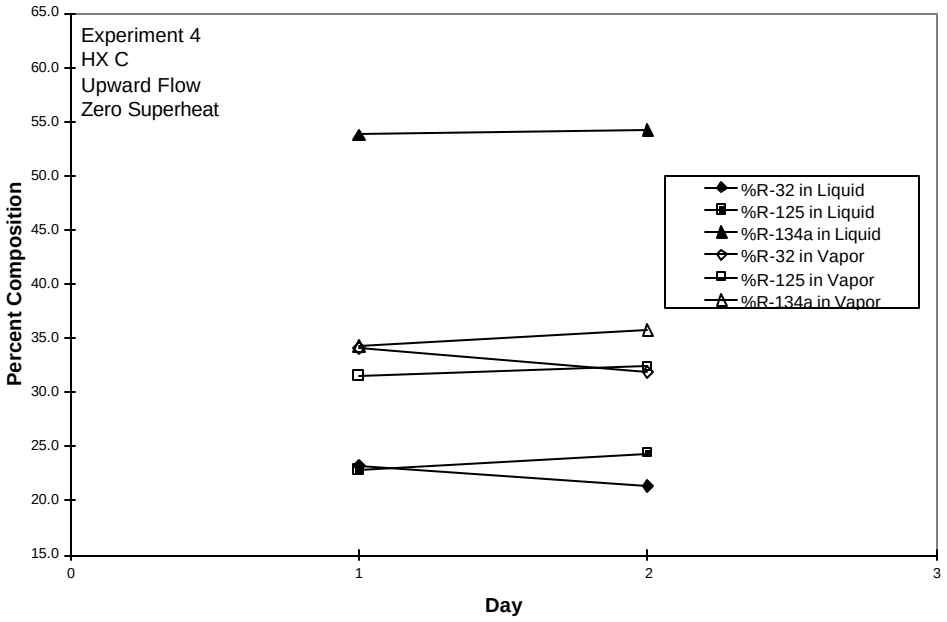

Figure C.10 Daily system composition (system not in operation) for Experiment 4

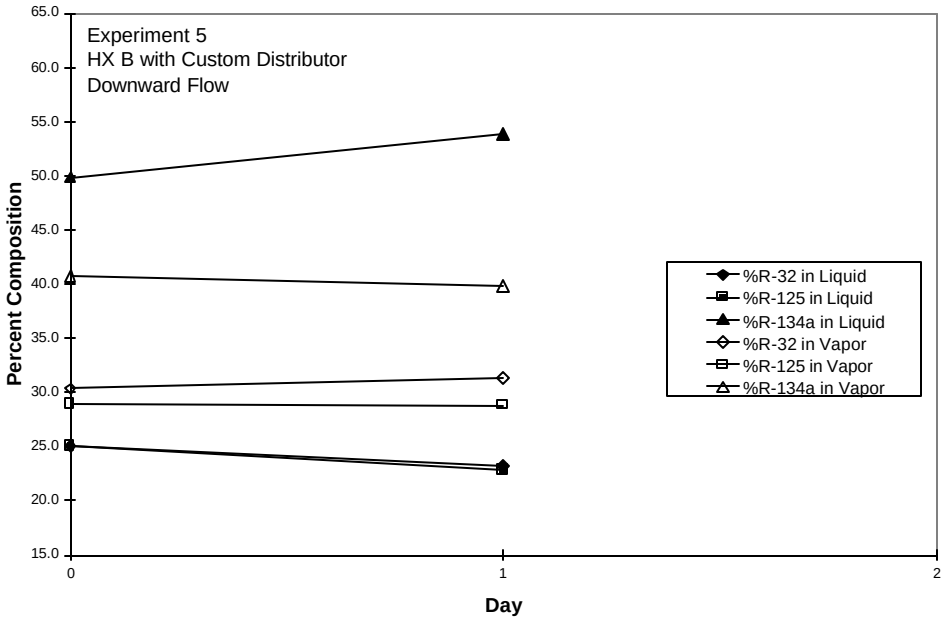

Figure C.11 Daily system composition (system not in operation) for Experiment 1

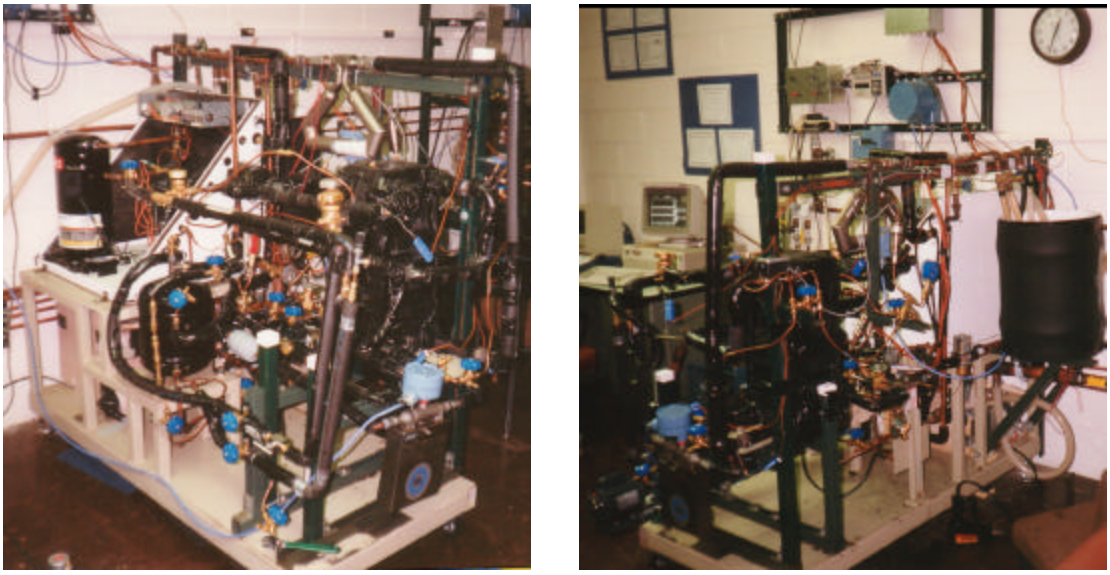

Figure C.12 Photographs of experimental facility (front and back)

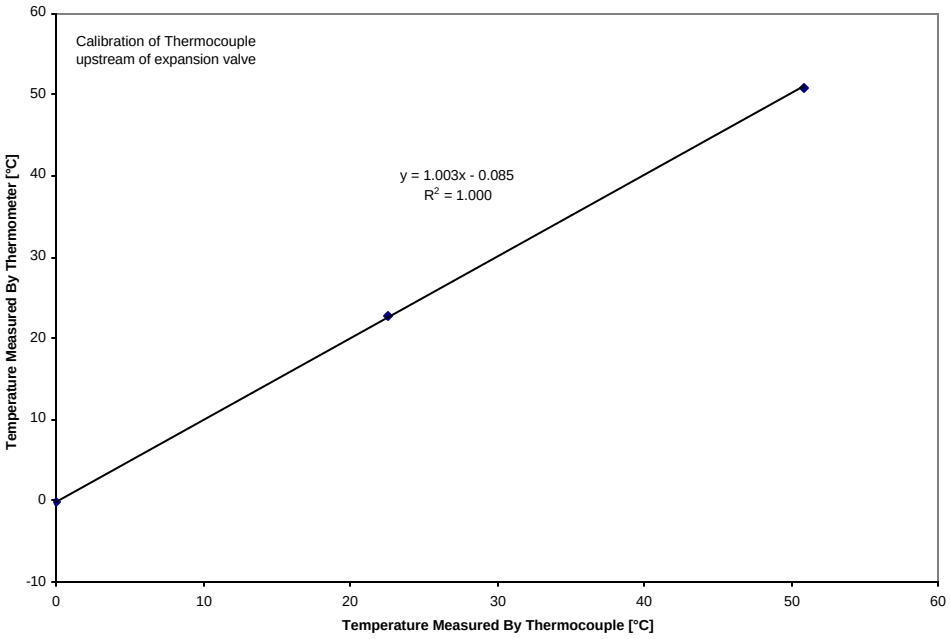

Figure C.13 Calibration Curve of thermocouple upstream of expansion valve

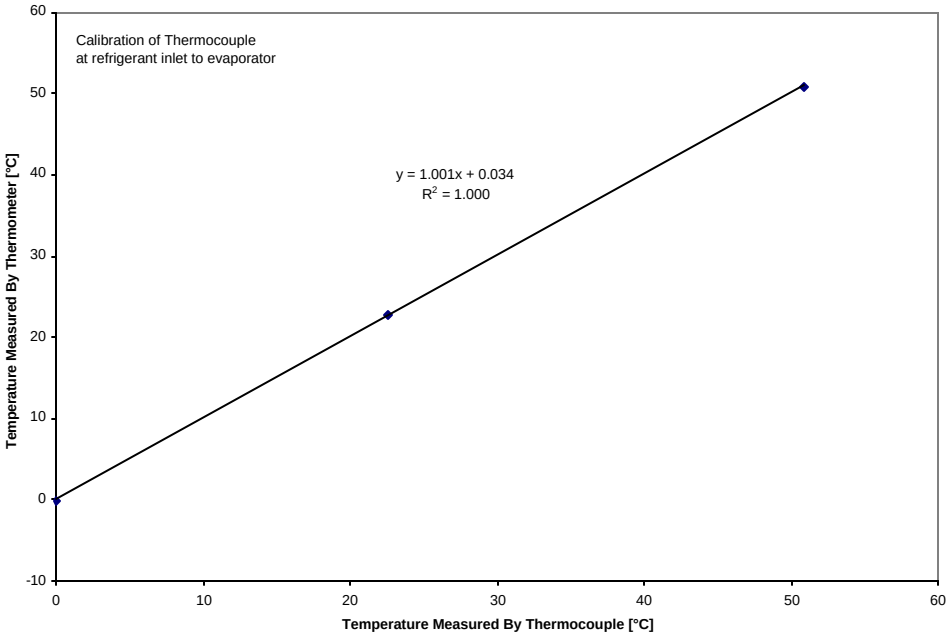

Figure C.14 Calibration Curve of thermocouple at refrigerant inlet of evaporator

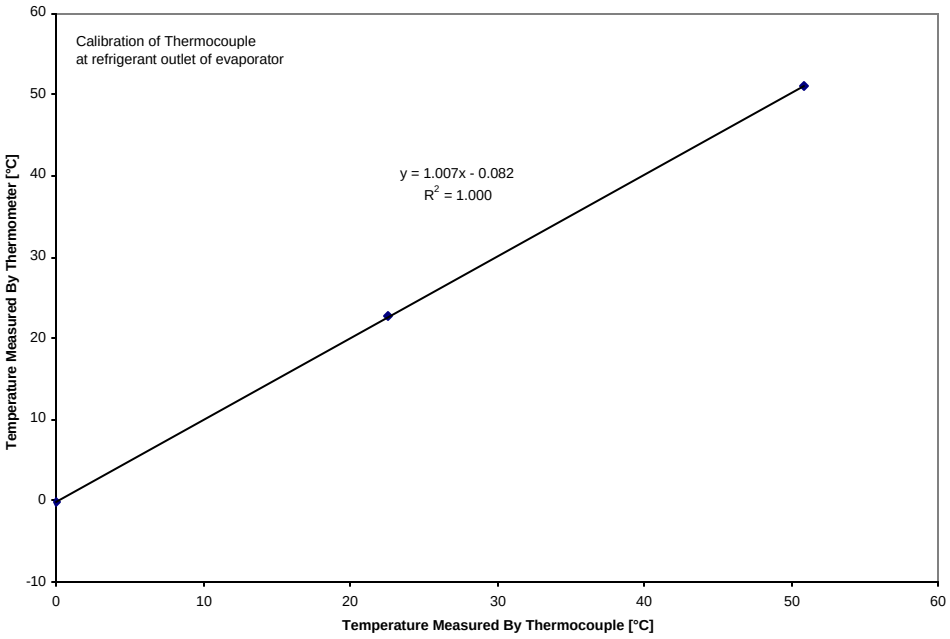

Figure C.15 Calibration Curve of thermocouple at refrigerant outlet of evaporator

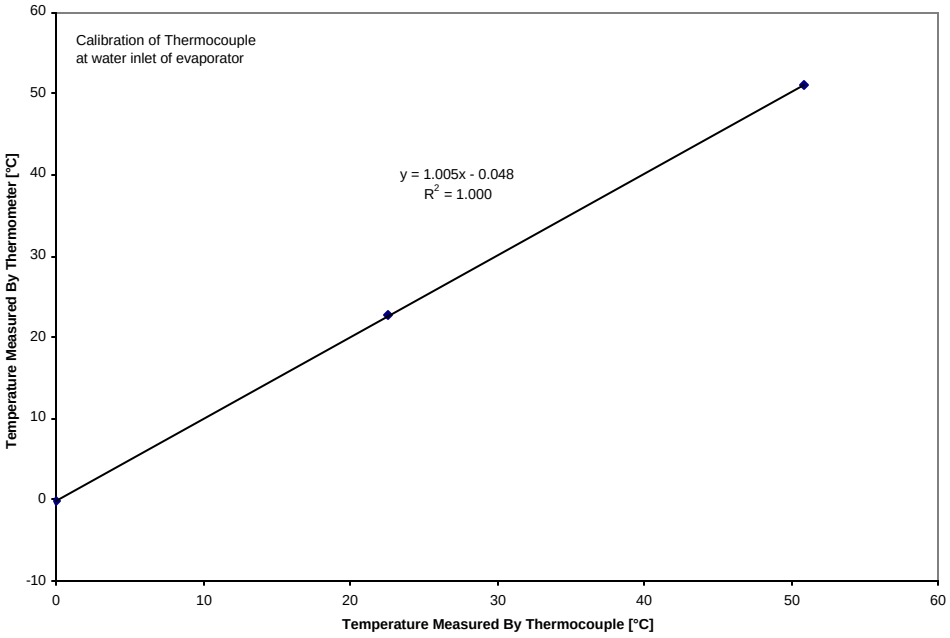

Figure C.16 Calibration Curve of thermocouple at water inlet of evaporator

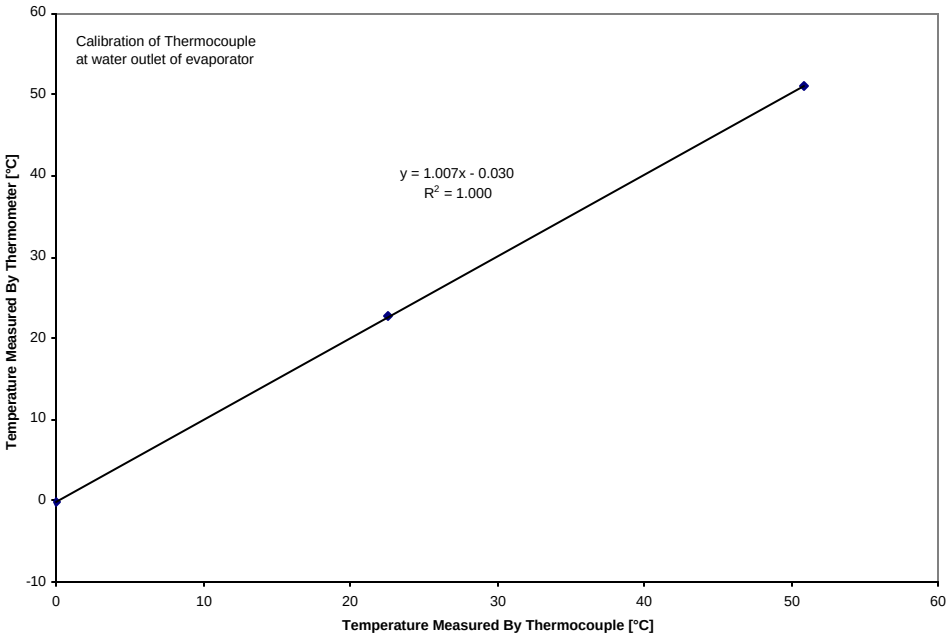

Figure C.17 Calibration Curve of thermocouple at water outlet of evaporator

Appendix D: EES Equations

The Engineering Equation Solver (EES) program was used to analyze data. This Appendix contains sample equations for both R-22 and R-407c evaluation.

R-22 EES Equations

```
{Trane ATP project
 Experiment 1
 B15x40, HX A
 R-22}

{Refrigerant side Calculations}

hin = Enthalpy(R22,T=TTXV, P=Pin)
xin = Quality(R22,T=Trin,h=hin)
hout = Enthalpy(R22,T=Trout,P=Pout)
DPref = Pressure(R22,x=0.5,T=Trin) - Pout
Qref= mref*(hout-hin)/1000
Pevapin=Pout+(0.151*mref+2.700)
Trin=Temperature(R22,P=Pevapin,x=0.5)

{Water side}

Qw = mw *Cp * DT/1000
DT = (Twin-Twout)

{Energy Balance}

dQ = 100*(Qref-Qw)/Qref

{heat exchanger}

Trevap = Temperature(R22,x=0.5,P=Pout)
LMTD = (abs(Twin-Trevap)-abs(Twout-Trin))/ln(abs(Twin -Trevap)/abs(Twout-Trin))
UAref =Qref/LMTD

{Water Side Correlation for plate evaporator  B15 x 40}

npw = 20  {number of water channels}
npr = 19 {number of refrigerant channels}
t = 0.0006  {plate thickness [m]}
k =  16.3 {thermal conductivity of plate material [W/(m*C)]}
ap = 0.036  {area of a plate [m^2]}
A = (npw+npr-1) * ap  {heat transfer area of the heat exchanger}
CRe = 28571  {constant in Re calculation based on specific plate geometry}
dh = 0.0040  {hydraulic diameter [m]}

Pr = mu*Cp*1000/kw
mu = Viscosity(Water,T=Twin,P=100)  {dynamic viscosity of water [kg/(m*s)]}
Cp = SpecHeat(Water,T = Twin,P = 100) {Specific heat of water [kJ/(kg*C)]}
kw = Conductivity(Water,T=Twin,P=100) {thermal conductivity of water [W/(m*C)]}

Y = 0.333*exp(6.4/(Pr+30))  {exponent for Pr}
```

```
Re = mw/1000*CRe/(mu*1000*npw)

C= if(Re,80,.63676,.63676,.330)
n= if(Re,80,0.53,0.53,0.68)

Nu = C*Re^n*Pr^Y
hw = Nu*kw/dh
U = Qw/(A*LMTD)
hr = 1/(1/(1000*U)-1/hw-t/k)

{Kedzierski's Method}

hsatvap = Enthalpy(R22,P=Pout,x=1)

Twmid = Q2ph*1000/(mw*Cp)+Twout

Q2ph = mref*(hsatvap-hin)/1000

Qsup=Qw-Q2ph

LMTD2ph = (Large2ph-Small2ph)/ln(Large2ph/Small2ph)
Large2ph = max(abs(Twout-Trin),abs(Twmid-Trevap))
Small2ph = min(abs(Twout-Trin),abs(Twmid-Trevap))

LMTDsup = (Largesup-Smallsup)/ln(Largesup/Smallsup)
Largesup = max(abs(Twin-Trout),abs(Twmid-Trevap))
Smallsup = min(abs(Twin-Trout),abs(Twmid-Trevap))

LMTD2zone = (Q2ph*LMTD2ph+Qsup*LMTDsup)/Qw

U2zone = Qw/(A*LMTD2zone)
```

R-407c EES Equations

```
Function Hl(T)
Tr:=(T+273.15)/359.938
X0:=0.5714562
X:=(1-Tr)^(1/3)-X0
A:=229.2501
B:=-547.75
C:=-502.544
D:=-208.25
E:=-221.75
F:=0.0
Hl:=A+B*X+C*X^2+D*X^3+E*X^4+F*X^5;
END


Procedure CONSTANTS(A:B,C)
If (A<10) Then GOTO 10
If (A>10) and (A<20) Then GOTO 20
If (A>20) and (A<40) Then GOTO 30
If (A>40) and (A<80) Then GOTO 40
If (A>80) Then GOTO 50
 10:  B := 0.61649
     C := 0.33;
20: B := 0.38305
     C := 0.54;
30: B := 0.04995
     C := 1.22;
40: B := 0.63676
     C := 0.53;
50: B := 0.330
     C := 0.68;
END


{Trane ATP project}
{Experiment 1}
{B15x40, HX A}
{R-407c}



{Refigerant side R-407c}

{Calculate inlet enthalpy using DuPont's formula for Saturated Liquid Enthalpy}

hin=Hl(Ttxv)

{Calculate outlet enthalpy using DuPont's formula for Vapor Enthalpy and Martin-Hou
EOS}

hout=A0*T+B0*T^2/2+C0*T^3/3+D0*T^4/4+Pout*V+(A2/(V-b)+A3/(2*(V-b)^2)+A4/(3*(V-
b)^3)+A5/(4*(V-b)^4))+exp(-k*T/Tc)*(1+k*T/Tc)*(C2/(V-b)+C3/(2*(V-b)^2)+C4/(3*(V-
b)^3)+C5/(4*(V-b)^4))+X
```

{where:}
T=Trout+273.15
A0=9.5220301e-2
B0=2.583136e-3
C0=-1.6933911e-6
D0=3.936350665e-10
Tc=359.938
X=282.9399
A2=-2.094775e-1
A3=3.159454e-4
A4=-1.809292e-7
A5=-5.449894e-11
B2=2.921993e-4
B3=-3.777023e-7
B4=0
B5=3.168756e-13
C2=-5.489855e-1
C3=-5.952803e-4
C4=0
C5=7.641826e-9
R=9.645379e-2
b=4.643328e-4
k=5.5
Pout=R*T/(V-b)+(A2+B2*T+C2*exp(-k*T/Tc))/(V-b)^2+(A3+B3*T+C3*exp(-k*T/Tc))/(V-b)^3+(A4+B4*T+C4*exp(-k*T/Tc))/(V-b)^4+(A5+B5*T+C5*exp(-k*T/Tc))/(V-b)^5

{calculate heat exchanged using refrigerant data}

Qref= mref*(hout-hin)/1000

{Water side}

Qw = mw *Cp * DT/1000

DT = (Twin-Twout)

dQ = 100*(Qref-Qw)/Qref

{Calculate temperature glide for LMTD determination using dew point formula}

ln(Pout/Pc)=1/Tr*(l+m*J+o*J^2+p*J^3+q*J^4+s*J^5)
J=(1-Tr)-J0
Tr=(Trglide+273.15)/Tc
Pc=4598.566
J0=0.2098958
l=-1.528743
m=-7.170891
o=-.9458618
p=-3.265625
q=.7246094
s=-8.10625e1

{heat exchanger}

LMDT = (Large-Small)/ln(Large/Small)
Large = max(abs(Twout-Trin),abs(Twin-Trglide))

```
        Small = min(abs(Twout-Trin),abs(Twin-Trglide))

UAref =Qw/LMDT

{calculate saturated liquid temperature at distributor pressure}

Pevapin=Pout+.151*mref+2.7

ln(Pevapin)=A6+B6/(Tsl+273.15)+C6*ln(Tsl+273.15)+D6*(Tsl+273.15)+E6*(F6/(Tsl+273.15)-1)*ln(F6-
(Tsl+273.15))
A6=8.518029e1
B6=-2.821167e3
C6=-1.315279e1
D6=2.430068e-2
E6=-6.303944e-1
F6=3.958659e2

{calculate saturated vapor temperature at distributor pressure}

ln(Pevapin/Pc)=1/Tr1*(l+m*J1+o*J1^2+p*J1^3+q*J1^4+s*J1^5)
J1=(1-Tr1)-J0
Tr1=(Tsv+273.15)/Tc

{calculate saturated liquid enthalpy at distributor pressure}

hsl = Hl(Tsl)

{calculate saturated vapor enthalpy at distributor pressure}

hsv=A0*T1+B0*T1^2/2+C0*T1^3/3+D0*T1^4/4+Pout*V1+(A2/(V1-b)+A3/(2*(V1-b)^2)+A4/(3*(V1-
b)^3)+A5/(4*(V1-b)^4))+exp(-k*T1/Tc)*(1+k*T1/Tc)*(C2/(V1-b)+C3/(2*(V1-b)^2)+C4/(3*(V1-
b)^3)+C5/(4*(V1-b)^4))+X
T1 = Tsv + 273.15
Pevapin=R*T1/(V1-b)+(A2+B2*T1+C2*exp(-k*T1/Tc))/(V1-b)^2+(A3+B3*T1+C3*exp(-k*T1/Tc))/(V1-
b)^3+(A4+B4*T1+C4*exp(-k*T1/Tc))/(V1-b)^4+(A5+B5*T1+C5*exp(-k*T1/Tc))/(V1-b)^5

{finally, calculate Trin}

(Trin-Tsl)/(Tsv-Tsl)=(hin-hsl)/(hsv-hsl)

{Water Side Correlation for plate evaporator  B15 x 40}

npw = 20  {number of water channels}
npr = 19 {number of refrigerant channels}
tplate = 0.0006  {plate thickness [m]}
kplate =  16.3 {thermal conductivity of plate material [W/(m*C)]}
ap = 0.036  {area of a plate [m^2]}
A = (npw+npr-1) * ap  {heat transfer area of the heat exchanger}
CRe = 28571  {constant in Re calculation based on specific plate geometry}
dh = 0.0040  {hydraulic diameter [m]}

Pr = mu*Cp*1000/kw
mu = Viscosity(Water,T=Twin,P=100)  {dynamic viscosity of water [kg/(m*s)]}
Cp = SpecHeat(Water,T = Twin,P = 100) {Specific heat of water [kJ/(kg*C)]}
kw = Conductivity(Water,T=Twin,P=100) {thermal conductivity of water [W/(m*C)]}
```

```
Y = 0.333*exp(6.4/(Pr+30))  {exponent for Pr}

Re = mw/1000*CRe/(mu*1000*npw)

Call CONSTANTS(Re:C,n)

Nu = C*Re^n*Pr^Y

hw = Nu*kw/dh

U = Qw/(A*LMDT)

hr = 1/(1/(1000*U)-1/hw-tplate/kplate)

{Kedzierski's Method}

hsatvap = Enthalpy(R407c,P=Pout,x=1)+(hin-Enthalpy(R407c,T=Ttxv,x=0))

Twmid = Q2ph*1000/(mw*Cp)+Twout

Q2ph = mref*(hsatvap-hin)/1000

Qsup=Qw-Q2ph

LMTD2ph = (Large2ph-Small2ph)/ln(Large2ph/Small2ph)
Large2ph = max(abs(Twout-Trin),abs(Twmid-Trglide))
Small2ph = min(abs(Twout-Trin),abs(Twmid-Trglide))

LMTDsup = (Largesup-Smallsup)/ln(Largesup/Smallsup)
Largesup = max(abs(Twin-Trout),abs(Twmid-Trglide))
Smallsup = min(abs(Twin-Trout),abs(Twmid-Trglide))

LMTD2zone = (Q2ph*LMTD2ph+Qsup*LMTDsup)/Qw

U2zone = Qw/(A*LMTD2zone)
```